

**A STUDY OF WEATHER IMPACTED KU BAND SATELLITE
CHANNEL: PROPAGATION IMPAIRMENT AND
IMPROVEMENT IN QUALITY OF SERVICE IN MOIST
TROPICAL CLIMATE**

**A THESIS SUBMITTED IN PARTIAL
FULFILMENT OF THE REQUIREMENTS
FOR THE DEGREE OF DOCTOR OF
PHILOSOPHY**

RAVINDRA NAITHANI

MZU REGN NO: 1506797

Ph.D REGN NO.MZU/Ph.D/915 OF 21.04.2016



**DEPARTMENT OF PHYSICS
SCHOOL OF PHYSICAL SCIENCES
APRIL 2023**

**A STUDY OF WEATHER IMPACTED KU BAND SATELLITE
CHANNEL: PROPAGATION IMPAIRMENT AND
IMPROVEMENT IN QUALITY OF SERVICE IN MOIST
TROPICAL CLIMATE**

BY

RAVINDRA NAITHANI

Department of Physics

Name of the Supervisor

Prof. RAMESH CHANDRA TIWARI

Submitted

**In partial fulfilment of the requirement of the Degree of Doctor of
Philosophy in Physics of
Mizoram University, Aizawl**



MIZORAM UNIVERSITY
DEPARTMENT OF PHYSICS
School of Physical Sciences

Aizawl - 796004, MIZORAM, India

(A Central University Established by an Act of Parliament of India)

Ph:+91-389-2330522(O) +91-9862300514 (M) Fax: +91-389-2330435
Supervisor Email: ramesh_mzu@rediffmail.com

Prof. R.C. Tiwari
Senior Professor

Date: April 2023

Certificate

This is to certify that the thesis entitled “A Study of weather Impacted KU Band Satellite Channel: Propagation Impairment and improvement in quality of service in moist Tropical climate”, submitted by Shri Ravindra Naithani, for the degree of Doctor of Philosophy of the Mizoram University, Aizawl, embodies the record of original Investigation carried out by him under my supervision. The thesis presented is worthy of being considered for the award of Ph.D. degree. This work has not been submitted for any degree to any other University.

Prof. Ramesh Chandra Tiwari
Supervisor

Declaration of the Candidate

Mizoram University

April 2023

I, Ravindra Naithani, hereby declare that the subject matter of this thesis is the record of the work done by me, that the contents of this thesis did not form basis for the award of any previous degree to me or to the best of my knowledge to anybody else, and that the thesis has not been submitted by me for any research degree in any other University/Institute.

This is being submitted to the Mizoram University for the degree of Doctor of Philosophy in Physics.

(RAVINDRA NAITHANI)

(Head of Department)

(Supervisor)

Acknowledgment

Many people and institutions have contributed immensely in completion of this research work. I would like to express my sincere gratitude and appreciation to all those who have supported me in the completion of my thesis.

I express my deep and sincere appreciation goes to my supervisor, Professor R. C. Tiwari, for his continuous guidance and motivation throughout this research. His intellectual ideas and never say die spirit encouraged me immensely to complete the research work.

I am also thankful to Prof. Zaithanzauva Pachuau, Head Department of Physics, and all the faculty members and non-teaching staff for their support and providing us with an intellectual atmosphere all through these years.

I am very grateful to my superiors at Directorate Doordrashan, New Delhi, for giving me necessary permission to carry out the research work at DDK Aizawl. My heartfelt thanks to my colleagues and staff at Doordrashan Aizawl for their technical help in installing the technical setup at Earth Station DDK Aizawl for data collection for my research study. My friend and fellow research scholars in the department, especially Dr. Thaisa Jawhly, deserve special mention for his help and support.

Last but not the least, I am immensely grateful to my family and wife, Nishi Naithani, for their unconditional support and belief in me. I thank all those who have helped me directly or indirectly in completing this thesis.

Dated: April 2023

(RAVINDRA NAITHANI)

Preface

Satellite communication is the most profound and widely used technology in modern world. This technology has revolutionized the way we communicate, navigate and access information. Here are some of the ways satellite communication has impacted our lives. With the help of satellite channel, corporate can now conduct video conferencing sessions with employees and clients across the globe. This has enabled better communication, faster decision making and increased productivity.

Satellite communication has also made it possible for medical sector to provide medical treatment and consultation to patients in remote areas through satellite links. This has been especially useful in emergencies where quick medical assistance is needed. It has enabled virtual classrooms where students from different parts of the world can connect with each other and learn together. This has opened up new opportunities for education and knowledge sharing.

Satellites are used to monitor weather pattern and natural disaster such as hurricane, earthquakes and tsunamis. This information is then used to predict and prepare for potential disasters, saving countless lives. Satellite communication has enabled the common man to use navigation tools and access the internet. Global positioning system (GPS) has made it easy for people to navigate and find their way around. GPS has also opened unimaginable business opportunities in travelling industry.

To conclude, the role of satellite communication in extending communication and navigation facilities is extensive. It has changed the way we communicate, navigate and access information. From virtual classrooms to medical treatment satellite communication has made it possible for people to connect with each other regardless of their location. It has truly made the world a small place.

With satellite communication it has become possible to provide seamless connectivity to remote and inaccessible areas where traditional mode of communication are not feasible. The north- eastern region of India is

one such region where satellite communication has significant importance due to its sparse population, rugged terrain and limited infrastructure.

The traditional satellite communication bands are congested, and hence, there is a need to migrate to higher frequencies bands to satiate the demands of higher bandwidth. However, higher frequencies bands are prone to atmospheric attenuation particularly rain attenuation, which can significantly impact the performance of satellite communication system.

Despite the significance of rain attenuation in satellite communication, all attenuation models available in the literature are based on measurements in temperate climatic conditions. Hence, it is crucial to study the impact of rain attenuation in the context of north- eastern region of India, which has a distinct climate and geography.

The current work aims to address this research gap by carrying out an experimental study of rain impacted Ku band satellite channels in Aizawl, the capital of Mizoram, a state in north- eastern region of India. This study will provide valuable insights into the behaviour of satellite channels under rain attenuation in the region, which can aid in design and optimization of satellite communication systems in the future.

The thesis is organised into chapters that provide a comprehensive understanding of the impact of rain attenuation on higher frequencies satellite channels. Chapter 1 provides an introduction to satellite communication and a brief introduction of theoretical framework for the current thesis. Chapter 2 reviews the literature on rain attenuation in satellite communication systems. Chapter 3 presents the experimental setup and methodology used in this study. Chapter 4 presents the result of experimental study and their analysis and brief description of various mitigation technique currently in use in satellite communication.

Finally, chapter 5 summarises the findings of the study and future scope of study.

Table of Contents

Page no

Inner cover page	2
Supervisor's certificate	3
Declaration of the candidate	4
Acknowledgments	5
Preface	6
Table of contents	8
List of figures	15
List of tables	18

Chapter 1

20-72

1	Introduction	21
----------	---------------------	----

1.1	Segments of satellite communication system	22
1.1.1	Frequencies allocated	23
1.1.2	Types of satellite services	24
1.1.3	Performance of satellite system	25
	1.1.3.1 Fidelity	25
	1.1.3.2 Availability	26
	1.1.3.3 Continuity	26
1.1.4	Signal parameters	26
1.2	Structure of atmosphere	28
1.2.1	Troposphere	30
1.2.2	Stratosphere	30
1.2.3	Mesosphere	31
1.2.3	Thermosphere(Ionosphere)	32
1.2.5	Exosphere	32
1.3	Basic transmission theory	33
1.4	World climate	38
1.4.1	Tropical wet climates	39

1.4.2	Tropical wet and dry climates	39
1.4.3	Semiarid and desert (arid) climates	40
1.4.4	Subtropical dry summer climates	41
1.4.5	Humid subtropical climates	41
1.4.6	Humid oceanic climates	41
1.4.7	Humid continental climates	42
1.4.8	Subarctic Climates	42
1.4.9	Subarctic Climates (Tundra Type)	42
1.4.10	Icecap climates	42
1.4.11	Highland climates	43
1.5	Classification of Precipitation (rainfall)	43
1.5.1	Convective rain	43
1.5.2	Stratiform rain	43
1.6	Propagation mechanism	44
1.6.1	Absorption	44
1.6.2	Scattering	45
1.6.3	Refraction	45
1.6.4	Diffraction	45
1.6.5	Multipath	45
1.6.6	Terrain scattering on the Earth's surface	45
1.7	Propagation Impairment Factor	49
1.7.1	Absorption	49
1.7.2	Scattering	50

1.7.3	Rayleigh scattering	51
1.7.4	Mie scattering	52
1.8	Characteristics of precipitation	52
1.8.1	Drop size distribution	53
1.8.2	Laws and Parson distribution	53
1.8.3	Marshall and Palmer model	54
1.8.4	Terminal velocity	55
1.8.5	Orientation and shape	56
1.8.6	Temperature	56
1.9	Measuring precipitation rate	57
1.9.1	Optical rain gauge	57
1.9.2	Tipping bucket rain gauge	58
1.9.3	Capacitance gauge	59
1.10	Frequency analysis of rainfall	59
1.10.1	Rainfall variability in time	59
1.10.2	Probability of Exceedance and return period	60
1.10.2.1	Rainfall depth expected for specific prob.	60
1.10.2.2	Probability of Exceedance	60
1.10.2.3	Return period	61
1.10.2.4	Time series of rainfall data	61
1.10.2.5	Frequency analysis and Prob. plotting	62
1.11	Estimation of Probability of Exceedance	63
1.11.1	Intensity duration frequency (IDF) curve	64
1.11.2	Attenuation due to precipitation	64
1.12	Conclusion	68

Chapter 2

2	Review of Literature	73-80
	References	80-82

Chapter 3

3	Methodology	83-112
3.1	Introduction	84
3.2	RF data collection Methodology	84
	3.2.1 Calculation of look angle	88
	3.2.2 Spectrum Analyzer	90
3.3	Rain data collection source	92
	3.3.1 Indian Metrological department, regional Centre, Guwahati	92
	3.3.2 State Metrological Centre, Government of Mizoram	92
	3.3.3 Indian Metrological department, New Delhi	92
3.4	Statistical tools for analysis	92
	3.4.1 The Chi- Square Test	93
	3.4.2 Bilinear Interpolation	95
	3.4.3 Statistical Test and Analysis	98
	3.4.3.1 Least Square Method	98
	3.4.3.2 Root mean square error (RMSE)	101
	3.4.3.3 Correlation coefficient	101
	3.4.3.4 Coefficient of Determination	102
3.5	Data analysis software	103
3.6	ITU Sectors	105
	3.7.1 Radio communication (ITU-R)	106
	3.7.2 Standardization (ITU-T)	106

3.7.3	Development (ITU-D)	106
3.7.4	ITU Telecom	106
3.8	ITU Recommendations	106
3.8.1	ITU- R.P. 839-4 (09-13)	106
3.8.2	ITU R-REC-P.837-7	108
3.8.3	Recommendation ITU-R-618-13	109
3.9	MATLAB Programme	109
3.9.1	Crane Model	110
3.9.2	ITU Model	111
3.10	Conclusion	111
3.11	Referencing	112

Chapter 4

4 Results and Discussion 113-191

4.1	Analysis of rainfall data	114
4.1.1	Source of rainfall data	117
4.2	Rain data Analysis	117
4.2.1	Point rainfall rate Statistics	120
4.2.2	Rainfall IDF curve	123
4.2.3	Rain depth exceedance curve integration time 24 hours	125
4.2.4	Experimental data	128
4.2.5	Comparison of experimental data with historical data	129
4.3	Conversion of rain rate from 60 minute to one minute integration time	130
4.4	Proposed Regression based rain model	134
4.4.1	Rain rate integration time one minute	134
4.4.2	Rain rate integration time 60 minutes	135
4.5	Comparison with other models	136

4.5.1	Mopfouma model	136
4.5.2	Segal Model	138
4.5.3	Burgueno Model	139
4.5.4	Comparison with Segal and Burgueno Model	140
4.6	Proposed power regression-based rain conversion model	140
4.7	Rain attenuation analysis	142
4.7.1	Introduction	142
4.8	Prediction of rain attenuation models	143
4.8.1	ITU model (ITU-RP.618-13,2017)	143
4.8.1.1	Calculation of rain attenuation using ITU model	145
4.8.2	SAM Model	154
4.8.3	DAS Model	156
4.8.4	Crane Model	158
4.8.5	ITU Model with MATLAB	163
4.8.6	Measured attenuation	165
4.9	Comparison of measured attenuation with predicted attenuation	167
4.9.1	Comparison with SAM and DAS model	167
4.9.2	Comparison with Crane and ITU model	168
4.9.3	Evaluation of Model in terms of Comparison Metrics	169
4.10	Regression analysis of measured and ITU predicted attenuation	170
4.11	Proposed rain attenuation model	171
4.11.1	Single component rain attenuation model	171
4.11.2	Two Component Rain attenuation model	172
4.11.3	Rain attenuation model for different frequencies	174
4.12	Fade Mitigation Technique	176
4.12.1	Static Fade Mitigation	176
4.12.2	Adaptive Fade Mitigation	176
4.13	FMT concepts	178
4.13.1	Measurements	178
4.13.2	Prediction	178
4.13.3	Statistical approach of Prediction	179
4.13.4	Regression based predictor	179
4.13.5	Artificial neural network method	180
4.13.6	Decisions	180

4.13.7	Mitigation Technique	180
4.13.8	Compensation type FMT	181
4.13.9	EIRP control	181
4.14	Adaptive waveform Technique	183
4.14.1	Adaptive coding	183
4.14.2	Adaptive Modulation	184
4.15	Avoidance type FMT	185
4.15.1	Diversity	185
4.16	References	188

Chapter 5

5	Conclusion and Summary	192-206
----------	-------------------------------	---------

5.1	Rainfall Analysis	193
5.2	Rain Attenuation Analysis	197
5.3	Proposed rain attenuation Model	199
5.3.1	Single component rain attenuation model	199
5.3.2	Two component rain attenuation model	200
5.3.3	Proposed rain attenuation model for different frequencies	202
5.4	Future scope of Study	204
5.5	References	206
	Bio-data of the candidate	207
	Publication and activities	208
	Particulars of the candidate	210

List of Figures

Chapter 1

1.1	Satellite communication systems	-	23
1.2	Structure of Atmosphere	-	29
1.3	Basic Communication link	-	33
1.4	wavelength	-	34
1.5	Inverse square law of radiation	-	35
1.6	Power flux Density	-	36
1.7	World climatic Map (Source: The World Book Encyclopedia)	-	38
1.8	Radio wave propagation mechanisms and their impact on parameters of communication signal (Ippolito, 1986)	-	1.8

Chapter 3

3.1	GSAT-15 (Picture: courtesy; google.com/pic)	-	85
3.2	Foot print of GSAT-15 (source: www.satstar.com)	-	86
3.3	Tektronix RSA306B spectrum Analyzer	-	90
3.4	Bilinear interpolation	-	95
3.5	Yearly average zero-degree isotherm height	-	107
3.6	ITU digital map for $R_{0.01}$ rate for the globe	-	108
3.7	Picture From recommendation P.837-6 (ITU-R)	-	109

Chapter 4

4.1	Map of Mizoram	-	115
4.2	Average monthly relative humidity of Aizawl (1986-2015)	-	116
4.3	Monthly Avg., Minimum and Maximum Temperature of Aizawl	-	116
4.4	Percentage of rainfall. Monsoon vs non-monsoon month	-	119
4.5	Average Monthly rainfall at Aizawl	-	119
4.6	Average rain-rate for different year blocks	-	120

4.7	Annual rainfall depth Exceedance curve for the district Aizawl Mizoram	-	124
4.8	Rain depth exceedance curve with integration time 24 hours	-	126
4.9	Measured and Historical rain rates with integration time one hour	-	129
4.10	GUI of ITU-R P.837.7	-	131
4.11	Exceedance rain-rate conversion from integration time one hour to 1 minute	-	132
4.12	Rain rate conversion	-	134
4.13	Figure 4.12: Estimated exceedance with rain-rate (mm/hour) integration time 1 minute	-	135
4.14	Exceedance rain rate with integration time one hour or 60 minutes	-	136
4.15	Comparison of the data with Mopfouma Model.	-	138
4.16	Comparison of measured rain rate with Segal and Burgueno Model	-	140
4.17	Proposed Rain Rate Conversion Model	-	141
4.18	The experimental set up	-	145
4.19	Space - earth signal path (courtesy ITU)	-	146
4.20	Attenuation vs. exceedance (ITU model)	-	154
4.21	Rain attenuation vs exceedance	-	156
4.22	Exceedence vs Attenuation DAS Model	-	158
4.23	Rain exceedance vs. attenuation (Crane model)	-	160
4.24	Rain attenuation at different frequencies (Crane model)	-	162
4.25	Predicted attenuation at different frequencies by Crane Model.	-	162
4.26	Rain attenuation vs. exceedance ITU model	-	164
4.27	Attenuation vs., frequency ITU model	-	165
4.28	ITU Attenuation at different frequencies	-	165
4.29	Exceedance vs. attenuation, Measured	-	166
4.30	Measured attenuation Vs. Predicted attenuation SAM and DAS Model	-	167
4.31	Comparison of measured attenuation with ITU and Crane model	-	168
4.32	Exceedance vs. attenuation for ITU and Crane model	-	169
4.33	Measured Attenuation Vs, Rain Exceedance	-	170
4,34	Exceedance vs. attenuation for ITU model	-	171
4.35	Proposed single Component Model for Rain Attenuation Ku Band	-	172

4.36	1st component of proposed two components Attenuation Model 2nd Component	-	173
4.37	2nd component of the proposed two component attenuation model	-	174
4.38	Proposed Attenuation frequency Model.	-	175
4.39	Schematics of Adaptive FMT loop	-	177

Chapter 5

5.1	Rain rate exceedance curve with integration time 60 Minutes	-	195
5.2	Rain rate conversion from integration 60 minute to 1 minute	-	196
5.3	Predicted rain attenuation at different frequencies by ITU model	-	198
5.4	ITU attenuation vs. frequency	-	199
5.5	Proposed single Component Model for Rain Attenuation Ku Band	-	200
5.6	1st component of proposed two components Attenuation Model	-	201
5.7	2nd component of proposed two component attenuation model	-	202
5.8	Proposed Attenuation frequency Model.	-	203

List of Tables

Chapter 1

1.1	Frequency Band And Frequency Allocation	-	24
1.2	Impairments Affecting Earth Space Communication System	-	47
1.3	Probability Of Rain-Rate Exceedance Calculation Method	-	63

Chapter 3

3.1	GSAT- 15 MISSION DATA	-	85
3.2	DISH SIZE ESTIMATE BASED ON EIRP (DBW)	-	86
3.3	Uplink Signal Parameters And Values	-	87
3.4	Diameter, Elevation Angle, And Azimuth Angle	-	87
3.5	Tabular Data to Calculate Bilinear Interpolation	-	96
3.6	Software/Programme Used	-	103

Chapter 4

4.1	Year-Wise Rainfall And Monsoon Months Rainfall	-	117
4.2	Relation Between Percentage Time And Absolute Time	-	112
4.3	C Value For Different Region Of India	-	127
4.4	Exceedance Rain Rate (Mm/Hour) With Integration Time One Hour.	-	128
4.5	Measured Rain Rate Vs. Exceedance	-	128
4.6	Table Of Comparison Metrics	-	129
4.7	Conversion Of Rain Rate From Integration Time 60 Minute To 1 Minute	-	133
4.8	Parameters For Segal And Burgueno Method	-	139
4.9	Geographical Location Of The Project Site	-	144

4.10	Rf Parameters For The Experimental Set-Up	-	144
4.11	Coefficients For K_H	-	149
4.12	Coefficients For K_V	-	149
4.13	Coefficients For α_v	-	149
4.14	FREQUENCY-DEPENDENT COEFFICIENTS FOR ESTIMATING SPECIFIC RAIN ATTENUATION	-	149
4.15	ATTENUATION (DB) WITH RAIN RATE BASED ON SAM MODEL	-	155
4.16	EXCEEDANCE AND ATTENUATION (DB)	-	157
4.17	RAIN ATTENUATION FROM CRANE MODEL	-	160
4.18	RAIN EXCEEDANCE AND ATTENUATION AT DIFFERENT FREQUENCIES	-	161
4.19	RAIN ATTENUATION FROM ITU MODEL	-	163
4.20	PREDICTED RAIN ATTENUATION AT DIFFERENT FREQUENCIES	-	164
4.21	MEASURED RAIN ATTENUATION	-	166
4.22	COMPARISON METRICS	-	169

Chapter 5

5.1	Comparison Metrics	-	197
5.2	Correlation Coefficient Between $\frac{E_b}{N_0}$ And Temperature	-	205

Chapter **1**

Introduction

CHAPTER 1: INTRODUCTION:

1 Introduction:

The history of satellite communication began with the launch of Sputnik by USSR in 1957 while the United State of America launched its own satellite in 1958 (Steeves et al., 2009). During early 1960 Moon was used to bounce teletypewriter signals between Hawaii and Washington D.C (Whalen, 2003) The Defence Satellite Communication Programme (DSCP) of USA was initiated in 1962 and during the phase 1 of DSCP, high quality voice transmission were conducted between a satellite and two earth stations. These early experiments with communication demonstrated that satellite systems can satisfy many requirements. They are survivable, reliable, secure and a cost-effective method of communication.

In the context of worldwide communication network, satellite communication systems are very important. Satellite communication because of its cost effectiveness, global availability, superior reliability, superior performance, scalability and versatility has unique advantages over conventional long distance communication technologies. In the past decade, new and demanding satellite applications evolved leading to spectral congestion of the conventional frequency bands allocated for satellite Services, namely *L* (1-2 GHz), *S* (2-4 GHz), and *C* (4-6 GHz) (Panagopoulos et al., 2009). Among the recent developments in the satellite industry, one can single out the proliferation of VSAT/USAT (very/ultra small aperture terminals) systems designed primarily for data applications, the provision of direct-to-home (DTH) services by Direct Broadcast Satellite (DBS) systems, and the extension of satellite communications to non-geostationary (NGSO) orbit

constellations. Further rapid emergence and deployment of terrestrial services such as Worldwide Interoperability for Microwave Access (WiMAX), terrestrial microwave network as well as sharing of limited C-band spectrum with radar systems is making conventional spectrum overcrowded. Concurrently there is growing global demand for mobiles, broadband (high data rate) applications via satellite such as airborne or maritime internet broadband connectivity and land based on the move applications.

All the above systems, including the Conventional Geostationary (GSO) satellite systems belonging to the Fixed Satellite Service (FSS), gradually tend to employ higher frequency bands to satisfy the growing capacity requirements. Therefore, besides operation at the Ku band (10-18 GHz), the Ka band (20-30 GHz) and the *V* band (40-50 GHz) had been investigated or even adopted in satellite systems recently put into operations.

1.1 Segments of Satellite communication System:

A satellite communication system consists of following three segments.

a. Control segment: The control segment is also known as command-and-control earth station. This segment consists of resources and facilities on ground to monitor, control and maintain the satellites. It sends control and configuration commands to space segment to carry out any specific task, reallocate the resources on board, maintains and discipline satellite in its parking slot. It also receives the health, housekeeping and other telemetric data from satellite.

b. Space segment: It comprises of a satellite or constellation of satellites orbiting the earth and exchanging data with other segments via appropriate signals.

c. User segment or User earth station: It consists of user who interact with the satellite and exchange data with the satellite through appropriate signals.

The schematics of the segments and their interaction is shown in Figure 1

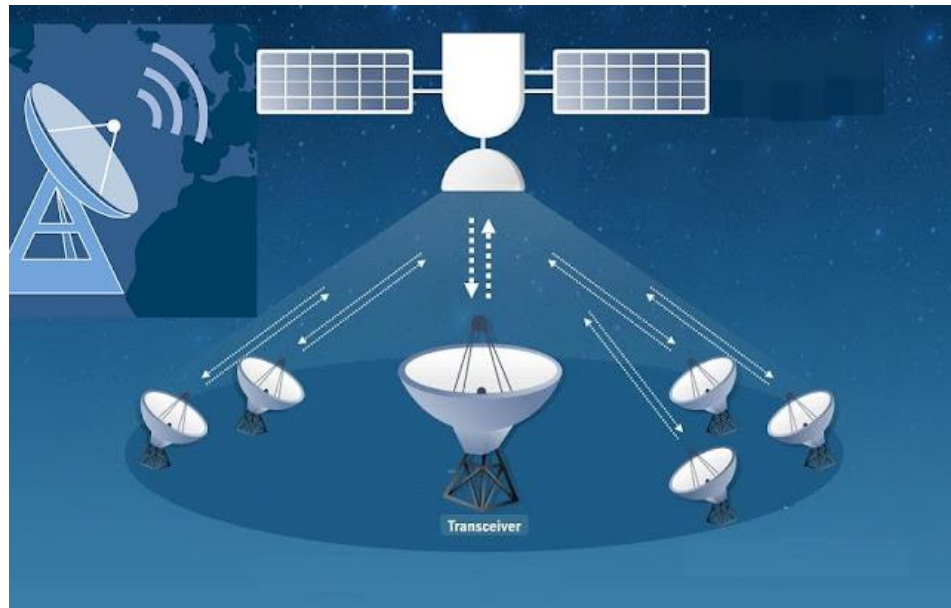


Figure 1.1: Satellite communication system

1.1.1 Frequencies allocated:

The table below gives the different frequency band and the range of frequencies allocated

TABLE 1.1: FREQUENCY BAND AND FREQUENCY ALLOCATION

Frequency band	Frequency
UHF Band	300 to 1000 MHz
L Band	1 to 2 GHz
S Band	2 to 4 GHz
C Band	4 to 8 GHz
X Band	8 to 12 GHz
Ku Band	12 to 18 GHz
Ka Band	27 to 40 GHz

1.1.2 Type of Satellite Services:

On the basis of height of satellite above earth surface satellite are classified as

1. Geostationary orbit (GEO)
2. Low Earth orbit (LEO)
3. Medium Earth orbit (MEO)
4. Polar orbit and Sun-synchronous orbit (SSO)
5. Transfer orbits and geostationary transfer orbit (GTO)
6. Lagrange points (L-points)

On the basis of type of service provided satellite are divided into

1. Fixed satellite services (FSS)
2. Mobile satellite services (MSS)
3. Broadcasting satellite services

4. Earth exploration satellite services (ESS)
5. Space research and operation satellite services (SRS)
6. Radio determination satellite services (RSS)

1.1.3 Performance of satellite system

Fidelity, availability and continuity are the important performance metric of any communication system. These parameters relate the physics affecting a propagating signal with the engineering parameters.

1.1.3.1 Fidelity:

Fidelity refers to the measure of correctness of the received information by the receiver. In satellite communication however Fidelity is not the popular term in use. In digital communication bits are the units carrying the information. Fidelity is quantitatively represented by a signal parameter known as bit error ratio (BER). BER is the ratio of bits in error in a stream of bits received by a receiver. Lesser the BER, better the fidelity and better the quality of communication system. Another signal parameter that can be associated with Fidelity is Bit error probability (BEP). BEP is the probability of a received information bit to be in error. BEP is the long-term statistical index of performance which is dependent upon how well the transmitted bits are received by the receiver.

1.1.3.2 Availability:

Availability is defined by the probability that the communication system will make the signal accessible to user within a specified coverage area and over a specified time with warranted quality.

1.1.3.3 Continuity:

Continuity is the probability that a service, once available, will continue to be available over a predefined duration. The number of time service goes in black out adds to the degradation of the continuity. There are a number of applications of satellite services like navigation, Telemedicine that cannot afford signal outage even temporarily.

1.1.4 Signal parameters

In analogue communication systems signal to noise ratio(S/N) or carrier to noise ratio (C/N) were the most important signal parameters for the performance of communication system. However, in digital communication system bit error ratio and E_b/N_0 are the most important and frequently used parameters to assess the quality of communication system.

$$\text{Signal to noise ratio} = \frac{\text{(signal power)}}{\text{(total noise power)}} = \frac{S}{N} \quad (1)$$

$$\text{Signal to spectral density of noise ratio} = \frac{\text{(signal power)}}{\text{(density of noise)}} = \frac{S}{N_0} \quad (2)$$

$$\text{Carrier to noise ratio} = \frac{\text{(carrier power)}}{\text{(total noise power)}} = \frac{C}{N} \quad (3)$$

$$\text{Carrier to spectral density of noise ratio} = \frac{(\text{carrier power})}{(\text{density of noise})} = \frac{C}{N_0} \quad (4)$$

If B is the band width of communication system

$$N_0 = \frac{N}{B} \quad (5)$$

$$\frac{Eb}{N_0} = \frac{(\text{energy per bit})}{(\text{noise density})} \quad (6)$$

The BER, Availability and Continuity are determined by the ability with which the receiver can acquire the signal and correctly decode the current state of the signal parameters like amplitude, phase and frequency. Only after decoding the received bits the receiver can faithfully recreate the signal.

Bits, the information bearing units in digital communication can assume values '0' or '1'. In a carrier signal, bits are represented by phase and amplitude. For example, in Quadrature phase shift keying (QPSK) type of modulation, the four possible codes corresponding to two bits of information are (0,0), (0,1), (1,0), (1,1) are represented by four different phase states of signal. So, with reference to an arbitrary zero phase of carrier signal, two of the codes may be represented by the phase $+\pi/4$ and $+3\pi/4$, while the other two codes may be $-\pi/4$ and $-3\pi/4$ of the signal. At the receiver side receiver has to correctly distinguish between these states of the signal. However, the random thermal noise in the system severely limits the capability of receiver to distinguish these states correctly. The overall probability of a bit being correctly identified by the receiver depends on both the energy carried by the signal and the random thermal noise. It is inversely proportional to the

variance of noise. The total added noise is a linear function of the noise power spectral density.

Hence the ratio $\frac{Eb}{N_0}$ is the most important parameter in satellite communication which in turn determines BER.

Eb = energy per bit = (signal power)/(bit rate)

$$Eb = S/Rb$$

Where Bit duration Tb is defined as

$$Tb = \frac{1}{Rb}$$

$$\therefore \frac{Eb}{N_0} = \frac{(S \times Tb)}{(N \times B)}$$

Where B is the bandwidth of the system

$$\frac{S}{N} = \left(\frac{Eb}{N_0}\right) \times \left(\frac{Rb}{B}\right)$$

Since signal to noise ratio is derived from RF signal, with C and N as power in carrier and noise, we can write

$$\frac{Eb}{N_0} = \left(\frac{C}{N_0}\right) \times \left(\frac{1}{Rb}\right) \quad (7)$$

1.2 Structure of the atmosphere

In satellite communication signal goes through the atmosphere which interacts with the signal through its constitutes and electrical properties. To

understand the impairment of the signal in atmosphere it is important to understand the structure of atmosphere.

The atmosphere can be divided into five layers according to the diversity of temperature and density:

1. Troposphere
2. Stratosphere
3. Mesosphere
4. Thermosphere (Ionosphere)
5. Exosphere

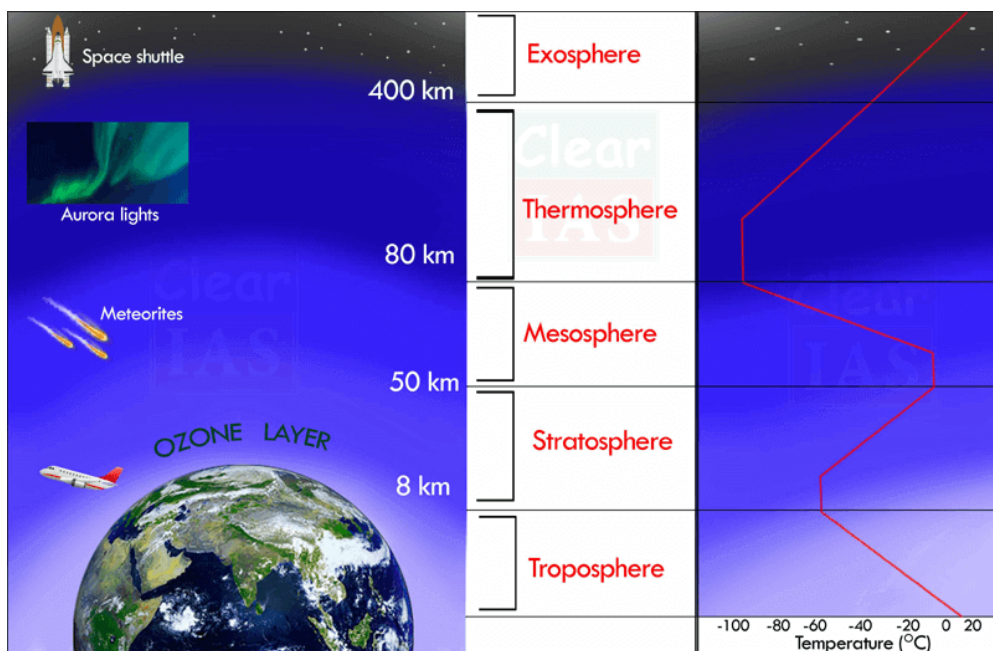


Figure 1.2: Structure of Atmosphere

1.2.1. Troposphere:

It is the lowermost layer of the atmosphere.

The height of this layer is about 18 km on the equator and 8 km on the poles.

The thickness of the troposphere is greatest at the equator because heat is transported to great heights by strong convectional currents.

Troposphere contains dust particles and water vapours.

This is the most important layer of the atmosphere because all kinds of weather changes take place only in this layer.

The air never remains static in this layer. Therefore, this layer is called 'changing sphere' or troposphere.

The environmental temperature decreases with increasing height of the atmosphere.

It decreases at the rate of 1° Celsius for every 165 m of height. This is called Normal Lapse Rate.

The zone separating troposphere from the stratosphere is known as tropopause.

The air temperature at the tropopause is about – 80° Celsius over the equator and about – 45° Celsius over the poles. The temperature here is nearly constant, and hence, it is called tropopause.

1.2.2. Stratosphere:

Stratosphere is found just above the troposphere.

It extends up to a height of 50 km.

The temperature remains almost the same in the lower part of this layer up to the height of 20 km. After this, the temperature increases slowly with the increase in the

height. The temperature increases due to the presence of ozone gas in the upper part of this layer.

Weather related incidents do not take place in this layer. The air blows horizontally here. Therefore, this layer is considered ideal for flying of aircraft.

The upper limit of the stratosphere is known as stratopause.

One important feature of stratosphere is that it contains a layer of ozone gas.

The relative thickness of the ozone layer is measured in Dobson Units.

It is mainly found in the lower portion of the stratosphere, from approximately 20 to 30 km above the earth's surface.

It contains a high concentration of ozone (O_3) in relation to other parts of the atmosphere.

It is the region of the stratosphere that absorbs most of the sun's ultra-violet radiations.

1.2.3. Mesosphere

It is the third layer of the atmosphere spreading over the stratosphere.

It extends up to a height of 80 km.

In this layer, the temperature starts decreasing with increasing altitude and reaches up to -100° Celsius at the height of 80 km.

Meteors or falling stars occur in this layer.

The upper limit of the mesosphere is known as mesopause.

1.2.4. Thermosphere

This layer is located between 80 and 400 km above the mesopause.

It contains electrically charged particles known as ions, and hence, it is known as the **ionosphere**.

Radio waves transmitted from the earth are reflected back to the earth by this layer and due to this, radio broadcasting has become possible.

The temperature here starts increasing with heights.

1.2.5. Exosphere

The exosphere is the uppermost layer of the atmosphere.

Gases are very sparse in this sphere due to the lack of gravitational force. Therefore, the density of air is very less here.

1.3. Basic transmission theory

The RF (or free space) segment of the satellite communications link is a critical element that impacts the design and performance of communications over the satellite. The basic communications link, shown in Figure 4.1, identifies the basic parameters of the link.

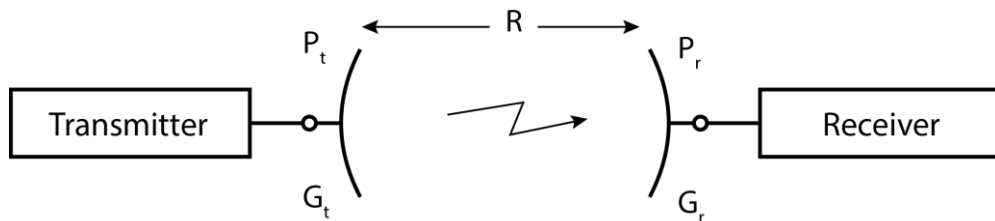


Figure 1.3: Basic Communication Link

The parameters of the link are defined as:

$$P_t = \text{Transmitted power (watt)}$$

$$P_r = \text{Received power (watt)}$$

$$G_t = \text{Transmitting antenna gain}$$

$$G_r = \text{Receive antenna gain}$$

$$R = \text{Path distance}$$

An electromagnetic wave, referred to as a radio wave at radio frequencies, is nominally defined in the range of ~ 100 MHz to 100+ GHz. The radio wave is characterized by variations of its electric and magnetic fields. The

oscillating motion of the field intensities vibrating at a particular point in space at a frequency f excites similar vibrations at neighboring points, and the radio wave is said to travel or propagate. The wavelength (λ) of the radio wave is the spatial separation of two successive oscillations, which is the distance the wave travels during one cycle of oscillation (Figure 4.2).

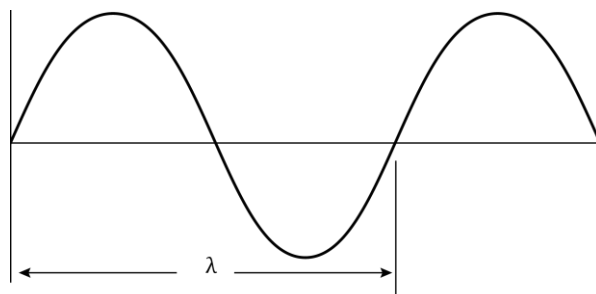


Figure 1.4: Wavelength

Wavelength and frequency in free space are related by

$$\lambda = \frac{c}{f}$$

Where c being the velocity of light, and f is the frequency of the wave.

The wave propagating in free space from a point source of power P_t watt is isotropic, i.e., spherically radiating from the point source as shown in Figure 4

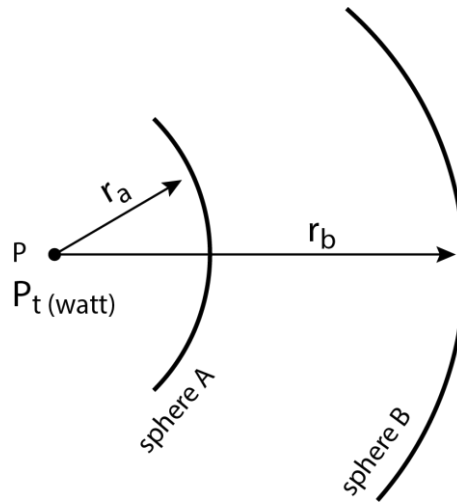


Figure 1.5: Inverse square law of radiation

The power density or the power flux density (P_A) over the surface of a sphere of radius r_a from the point source A is given by

$$P_A = \frac{P_t}{4\pi r_a^2} \quad (8)$$

Similarly, power density at the surface of sphere B is given by

$$P_B = \frac{P_t}{4\pi r_b^2} \quad (9)$$

From above equations it follows

$$\frac{P_A}{P_B} = \frac{r_b^2}{r_a^2} \quad (10)$$

The above relation is the well-known inverse square law in physics.

In microwave communication the antenna employed are highly direction and they

have very high directional gain. The transmitting system in satellite communication comprises of a directional antenna getting driven by the final stage of an amplifier as shown in figure below.

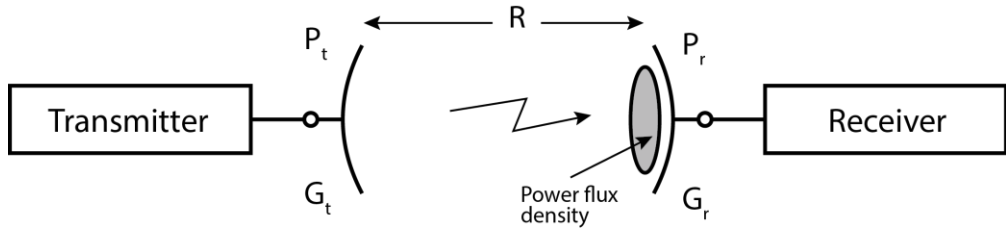


Figure 1.6: Power flux density

If P_t is the power and G_t is the gain of antenna the flux density at a distance R is given by

$$F = \frac{P_t G_t}{4\pi R^2} \quad (11)$$

If the gain of receiver antenna is G_r and effective aperture area is A_r then the power received by the receiver antenna

$$P_r = \left(\frac{P_t G_t}{4\pi R^2} \right) A_r \quad (12)$$

Directive gain of an antenna is related to the wavelength of the signal

$$G_r = \frac{4\pi A_r}{\lambda^2} \quad (13)$$

Substituting for A_r in above equation

$$P_r = P_t G_t G_r \times \left(\frac{\lambda}{4\pi R} \right)^2 \quad (14)$$

The expression above is known as Friss transmission equation (Rappaport, 2001) which is of prime importance for current study for the measurement of received power. The above equation relates the received power with two measurable parameters

$$\text{Effective Isotropic Radiated Power (EIRP)} \equiv P_t G_t$$

$$\text{Path loss } (L_p) = \left(\frac{4\pi R}{\lambda} \right)^2 \quad (15)$$

Collecting various factors together we can write

$$\text{Power Received} = \frac{\text{EIRP} \times (\text{Receiving antenna gain})}{(\text{path loss})} \quad (16)$$

In satellite communication we use decibels widely to simplify the expressions. The above equation expressed in dBw has the following form.

$$P_r = (\text{EIRP} + G_r - L_p) \text{ dBw} \quad (17)$$

Where

$$\text{EIRP} = 10 \log_{10}(P_t G_t) \quad (18)$$

$$G_r = 10 \log_{10} \left(\frac{4\pi A_r}{\lambda^2} \right) \quad (19)$$

$$L_p = 20 \log_{10} \left(\frac{4\pi R}{\lambda} \right) \quad (20)$$

The above equation represents an idealized case in which there are no more additional losses in the link. We as a system designer need to take into account of a

more complex situation in which we have losses in the atmosphere due to attenuation by rain (L_{RAIN}), losses in antenna at each end of the link, and possible loss due to antenna misalignment.

$$P_r = \left(EIRP + G_{rLp} - L_{RAIN} - L_{Antenna\ loss} \right) dBW \quad (21)$$

1.4. World Climate

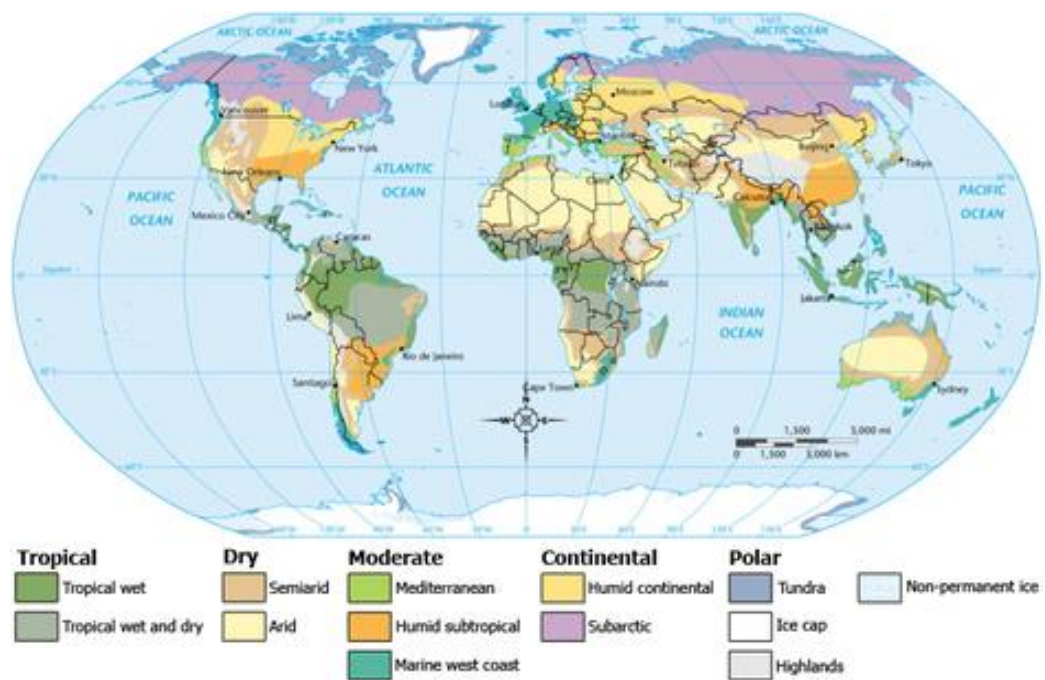


Figure 1.7: World climatic Map (Source: The world Book Encyclopedia)

The early climatologist has classified the earth climate into tropical, temperate and polar climates, considering only the temperature as the differentiating parameter. Wladimir Koppen, a German climatologist introduced a modified version of world climate in 1918 (Kottek et al., 2006).

Koppen based his system on a region's vegetation, average monthly and annual temperature, and average monthly and annual precipitation. His modified version specifies 12 climate groups identified as: (1) tropical wet / equatorial, (2) tropical wetland dry, (3) semiarid, (4) desert, (5) subtropical dry summer, (6) humid subtropical, (7) humid oceanic, (8) humid continental, (9) sub-arctic, (10) tundra, (11) icecap, and (12) highland. Descriptions and contours of each climate group as categorized by Koppen, adapted from literatures (Grefrath, 2000; Sutcliffe, 1966) are reproduced on the following subsection.

1.4.1. Tropical wet climates

Tropical wet climates are hot and muggy the year around. They support dense tropical rain forests. Rainfall is heavy and occurs in frequent showers and thunderstorms throughout the year. Average annual rainfall varies from about 70 to 100 inches (175 to 250 centimeters). Temperatures are high, and they change little during the year. The coolest month has an average temperature no lower than 64 degrees F (18 degrees C). The temperature difference between day and night is greater than the temperature difference between summer and winter. Frost and freezing temperatures do not occur. Plants grow all year.

1.4.2. Tropical wet and dry climates

Tropical wet and dry climates occur in areas next to regions that have tropical wet climates. Temperatures in tropical wet and dry climates are similar to those in tropical wet climates, where they remain high throughout the year. The main difference between the two climates lies in their rainfall. In tropical wet and dry

climates, winters are dry, and summers are wet. Generally, the length of the rainy season and the average rainfall decrease with increasing latitude. Not enough rain falls in tropical wet and dry climates to support rain forests. Instead, they support savannahs--grasslands with scattered trees.

1.4.3. Semiarid and desert (arid) climates

Semiarid and desert climates occur in regions with little precipitation. Desert climates are drier than semiarid climates. Semiarid climates, also called steppe climates, usually border desert climates. In both climate groups, the temperature change between day and night is considerable. One reason for the wide swings in temperature is that the skies are clear and the air is dry. Clouds would reflect much of the sun's intense radiation during the day, slowing the rate of heating of the air near the surface. At night, clouds and water vapor would absorb much of the earth's radiation, most of which consists of infrared rays, slowing the rate of cooling.

Semiarid and desert climates occur over a greater land area than any other climate grouping. They occur in both tropical and middle latitudes. They cover broad east-west bands near 30 degrees north and south latitude.

Middle latitude semiarid and desert climates are in the rain shadows of mountain ranges. Winds that descend the leeward slopes of these ranges are warm and dry. Middle latitude semiarid areas and deserts differ from their tropical counterparts mainly in their seasonal temperature changes. Winters are much colder in middle latitude semiarid areas and deserts.

1.4.4. Subtropical dry summer climates (Mediterranean)

Subtropical dry summer climates feature warm to hot, dry summers and mild, rainy winters. These climates, sometimes called Mediterranean climates, occur on the west side of continents roughly between 30 degrees and 45 degrees latitude. The closer to the coast the area is, the more moderate the temperatures and the less the contrast between summer and winter temperatures.

1.4.5. Humid subtropical climates

Humid subtropical climates are characterized by warm to hot summers and cool winters. Rainfall is distributed fairly evenly throughout the year. Winter rainfall and occasionally snowfall is associated with large storm systems that the westerlies steer from west to east. Most summer rainfall occurs during thunderstorms and an occasional tropical storm or hurricane. Humid subtropical climates lie on the southeast side of continents, roughly between 25 degrees and 40 degrees latitude.

1.4.6. Humid oceanic climates (Marine West Coast)

Humid oceanic climates are found only on the western sides of continents where prevailing winds blow from sea to land. The moderating influence of the ocean reduces the seasonal temperature contrast so that winters are cool to mild and summers are warm. Moderate precipitation occurs throughout the year. Low clouds, fog, and drizzle are common. Thunderstorms, cold waves, heat waves, and droughts are rare.

1.4.7. Humid continental climates

Humid continental climates feature mild to warm summers and cold winters. The temperature difference between the warmest and coldest months of the year increases inland. The difference is as great as 45 to 63 degrees Fahrenheit (25 to 35 Celsius degrees). Precipitation is distributed fairly evenly throughout the year, though many locations well inland have more precipitation in the summer.

Snow is a major element in humid continental climates. Winter temperatures are so low that snowfall can be substantial and snow cover persistent. Snow cover has a chilling effect on climate. Snow strongly reflects solar radiation back into space, lowering daytime temperatures. Snow also efficiently sends out infrared radiation, lowering night-time temperatures.

1.4.8. Subarctic climates

Subarctic climates have short, cool summers and long, bitterly cold winters. Freezes can occur even in midsummer. Most precipitation falls in the summer. Snow comes early in the fall and lasts on the ground into early summer.

1.4.9. Subarctic climates

Tundra climates are dry, with a brief, chilly summer and a bitterly cold winter. Continuous permafrost (permanently frozen ground) lies under much of the treeless tundra regions.

1.4.10. Icecap climates

Icecap climates are the coldest on earth. Summer temperatures rarely rise

above the freezing point. Temperatures are extremely low during the long, dark winter. Precipitation is meager and is almost always in the form of snow

1.4.11. Highland climates

Highland climates occur in mountainous regions. A highland climate zone is composed of several areas whose climates are like those found in flat terrain. Because air temperature decreases with increasing elevation in the mountains, each climate area is restricted to a certain range of altitude.

1.5. Classification of Precipitation (Rain fall)

Initial understanding of precipitation has revealed two broad classes of rainfall event.

1.5.1. Convective Rain

Characterized by a very intense and short-lived rainfall event with variable rain fall height that might go up to 10 Km or more. Usually, convective rain event is confined to small or localized area.

1.5.2. Stratiform Rain

The Stratiform rain on the other hand can be characterized by medium and low-rate events that occur for a longer period of time. This type of rain comprises a long period of Stratiform precipitation with a very well-developed melting layer at a constant height.

Further studies are now being carried out by organization such as Rutherford Appleton Laboratory, United Kingdom with radar data on precipitation events.

Attempts are being made to characterize the vertical distribution of ice and water regions, and to determine the precipitation drop size distribution from measurements of fall velocity. Both parameters are considered important for improved radio wave propagation modeling. According to the ITU Handbook on Radio meteorology (Bureau, 1996; Houze, 1981), precipitation that occurs all over the world may be grouped into four different types. The fifth type of precipitation identified as ‘warm rain’ excerpted from literatures (Huffman & Norman, 1988; Murakami et al., 1994) is also included below.

1.6. Propagation Mechanisms

The general terms used to describe the propagation phenomena or mechanisms that can affect the characteristics of radio waves, adapted from literatures (Allnutt, 2011; Ippolito, 1986) are reproduced below. These mechanisms are usually described in terms of variations in the signal characteristics of the wave, as compared to the natural or free space values, found in the absence of the mechanism. Most of the definitions are based on the Institute of Electrical and Electronics Engineers (IEEE) Standard

Definitions of Terms for Radio Wave Propagation (“IEEE Standard Dictionary of Electrical and Electronics Terms,” 1980)

1.6.1. Absorption: A reduction in the amplitude or field strength of a radio wave due to an irreversible conversion of energy from the radio wave to matter in the propagation path.

1.6.2. Scattering: A process in which the energy of a radio wave is dispersed in direction caused by interaction with inhomogeneity in the propagation medium

1.6.3. Refraction: A change in the direction of propagation of a radio wave resulting from the spatial variation of refractive index of the medium.

1.6.4. Diffraction: A change in the direction of propagation of a radio wave resulting from the presence of an obstacle, a restricted aperture, or other object in the medium.

1.6.5. Multipath: The propagation condition that results in a transmitted radio wave reaching the receiving antenna by two or more propagation paths. Multipath can result from refractive index irregularities in the troposphere or ionosphere, or from structural and

1.6.6. Terrain scattering on the Earth's surface:

a. Scintillation: Rapid fluctuations of the amplitude and the phase of a radio wave caused by small-scale irregularities in the transmission path or paths with time.

b. Fading: The variation of the amplitude of a radio wave caused by changes in the transmission path or paths with time. The terms fading and scintillation are often used interchangeably; however, fading is usually used to describe slower time variations, on the order of seconds or minutes, while scintillation refers to more rapid variations, on the order of fractions of a second in duration.

c. Frequency Dispersion: A change in the frequency and phase components across the bandwidth of a radio wave, caused by a dispersive medium. A dispersive medium is one whose constitutive components (permittivity, permeability, and conductivity) depend on frequency (temporal dispersion) or wave direction (spatial dispersion)

Many of the mechanisms described above can be present on the transmission path at the same time and it is very difficult to distinguish the mechanism or the mechanisms that produce a change in the characteristics of the transmitted signal. Propagation effects on communications links are usually defined in terms of variations in the signal parameters. The parameters that can be observed or measured on a typical link are amplitude, phase, polarization, frequency, bandwidth, and angle of arrival. Each of the mechanisms above if present in the path, could affect one or more of the signal parameters. Figure 2.1 illustrates how the various mechanisms affect the measurable parameters of a signal on communications links.

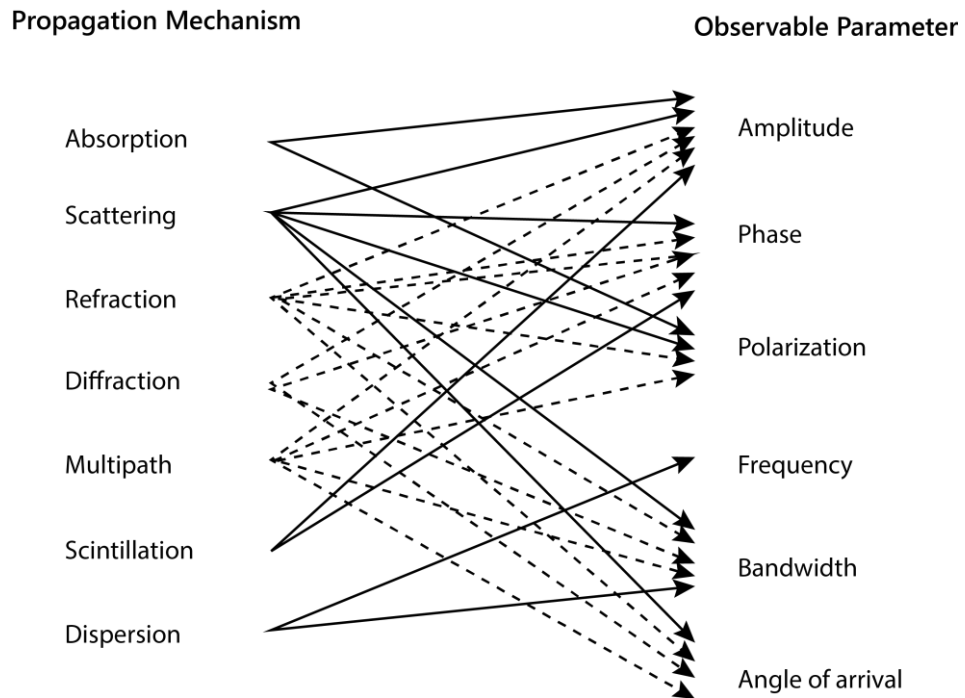


Figure 1.8: Radio wave propagation mechanisms and their Impact on the parameters of communication signal (Ippolito, 1986)

TABLE 1.2: Impairments affecting earth space communication system

Impairment	Physical causes	Affected systems	Frequency
	Atmospheric gases, clouds, precipitation, sand and dust		$f > 10$ GHz
	Low ionospheric layers		$f < 70$ MHz
	Raindrops, ice, crystals		6/4, 14/11 and 30/20 GHz
	Faraday rotation		Below 1 GHz
			$f > 10$ GHz
			10 MHz – 12 GHz

Refraction, atmospheric Multipath	Atmospheric gases Ionospheric electron Distribution	Systems operating at low elevation angles; antenna tracking	1 – 45 GHz
Refraction multipath, shadowing, blockage	Objects, vegetation on Earth's surface	Mobile-satellite Services	
Propagation delays and delays variations	Free-space, variations in troposphere, total electron content	IDMA and position location system, closed loop adaptive control system	
	Ducting, precipitation scatter, diffraction		6/4 GHz system
	Ionospheric scattering and reflection		$f < 300$ MHz
Dispersion	Total electron content multipath	Wide bandwidth systems	

Design, implementation and operation of satellite communication system requires accurate propagation information. The propagation behavior of electromagnetic waves in ionosphere and troposphere are of prime concern for a satellite communication system designer. The table above taken from ITU literature identifies the relevant propagation effects along with those system for which they are of significant importance.

Among the various propagation factors summarized in above table, absorption and scattering of radio waves by the medium are of prime importance for satellite signals of frequency greater than 10 GHz. Physics of these two factors is explained in below few paragraphs

1.7: Propagation Impairment Factors:

The change in intensity of electromagnetic wave as it passes through a medium is known as impairment. The phenomenon of absorption, scattering and atmospheric diffraction are responsible for the change in intensity of incoming electromagnetic wave as it traverses through a medium.

1.7.1 Absorption:

When electromagnetic wave passes through a material medium the free electrons of the medium respond to the incident wave and start oscillating. In due process they absorb energy from the wave. In case of dielectric medium where the resistance to oscillation of bound charges is non-trivial, the permittivity of the medium become complex. The imaginary component of permittivity leads to loss in power due to absorption. Both the dielectric constant and permittivity of medium are complex having real and imaginary part. When electromagnetic wave of electric field intensity E angular frequency ω passes through a medium having conductivity σ and complex permittivity part ϵ then energy absorbed from the medium is given by

$$W = E(\sigma - w\epsilon) \quad (22)$$

Therefore, even for non-conducting medium with $\sigma = 0$ there is definite absorption of energy from the wave due to complex permittivity part. The absorbed power is dissipated as heat in the medium and result as impairment of signal.

1.7.2 Scattering

The phenomenon of scattering may be thought as redirection of incoming electromagnetic wave as it encounters an obstacle in its path (Olivares & Carrazana, 2020). In fact, the phenomenon of scattering is the complex interaction between the complex atomic structures of scattering particle with the electromagnetic wave.

Whenever electromagnetic waves are incident on a neutral dielectric medium such as a rain drop the bound charges within the medium respond to incoming field and get displaced from their position of equilibrium causing the polarization of the medium and creation of dipoles within the medium. Incident electromagnetic wave thus induces electric dipole moment in the direction of field. With the changing direction of incident electromagnetic field, the direction of dipole moment also changes and dipoles start oscillating with the field. These oscillating dipoles generate secondary electromagnetic waves and hence radiate energy in a direction different from that of incoming wave.

Scattering cross section $\sigma_s(\phi)$ of a scattering particle in a direction making angle Φ with the direction of incident wave is the fraction of total power that is reradiated in that particular direction per unit solid angle. If permittivity and refractive index of the scattering particle is non-complex then only scattering takes place. If the permittivity and refractive index of scattering particle is complex then along with scattering absorption also takes place.

Based on relative size of scattering particle and the wavelength of incoming wave there are two classes of electromagnetic wave scattering, The Rayleigh Scattering and Mie scattering.

1.7.3 Rayleigh Scattering:

Named after Lord Rayleigh this type of scattering is formulated when the wavelength of electromagnetic wave is larger than the diameter of the scattering particle. If d is the diameter of particle and λ is the wavelength of electromagnetic wave then for Rayleigh scattering

The smaller dimension of scattering particle compared to the Wavelength implies that the time for the electromagnetic wave to pass the object is less compared to the time period of the wave which in turn means that there is no appreciable change in the phase of electromagnetic wave.

The total scattering cross section in case of Rayleigh scattering of electromagnetic wave of wavelength λ by a particle of diameter d and refractive index n (with respect to medium surrounding it) is given by (Rajat Acharya, 2017)

$$\sigma_{scat} = \left(\frac{2}{3}\right) \pi^5 \left(\frac{d^6}{\lambda^4}\right) \left[\frac{n_2 - 1}{n_2 + 2}\right]^2 \quad (23)$$

- Power radiated by the scattering particle depend upon the refractive index of scattering particle with respect to medium surrounding.
- Power radiated is proportional to the 6th power of size of scattering particle
- Power is inversely proportional to the fourth power of wavelength λ

For satellite signal which operate in GHz range, the atmospheric gaseous particle manifest absorption but they have very low scattering cross section to show scattering effect. The tiny water droplet in cloud shows Rayleigh scattering.

1.7.4 Mie Scattering:

- Named after Gustav Mie is the most dominant process through which microwave signals suffer rain attenuation.
- Mie scattering applies when the size of the scattering particle is comparable or larger than the wavelength of the incident radio wave.
- Mie scattering is not an independent phenomenon; it is only a solution to the Maxwell equation for scattering where the phase of the incident wave can change appreciably over the dimension of the scattering particle.
- The Mie scattering process is accompanied by an absorption process, and another total extinction cross section is defined in this scattering process.
- Total Extinction cross section is the ratio of total combined power lost by the wave due to absorption and scattering to the power incident on the particle.
- Absorption cross section is the difference of total extinction cross section and the scattering cross section.

1.8 Characteristics of Precipitation

The specific attenuation of precipitation relies on its microstructures such as drop size distribution, terminal velocity, orientation and shape, and temperature. All these structures have to be established in each point of the radio wave path. However, precipitation deviates notably in space and time and thus complicates the calculation of precipitation attenuation. Brief description of each microstructure is presented in the following subsections.

1.8.1 Drop Size Distribution:

The rain drop size also plays an important role in determining the propagation impairments. Absorptions and scattering take place in individual rain drop, resulting in signal attenuation. The amount of attenuation is determined by the size of drop and frequency of wave. The rain drop size varies between 0.5 mm to 5.0 mm. The size distribution density $n(D)$ of the rain droplets is the number of raindrops per unit volume of space within the diameter range D to $(D + dD)$. The distribution depends upon the rain rate R and can be well represented by the standard statistical models as well as by definite empirical expressions. Broadly, three type of statistical distributions are used to represent drop size distribution.

1. Exponential Distribution
2. Gamma distribution
3. Log normal distribution.

The distribution also showed a significant variation between different climatic regions.

1.8.2 Laws and Parson distribution

Laws and Parson (Laws & Parsons, 1943) conducted the first systematic measurements of drop size distribution and observed that the number of rain drops ' n ' decreases with decreasing drop diameter D . The median drop size shifts with increasing rain rates. Quantitatively, $n(D)$ can be represented from their measurement as an exponentially decaying function.

1.8.3 Marshall and Palmer Model

The Laws and Parson (Laws & Parsons, 1943) drop size distribution has been found effective for most estimation of the attenuation and scattering properties of rain at frequencies up to about 40 GHz. The rain drops size distribution changes mainly with the rainfall rates and therefore the distribution may deviate within a storm. The use of a single distribution model may not be adequate for all locations in the world. This is because relative concentration of small drops can be highly variable. Different rain drops size distributions have been reported for tropical and temperate climates. It is also reported that relative densities of small drops having diameters less than 0.5 mm could not be well modelled by Laws and Parsons. Therefore, the use of the Marshal Palmer (Marshall & Palmer, 1948) drop size distribution is sometimes employed to aid the drawback. The Marshall-Palmer distribution is given by

$$n(D) = n_0 \exp(-\gamma D)$$

where

$$n_0 = 8 \times 10^3 \text{ m}^{-3} \text{ mm}^{-1}$$

$$\gamma = 4.1R^{0.21}$$

R being the rain rate in mm/hr

The Laws and Parson and Marshall-Palmer distributions represent on-average distribution reflecting in the stratiform or widespread rain. In climates where showery convection is evident, other distributions are sometimes used. The other most often referenced distribution is the Joss and Waldvogel (Joss and Waldvogel, 1968). The Joss distributions are classified into three rain types (drizzle, widespread rain and thunderstorm), while the Laws and Parson and Marshall-Palmer

distributions include all the measurements in a single distribution. In Japan, a group of researchers (Jiang et al., 1997) has proposed the use of Weibull distribution to represent the drop size distribution for rain measured in Tokyo. The measurements is obtained in the year 1993 and they also reported that the rain induced attenuation coefficients from the Weibull drop size distribution have given a very good agreement with experimental data obtained at Nagoya back in 1990. Another investigator (Gloaguen & Lavergnat, 1995) also suggested that the rain drop size distribution near Paris, France could be modelled by the Weibull distribution. Ajayi and Olsen (Ajayi & Olsen, 1985) on the other hand, by employing the 'method of moment regression', have described a single lognormal function to be accurately fitted over the entire range of rain rates measured in Nigeria.

1.8.4 Terminal Velocity:

Measurements to determine the terminal velocity were made in quiet conditions in a laboratory but had been assumed to apply in the atmosphere was conducted by previous researchers (Gunn & Kinzer, 1949). They reported that the terminal velocity of a raindrop is a function of drops' sizes. Radar observations (which most of them are usually stratiform events) generally show only small differences in reflectivity values are detected for the region below the rain height. Therefore, it is generally assumed that the number of raindrops, the size of raindrops and the liquid water content of a volume of raindrops deviates only slightly with height. Based on such assumption, the specific attenuation can also be postulated to have very small deviation with height below the rain height because it depends primarily on liquid water content.

1.8.5 Orientation and Shape:

The raindrop shape depends upon a number of various factors. The shape is a function of their falling terminal velocity, sizes, and internal-and-external pressure at their surfaces. The force of gravity is a major orientation force on the raindrops. Falling drops assume nearly spheroidal shape when affected by gravity and surface tension of the water. While falling, drops may vibrate and oscillate but the net shape is oblate spheroidal with the symmetry axis close to vertical. Investigators (Pruppacher & Pitter, 1971) have modelled the drop shape of rain as a function of drop size. Observations made in a laboratory reported earlier (Pruppacher & Beard, 1971) agreed with the shape predictions by (Pruppacher & Pitter, 1971). Raindrops could exist in size varying from very small to fairly large ones. The smallest drop may be equivalent to those found in the cloud, whereas the largest drop does not usually exceed 4-mm radius. This is because drop with the radii bigger than 4 mm is hydrodynamically unstable and will break up. Measurements show that water drops larger than 1 mm in-radius are oblate in spheroidal shape with a flattened shape.

1.8.6 Temperature:

Falling raindrops have a temperature that approximates the wet bulb temperature for the temperature, pressure and humidity of the surrounding air (Bureau, 1996). In the tropical regions, rainfall is predominantly convective, and researchers (Pan & Bryant, 1994) reported that it has been confirmed by radar observations that supercooled water drops can rise on the strong updraft to area well above the 0°C isotherm. This proves that small liquid droplets can exist at

temperature below 0°C (especially in the updraft region of a convective storm). Nevertheless, attenuation by rain is generally contributed by significant numbers of large liquid water drops that exist between the height of the 0°C isotherm and the surface.

1.9. Measuring precipitation rate:

Precipitation rate or rainfall rate is defined as 'a measure of the intensity of precipitation expressed by the increase in the height of water reaching the ground per unit time' (ITU-R, 1992). Precipitation rate is generally expressed in millimetres per hour and commonly presented in units of mm/hr. There are several equipment that can be employed to obtain precipitation intensity measurements.

Descriptions of several precipitation measuring equipment also commonly known as rain gauges that are commercially available are described briefly below.

1.9.1 Optical Rain Gauge:

The device is an optical sensor that measures precipitation rate and provides an analogue voltage equivalent to the measured precipitation intensity. The equipment employs the focusing and defocusing of an optical beam principle to estimate precipitation rate. It measures the precipitation rate by detecting the optical irregularities induced within the sample volume by precipitation particles falling through the beam of partially coherent infrared light. These irregularities are known as scintillation, and by detecting the intensity of scintillation, which are characteristics to precipitation the actual rainfall rate can be determined.

Impact disdrometer:

A disdrometer is a device that able to convert the raindrop impact momentum into rain drop size and rainfall rate (Bringi et al., 2003). The instrument operates base on the principle of transforming the vertical momentum of impacting drops into electric pulses, the amplitude of which is a function of the drop diameter. The equipment obtains additional information about the number of drops, and from such knowledge the drop size distribution and rainfall intensity can be derived.

Rain sensor:

The device uses the principle of a precision volume drop passing through an optical beam. The sensor is plastic-moulded and aerodynamically shaped to lessen the effect of wind on the reading. The rain gauge operates on the principal of counting known volume drops as they pass an optical sensor. The sensor measures the amount of rain passing through it by an infrared optical system with no moving parts.

1.9.2 Tipping Bucket Rain Gauge:

The rain gauge comprises a divided bucket assembly that is pivoted at the centre. Rain collects in one side of the bucket that then tips when a predetermined volume of water has been collected. Toe tipping action discharges the collected water and repositions the opposite side of the bucket under the discharge nozzle. a switch is activated when the bucket tips on its pivot. The number of times the switch is closed in a given period provides a measure of rainfall rate.

1.9.3 Capacitance Gauge:

The device collects water into a measuring chamber, which surrounds a capacitance probe. The capacitance of the system changes as the water level, in the chamber, rises. Therefore, the rainfall accumulation can be determined. The system is automatically emptied and reset at every predetermined accumulation.

1.10. Frequency Analysis of Rainfall:

1.10.1 Rainfall variability in time

The total rainfall received in a given period at a location is highly variable from one year to another. The variability depends on the type of climate and the length of the considered period. In general, it can be stated that the drier the climate, the higher the variability of rainfall in time. The same hold for the length of the period: the shorter the period the higher the annual variability of rainfall in that period.

Because of the strong variability of rainfall in time, the design and management of irrigation water supply and flood control systems are not based on the long-term average of rainfall records but on particular rainfall depths that can be expected for a specific probability or return period. These rainfall depths can only be obtained by a thoroughly analysis of long time series of historic rainfall data.

Although time series of historic rainfall data are characterized by their average and standard variation, these values cannot be blindly used to estimate design rainfall depths that can be expected with a specific probability or return period. Applying this technique to a data set can produce misleading results since the actual characteristics of the distribution are ignored and it is assumed that they follow

a particular distribution. To avoid this type of error, it is essential that the goodness of the assumed distribution be checked before design rainfall depths are estimated.

1.10.2 Probability of Exceedance and Return period:

1.10.2.1 Rainfall depth expected for specific probability

Estimates of rainfall depths (XP) or intensities that can be expected for a specific probability during a specific reference period (hour, day, week, 10-day, month, year) are required for the management and design of irrigation, drainage and satellite communication project. Here the probability refers to the probability of exceedance and it specifies the likelihood that the actual rainfall during that period will be equal to or higher than the estimated rainfall depth XP.

1.10.2.2 Probability of Exceedance (PX):

The probability of exceedance refers to the probability of the occurrence of a rainfall depth greater than some given value XP. The probability of exceedance (PX) is expressed as a fraction (on a scale ranging from zero to one) or as a percentage chance with a scale ranging from 0 to 100 percent. If the estimates refer to the rainfall depth that can be expected or might be exceeded in a year during the reference period than it can be expressed as a set number of years out of a total number of years.

1.10.2.3 Return Period (TX):

The return period (also called the recurrence interval) TX is the period expressed in number of years in which the annual observation is expected to return. It is the reciprocal value of the probability when expressed as a fraction

$$TX = \frac{1}{PX} \quad (24)$$

1.10.2.4 Time series of rain fall data

In a frequency analysis, estimates of the probability of occurrence of future events are based on the analysis of historical rainfall records. By assuming that the past and future data sets are stationary and have no apparent trend one may expect that future time series will reveal frequency distributions similar to the observed one. It is obvious that the longer the data series the more similar the frequency distribution will be to the probability distribution. In short series accurate determination for rainfall depths that can be expected for selected return periods is not possible. Estimates of dependable rainfall are less reliable if the corresponding return period exceeds the observation period. As the number of observations increases, the error in determining expected rainfall gradually diminishes. Although the required length of the time series depends on the magnitude of variability of the precipitation climate, a period of 30 years and over normally is thought to be very satisfactory. However, if interest lies in extreme rainfall events, larger number of years will be required

The basis of all statistical analysis is that the data series must be composed of random variables selected from a single population usually infinite in extent.

Therefore, rainfall records from a climatic station should be carefully checked for homogeneity, or in other words, it should be checked if the collected observations are from the same population. If there is an apparent trend in time, the observation period should be restricted to the period where the data is homogeneous and representative for the planned use.

1.10.2.5 Frequency analysis and Probability plotting:

From a frequency analysis, the estimates of rainfall depths for selected probabilities or return periods required for the design can be obtained. The analysis consists in collecting historical data over a sufficient number of years and subsequently:

- a. ranking the data and assigning plotting positions by estimating the probability of exceedance with one or another method
- b. selecting a distributional assumption and plotting the data in a probability plot
- c. verifying the goodness of the selected distribution. If unsatisfactory another distribution should be selected or the data should be transformed so that the transformed data follow the selected distribution
- d. Determining rainfall depths (XP) that can be expected for selected probabilities or return period from the probability plot.

1.11. Estimation of probability of Exceedance:

The first step in the frequency analysis is the ranking of the rainfall data. After the rainfall data are ranked, a serial rank number (r) ranging from 1 to n (number of observations) is assigned. Subsequently, the probability had to be determined which should be assigned to each of the rainfall depths. If the data are

ranked in descending order, the highest value first and the lowest value last, the probability is an estimate of the probability that the corresponding rainfall depth will be exceeded. When data are ranked from the lowest to the highest value, the probability refers to the probability of non-exceedance. Hence the probabilities are estimates of cumulative probabilities. They are formed by summing the probabilities of occurrence of all events greater than (probability of exceedance) or less than (probability of non-exceedance) some given rainfall depth. Since these probabilities are unknown the probabilities of exceedance have to be estimated by one or another method. Several methods are listed in Table below. The Weibull (Bergman, 1984), Sevruk and Geiger (Sevruk & Geiger, 1981), and the Gringorten (Gringorten, 1963) methods are theoretically better sound. The probabilities will be the plotting positions of the ranked rainfall data in the probability plot.

TABLE 1.3: PROBABILITY OF RAIN-RATE EXCEEDANCE CALCULATION METHOD

Method	Probability of exceedance or non-exceedance (%)
California	$\frac{r}{n} \times 100$
Hazen	$\frac{(r - 0.5)}{n} \times 100$
Weibull	$\frac{r}{(n + 1)} \times 100$
Gringorten	$\frac{(r - 0.44)}{(n + 0.12)} \times 100$
Sevruk and Geiger	$\frac{\left(r - \frac{3}{8}\right)}{\left(n + \frac{1}{4}\right)} \times 100$

Table: Methods for estimating probabilities of exceedance of ranked data, where r is the rank number and n the number of observations

1.11.1 Intensity Duration Frequency (IDE) Curve

Estimates of precipitation intensity for selected return periods are often required for the design of sewer or surface drainage systems. Reliable estimates can only be obtained from a frequency analysis of long time series. IDE curve are relation between intensity(mm/hour), duration (integration time) and return period.

The empirical relation describing the IDE relationship is of the form.

$$R_t^T = a \frac{T^b}{t^c} \quad (25)$$

Where a , b , and c are empirical constants

t = duration of rain

T = *return period*

R = rain rate or intensity

1.11.2 Attenuation due to precipitation

In most radio system design, the operating limit is usually predetermined by the variation about the clear sky level. The negative variation below the mean clear sky level is called excess attenuation (Allnutt, 2011). Attenuation is usually measured in decibels denoted by unit of dB. The excess attenuation of a radio wave due to precipitation is formed from two components. The components are described as absorption and scattering.

Signal attenuation on a path is sometimes referred as extinction. Extinction is the algebraic sum of component due to scattering and absorption (Oguchi, 1983).

Two relative importance of scattering and absorption is a function of the complex refraction of the absorbing/ scattering particle. Two complex index of refraction itself is a function of signal wavelength, temperature, and the size of the particle, relative to the wavelength of the radio wave. It is important to examine the variation of the scattering and/or absorption contributions to extinction, for water spheres of various radii. As illustrated in Figure 2.6 below, it is clear that for longer wavelengths and smaller particles, absorption dominates the extinction process, whereas for shorter wavelengths and larger particles, the scattering dominates (Brussaard & Watson, 1994).

In conditions where a particle is very small compared to a wavelength of the radio wave, Rayleigh scattering theory can be applied. In these situations, the signal extinction will be mainly due to absorption. These conditions generally hold for signals well below the frequency of 10 GHz, propagating through an ensemble of hydrometeors. As the frequency goes up, the size of the raindrops becomes a substantial fraction of the wavelength. The raindrops now not only absorb the signal but also scatter it. There is increasing significance of the scattering as the wavelengths decreases. The imaginary part of the complex permittivity of water becomes significant. In this situation, Mie scattering theory is used. To calculate the attenuation of a radio wave as it passes through precipitation, it is necessary to aggregate the individual extinction contributions of each raindrop encountered along the path. Since the drops are all of different sizes, it is necessary to invoke a drop size distribution $N(D)$ and integrate the extinction contributions. The attenuation A can be expressed as follows (Allnutt, 2011)

$$A = 4.343 \times L \int_0^{\infty} [\sigma(D)N(D)] dD \quad (26)$$

Where $\sigma(D)$ is the extinction cross section of a drops of diameter D and L is the length of path through precipitation in km and $N(D)$ represent the particle size distribution in $\text{mm}^{-1} \text{m}^{-3}$.

If the length of path through precipitation is equal to 1 km , the above equation gives the specific attenuation γ

$$\Gamma = 4.343 \int_0^{\infty} [\sigma(D)N(D)] dD \quad \text{dBkm}^{-1} \quad (27)$$

In relating such attenuation to the amount of precipitation volume falling in per unit area on the ground, the dependence of terminal velocities of precipitation in still air of radius D must be established. Hence, the rainfall rate R where $V(D)$ as the fall velocity of a particle of radius D in ms^{-1} can be described as follows (Mitra et al., 1987)

$$R = 4.8 \pi \times 10^{-3} \int_0^{\infty} [D^3 V(D)N(D)] dD \quad \text{mm hr}^{-1} \quad (28)$$

The calculation of the specific attenuation is quite complicated since characteristics of precipitation vary so much in both space and time. Simplification can be made to obtain results well within the accuracy achievable in most measurement. The well-

known specific attenuation equation given by power-law relationship to the rainfall rate is defined as (Bureau, 1996)

$$\gamma_R = k(R_0)^\alpha \quad \text{dBkm}^{-1} \quad (29)$$

Where k and α are frequency and polarization dependent coefficient.

Selected values of these two frequency-dependent coefficients as a function of frequency can be found in the Recommendation ITU-R P.838 (ITU-R, 1992).

Olsen et al. (Olsen et al., 1978) have examined the theoretical background of the $A = a R^b$ equation which is the same as equation (1) described earlier. They expanded the Mie coefficients for a sphere in a power series of $ka/2$ where k is the free space propagation constant. Substituting the resulting power series expression of $\sigma(D)$ into the attenuation integral shown in equation (1) together with the negative exponential rain drop size distribution and the modified gamma distribution function. they found that the $A = aR^b$ relationship is exact in the limit of low frequencies and low rainfall rates. The relationship is not exact in the higher optical limit because for a very large drop in comparison with the wavelength, the total energy lost from the incident beam is made up of two components. One, energy is removed from the beam by scattering or absorption that exactly corresponds to the geometrical cross-section. The other, energy is lost by diffraction in the forward direction that again corresponds to the geometrical cross-section.

In frequency range between two extremes such as microwave and millimetre wave regions, the relationship could not be exact. There is possible error in assuming

Rayleigh scattering instead of Mie scattering or vice versa for various cases as the frequency increases. However, examinations showed that the $\gamma_R = k(R_0)^\alpha$ relationship is a good approximation to the exact relationship. The values of k and a were obtained from logarithmic regression, fit to the exact specific attenuation values in the frequency range of 1 – 1000 GHz for the drop size distribution functions and for the temperature of 20,0 and –10 degree celsius. A comparison of the exact Mie calculations and calculations based on $\gamma = k (R_0)^\alpha$ relationship showed that the accuracy of the approximate expression is reasonably good for the frequencies, temperature and rainfall rates used in the regressions.

Oguchi (Oguchi, 1977) reviewed some of the features of the calculated single-scattering properties of non-spherical raindrops in the Mie scattering region. For a distorted raindrop, the cross-section at depends on polarisation. Thus, the attenuation is polarisation dependent. Several measurement results did suggest that the general procedure of calculating cross-section from Mie theory with a known refractive index could also be valid.

1.12 Conclusion:

All the theoretical framework on which this thesis is based has been presented in this chapter. Radio wave propagation mechanisms have been discussed briefly and propagation Impairments affecting space communications have been highlighted. Definition of rainfall rate and description of different equipment that can be utilised to measure rain intensity have been presented. The relevance between rain and signal attenuation has been described on conceptual basic.

A factor that complicates the determination or prediction of rain-induced attenuation along the slant path is its variability in space and time. The rain specific attenuation depends on the microstructures of rain fall i.e., size distribution, temperature, terminal velocity and shape of the rain drops (Bureau, 1996)\ and these structures need to be identified at each point of radio path to calculate the attenuation accurately. Microstructure such as rain drop size distribution varies according to type of precipitation. Some of the rain microstructures are climate dependent. One climate differs from another, and brief narrations of world climate types have also been presented in this chapter.

1.13 Reference:

- Ajayi, G. O., & Olsen, R. L. (1985). Modeling of a tropical raindrop size distribution for microwave and millimeter wave applications. *Radio Science*. <https://doi.org/10.1029/RS020i002p00193>
- Allnutt, J. E. (2011). Satellite-to-ground radiowave propagation, 2nd edition. In *Satellite-to-Ground Radiowave Propagation, 2nd Edition*. <https://doi.org/10.1049/PBEW054E>
- Bergman, B. (1984). On the estimation of the Weibull modulus. *Journal of Materials Science Letters*. <https://doi.org/10.1007/BF00719924>
- Bringi, V. N., Chandrasekar, V., Hubbert, J., Gorgucci, E., Randeu, W. L., & Schoenhuber, M. (2003). Raindrop size distribution in different climatic regimes from disdrometer and dual-polarized radar analysis. *Journal of the Atmospheric Sciences*. [https://doi.org/10.1175/1520-0469\(2003\)060<0354:RSDIDC>2.0.CO;2](https://doi.org/10.1175/1520-0469(2003)060<0354:RSDIDC>2.0.CO;2)
- Brussaard, G., & Watson, P. A. (1994). *Atmospheric modelling and millimetre wave propagation*. Springer Science & Business Media.
- Bureau, R. C. (1996). *Radiocommunication Bureau* (pp. 1–8). Geneva.
- Gloaguen, C., & Lavergnat, J. (1995). Raindrop size distribution near Paris.

- Electronics Letters*. <https://doi.org/10.1049/el:19950272>
- Grefrath, R. W. (2000). The world book encyclopedia. *Reference & User Services Quarterly*, 40(2), 192.
- Gringorten, I. I. (1963). A plotting rule for extreme probability paper. *Journal of Geophysical Research*. <https://doi.org/10.1029/jz068i003p00813>
- Gunn, R., & Kinzer, G. D. (1949). THE TERMINAL VELOCITY OF FALL FOR WATER DROPLETS IN STAGNANT AIR. *Journal of Meteorology*. [https://doi.org/10.1175/1520-0469\(1949\)006<0243:ttvoff>2.0.co;2](https://doi.org/10.1175/1520-0469(1949)006<0243:ttvoff>2.0.co;2)
- Houze, R. A. (1981). Structures of atmospheric precipitation systems: A global survey. *Radio Science*. <https://doi.org/10.1029/RS016i005p00671>
- Huffman, G. J., & Norman, G. A. (1988). The supercooled warm rain process and the specification of freezing precipitation. *Monthly Weather Review*. [https://doi.org/10.1175/1520-0493\(1988\)116<2172:TSWRPA>2.0.CO;2](https://doi.org/10.1175/1520-0493(1988)116<2172:TSWRPA>2.0.CO;2)
- IEEE Standard Dictionary of Electrical and Electronics Terms. (1980). *IEEE Transactions on Microwave Theory and Techniques*. <https://doi.org/10.1109/TMTT.1980.1130033>
- Ippolito, L. J. (1986). Attenuation by Atmospheric Gases. In *Radiowave Propagation in Satellite Communications*. https://doi.org/10.1007/978-94-011-7027-7_3
- Ismail, Ahmad, Fadzil, (2001). Rain Induced attenuation Studies for Satellite communication in Tropical region. *Ph.D Thesis, University of Bath*.
- ITU-R. (1992). *Rec. ITU-R P.838-3 RECOMMENDATION ITU-R P.838-3*. https://www.itu.int/dms_pubrec/itu-r/rec/p/R-REC-P.838-3-200503-I!!PDF-E.pdf
- Jiang, H., Sano, M., & Sekine, M. (1997). Weibull raindrop-size distribution and its application to rain attenuation. *IEE Proceedings: Microwaves, Antennas and Propagation*. <https://doi.org/10.1049/ip-map:19971193>
- Kottek, M., Grieser, J., Beck, C., Rudolf, B., & Rubel, F. (2006). World map of the Köppen-Geiger climate classification updated. *Meteorologische Zeitschrift*. <https://doi.org/10.1127/0941-2948/2006/0130>
- Laws, J. O., & Parsons, D. A. (1943). The relation of raindrop- size to intensity. *Eos, Transactions American Geophysical Union*. <https://doi.org/10.1029/TR024i002p00452>

- Marshall, J. S., & Palmer, W. M. K. (1948). THE DISTRIBUTION OF RAINDROPS WITH SIZE. *Journal of Meteorology*. [https://doi.org/10.1175/1520-0469\(1948\)005<0165:tdorws>2.0.co;2](https://doi.org/10.1175/1520-0469(1948)005<0165:tdorws>2.0.co;2)
- Murakami, M., Matsuo, T., Mizuno, H., & Yamada, Y. (1994). Mesoscale and microscale structures of snow clouds over the sea of Japan part I: Evolution of microphysical structures in short-lived convective snow clouds. *Journal of the Meteorological Society of Japan*. https://doi.org/10.2151/jmsj1965.72.5_671
- Oguchi, T. (1977). Scattering properties of Pruppacher- and- Pitter form raindrops and cross polarization due to rain: Calculations at 11, 13, 19.3, and 34.8 GHz. *Radio Science*. <https://doi.org/10.1029/RS012i001p00041>
- Oguchi, T. (1983). Electromagnetic Wave Propagation and Scattering in Rain and Other Hydrometeors. *Proceedings of the IEEE*. <https://doi.org/10.1109/PROC.1983.12724>
- Olivares, I. E., & Carrazana, P. (2020). Mie scattering revisited: Study of bichromatic Mie scattering of electromagnetic waves by a distribution of spherical particles. *Review of Scientific Instruments*. <https://doi.org/10.1063/5.0015050>
- Olsen, R., Rogers, D. V, & Hodge, D. (1978). The aR b relation in the calculation of rain attenuation. *IEEE Transactions on Antennas and Propagation*, 26(2), 318–329.
- Pan, Q. W., & Bryant, G. H. (1994). Effective rain-cell diameters and rain-column heights in the tropics. *Electronics Letters*. <https://doi.org/10.1049/el:19941201>
- Panagopoulos, A. D., Arapoglou, P.-D. M., & Cottis, P. G. (2009). Satellite communications at KU, KA, and V bands: Propagation impairments and mitigation techniques. *IEEE Communications Surveys & Tutorials*. <https://doi.org/10.1109/comst.2004.5342290>
- Pruppacher, H. R., & Beard, K. V. (1971). A wind tunnel investigation of the internal circulation and shape of water drops falling at terminal velocity in air. In *Quarterly Journal of the Royal Meteorological Society*. <https://doi.org/10.1002/qj.49709741117>
- Pruppacher, H. R., & Pitter, R. L. (1971). Semi- empirical determination of the shape of cloud and rain drops. *Journal of the Atmospheric Sciences*.

- Rajat Acharya., *Satellite Signal Propagation, Impairments and Mitigation*, 2017.
Academic press, Elsevier Ltd.,
- Rappaport, T. S. (2001). *Wireless Communications: Principles and Practice* (Prentice Hall Communications Engineering & Emerging Technologies Series). In *Optimization*.
- Sevruk, B., & Geiger, H. (1981). Selection of distribution types for extremes of precipitation. In *Selection of distribution types for extremes of precipitation*.
- Steeves, K. A., Bernhardt, P. E., Burns, J. P., & Lombard, M. K. (2009). Transforming American Educational Identity after Sputnik. *American Educational History Journal*.
- Sutcliffe, J. V. (1966). The assessment of random errors in areal rainfall estimation. *International Association of Scientific Hydrology. Bulletin*.
<https://doi.org/10.1080/02626666609493477>
- Whalen, D. J. (2003). The origins of satellite communications 1945 - 1965. *41st Aerospace Sciences Meeting and Exhibit*. <https://doi.org/10.2514/6.2003-661>

Chapter 2

Review of Literature

CHAPTER 2: REVIEW OF LITERATURE

Review of Literature:

Our study aims to find the prediction method for satellite earth communication attenuation which also entails the rain rate statistics. In the Introduction of the first chapter, we have highlighted the different aspects of precipitation measurement methods derived from different literature works. Therefore, in this chapter we will not list the segregation of the rain statistics and the signal attenuation. It would be misleading to separate these two as the majority of the existing satellite attenuation models incorporates the precipitation parameters, which is the dominant parameter responsible for large scale earth-satellite signal impairment.

Rain can affect electromagnetic signals in a wide range of frequency bands, but the extent of the impact varies depending on the specific frequency band. Generally, the higher the frequency, the greater the attenuation due to rain. In satellite communication systems, the most commonly affected frequency bands due to rain attenuation are the Ku-band (12-18 GHz), Ka-band (26.5-40 GHz), and V-band (40-75 GHz). These frequency bands are used for a variety of applications, including satellite television, broadband internet, and remote sensing. In addition to these frequency bands, rain can also affect other microwave communication bands such as the L-band (1-2 GHz), C-band (4-8 GHz), X-band (8-12 GHz), and Q-band

(33-50 GHz). These bands are used for a range of applications, such as weather radar, microwave links, and military communications.

Our initial acquaintance of satellite propagation mechanism was purely based on a theoretical treatment. RK Crane (R. K. Crane 1971) reviewed the theories describing the effect of troposphere on satellite communication system operating in the microwave band with frequency ranging from 7.5 GHz to 34.9 GHz. In his paper he presents the results of the computation-based theories and atmospheric models which he compared with the available experimental data. His analysis showed that rain causes the major difficulties in microwave transmission. Rain attenuation at frequencies above 16 GHz is severe and that the rain scattering also provides the dominant mechanism for interference between the ground systems operating at the same frequency and beyond each other's radio horizon. In his study he detailed the importance of understanding the statistical properties of rain and its relation with microwave transmission attenuation.

Crane (Robert K. Crane 1977) in his analysis of satellite-to-ground effect of microwave operating in the frequency range of 4 GHz and 20 GHz found that the major propagation effect of satellite communication system operating above 4 GHz are caused by rain. And that there is a possible exception of depolarization and multiple scattering at frequencies above 20 GHz. He also showed that the effects of depolarization effect could be calculated if the distribution of the rain intensity both in spatial and temporal variation measured by rain rate, liquid-water content, or reflectivity property is known.

By the year 1980s, two distinguished models with worldwide applicability for the prediction of the radio wave propagation attenuation statistics are the Global

Crane (Robert K. Crane 1980) and the CCIR model. These two models have been evaluated by comparing the model predictions with rain rate measurements (Robert K. Crane 1985). The use of single-year, measured rain rate statistics as a model for the prediction of the statistics for subsequent years was also considered. Surface rain rate distributions for one or more years of observations at 52 locations were employed for the model evaluations. On the basis of the available data the Global model or the Crane model showed a superior performance to the CCIR model. It was found that the lognormal distributions well-described the location-to-location variations in rain rate at specified probability levels and in probability at specified rain rate levels. No significant differences were observed between year-to-year and location-to-location variability estimates relative to the two rain rate prediction models. The data correspondingly showed that the climate models are comparable to inference from limited-duration records and suggest that prediction variability can be minimized by dividing the rain climate zones into smaller regions

In 1982, the CCIR plenary assembly held in Geneva (CCIR 1982) presented a contour maps of rainfall intensity $R_{0.01}$ (mm/hr) exceeded for 0.01% of the time in different hydrometeorological regions of the world. The CCIR rain model, also known as the CCIR 837 model, was a widely used rain attenuation model developed by the International Radio Consultative Committee (CCIR) in the 1980s. The model was based on empirical measurements of rain attenuation data obtained from a number of different locations around the world, and was intended to provide a simplified method for predicting rain attenuation in satellite communication systems. The CCIR model was widely used in the 1990s and early 2000s, but was later replaced by newer rain attenuation models developed by the International

Telecommunication Union (ITU). One of the reasons for this was that the CCIR model did not take into account the variability of raindrop size distributions, which can have a significant impact on rain attenuation.

Following the CCIR Planetary Assembly report, Moupfouma (Moupfouma 1985) proposed an empirical rain rate model to design the satellite and terrestrial microwave radio link. In the proposed model, Mopfouma expressed the variable parameters as a function of the rainfall intensity exceeded during 0.01% of the time, which is the rainfall-rate intensity recommended by the International Radio Consultative Committee (CCIR) to evaluate the availability of terrestrial and satellite radiowave links. The proposed probability law model exhibits a log-normal asymptotic behavior for the low rain rates, and a gamma asymptotic behavior for the high rain rates. The probability law proposed here gives a good representation of intensity cumulative distributions for most of the hydrometeorological zones of the world classified by the CCIR.

Segal examined two modes of expression for rainfall statistics derived on the basis of rain-gauge recording having an effective integration time of five minutes or more (Segal 1986). Data from 45 locations in Canada, which were spread across more than 5000 km was used for analyzing the problems of converting cumulative distribution of rainfall intensity with a rain-gauge having 5 to 10 min integration time into equivalent 1-minute statistics. Mode II follows the logarithmic treatments while Mode I follows a power-law treatment. In his analysis, he observed that the power-law relation gives a very good precision over the range of different locations.

A simple attenuation model was proposed by authors in (Stutzman and Yon 1986) incorporating the wave polarization effect. This model is labeled Simple

Attenuation Model (SAM), which applies for the prediction of rain attenuation statistics on earth-space communication links operating in the 10-35 GHz band. In their evaluation they observed that the SAM model yields better result compared to the CCIR model at a higher percentage of time (≤ 0.1 %) while the CCIR model presents a better result at lower percentages of time (≤ 0.01 %)

The Moupfouma rain attenuation model provides a method for estimating the specific attenuation caused by rain as a function of frequency, path length, and other factors. The model is known for its simplicity and accuracy. Authors in (Chebil and Rahman 1999) have examined the relationship between the hourly and 1 min cumulative rain rate statistics in different regions of Malaysia for the Microwave system design. They have collected two types of rainfall data: hourly and 1 min time interval rainfall data were measured over three years. In their study they found that the estimate of the rain rate conversion factor is best described from the Moupfouma and linear logarithmic model compared to the Segal's model.

It is worthwhile noting that the CCIR existed as an individual organ of the International Telecommunication Union (ITU) since 1929, which was replaced with the ITU-R in 1993 (ITU 1993). The technical studies and recommendations from both these organs have been of great assets in all sectors of wireless communication development around the world. The International Telecommunications Union (ITU) is the leading United Nations agency for Radio and Telecommunications coordination worldwide. These Study Groups and their Parties, dedicated to specialized technical areas, provide the mechanism for Member Nations to contribute, study and recommend standards and practices to ensure impartial and interference-free operation within the radio spectrum(Beard 2011).

The International Telecommunication Union Recommendation (ITU-R) recommends the use of the 1 min integration time rainfall rate $R_{0.01}$ (mm/h) exceeded for 0.01% of the time. This recommendation is one of the most widely referenced and adapted rain rate attenuation models in literature. The ITU provides recommendation and gives rectification to any recommendation's underperformance through a series of revised recommendations which is updated from time to time. The performance of such recommendations could differ from region to region.

A prediction model that combines rain attenuation and other propagation impairments for earth-satellite path by authors in (Dissanayake and Allnut 1997). This model is labeled as DAH model. In their work they have analyzed the cloud attenuation, melting layer attenuation, gaseous attenuation, rain attenuation and have proposed a method apt for the prediction of propagation loss along the earth-satellite path. Their model applies between 4 and 35 GHz. This model was projected to provide prediction across the probable range of 0.01 % to 50 %, which is adequate for most telecommunication system design purpose.

The SAM and ITU-R model were evaluated for the Ku-band in the tropical region of India (Kolkata) by author in (Adhikari et al. 2011). In their study they have proposed a model considering the instantaneous rain rate instead of $R_{0.01}$ where the effective path length is modified as a function of rain rate. Although their proposed model outperforms the SAM model, they learned that the ITU model is the best performing model for rain attenuation values up to 8 dB, while their proposed model improved to some extent for attenuation > 8 dB for the higher rain attenuation.

Evaluation of the ITU-R model was done by authors in (Dafda and Maradia 2019) for different region of India using the 0.01% Rain Rate values suggested by

ITU-R model. In their study they have made analysis for different states of India excluding North-eastern states. Their analysis suggested that the ITU-R model vary widely compared to actual Rain Rate values considered from the Monsoon Rainfall data of 64 years obtained from India Meteorological Department (IMD). Due to predictions from longer duration of data, statistical accuracy is obtained. Consequently, they proposed a new Rain attenuation model based on the ITU-R model for India. The DM model suggests a reduced Rain Attenuation as compared to that suggested by ITU-R model. The rain attenuation proposed is 5–15 dB lower than as defined by ITU-R model. DM model is proposed taking data from 5 meteorological subdivisions.

2.1 References

- Adhikari, A., S. Das, A. Bhattacharya, and A. Maitra. 2011. “Improving Rain Attenuation Estimation: Modelling of Effective Path Length Using Ku-Band Measurements at a Tropical Location.” *Progress In Electromagnetics Research B*.
- Beard, Ronald L. 2011. “Role of the ITU-R in Time Scale Definition and Dissemination.” *Metrologia*.
- CCIR. 1982. “CCIR XVth Plen. Ass., Geneva, 1982, V, Report 563-2.” In *Planetary Assessment*, , 563–2.
- Chebil, J., and T. A. Rahman. 1999. “Rain Rate Statistical Conversion for the Prediction of Rain Attenuation in Malaysia.” *Electronics Letters*.
- Crane, R. K. 1971. “Propagation Phenomena Affecting Satellite Communication

- Systems Operating in the Centimeter and Millimeter Wavelength Bands.”
Proceedings of the IEEE.
- Crane, Robert K. 1977. “Prediction of the Effects of Rain on Satellite Communication Systems.” *Proceedings of the IEEE*.
- . 1980. “Prediction of Attenuation by Rain.” *IEEE Transactions on Communications*.
- . 1985. “Evaluation of Global and CCIR Models for Estimation of Rain Rate Statistics.” *Radio Science*.
- Dafda, Alpesh H., and Kishor G. Maradia. 2019. “A Novel Method for Estimation of Rainfall Attenuation Using Coarse Rainfall Data and Proposal of Modified ITU-R Rain Model for India.” *SN Applied Sciences*.
- Dissanayake, Asoka, and Jeremy Allnutt. 1997. “A Prediction Model That Combines Rain Attenuation and Other Propagation Impairments along Earth-Satellite Paths.” *IEEE Transactions on Antennas and Propagation*.
- ITU. 1993. “FROM CCIR TO ITU-R 75 YEARS OF CONTRIBUTION TO RADIO DEVELOPMENT.” *itunews*: 1.
<https://www.itu.int/itunews/manager/display.asp?lang=en&year=2004&issue=09&ipage=ccir-revolution&ext=html> (March 23, 2023).
- Moufouma, F. 1985. “MODEL OF RAINFALL-RATE DISTRIBUTION FOR RADIO SYSTEM DESIGN.” *IEE Proceedings H: Microwaves Optics and Antennas*.
- Segal, B. 1986. “The Influence of Rainage Integration Time, on Measured Rainfall-Intensity Distribution Functions.” *Journal of Atmospheric and Oceanic Technology*.

Stutzman, W. L., and K. M. Yon. 1986. "A Simple Rain Attenuation Model for Earth- space Radio Links Operating at 10–35 GHz." *Radio Science*.

Chapter 3

Methodology

Chapter 3 Methodology:

3.1 Introduction:

The Ku-band satellite links have been widely used for communications in countries with temperate climates since margins can be built into link budget to cope with fading in those climates. Initially, contributions on rain induced attenuation measurements in the tropical climate are very limited and prediction models of rain induced attenuation in satellite links have to depend almost entirely on "measurements in temperate climates. Even until recently, still very few experimental results are made available on earth-space communication links in tropical-equatorial region. Sufficient measurements are required to understand the complete propagation mechanisms in this region.

3.2 RF Data collection Methodology:

For our current study the Ku band down link of GSAT-15 parked at parking slot of 93.5 degrees east was used. GSAT-15, India's latest Communication Satellite is a high-power satellite being inducted into the INSAT/GSAT system. Weighing 3164 kg at lift-off, GSAT-15 carried a total of 24 communication transponders in Ku-band as well as a GPS Aided GEO Augmented Navigation (GAGAN) payload operating in L1 and L5 bands. GSAT-15 is the third satellite to carry GAGAN payload after GAST-8 and GSAT-10, which are already providing navigation services from orbit. GSAT-15, carried a Ku-band beacon as well to help in accurately pointing ground antennas towards the satellite.

GSAT-15 was launched by Ariane-5 VA-227 launch vehicle from Kourou, French Guiana on early morning of November 11, 2015 (Suryanarayana Rao, 2007).

TABLE 3.1: GSAT-15 MISSION DATA

Mission	Communication and Satellite Navigation
Weight	3164 kg (Mass at Lift – off) 1440 kg (Dry Mass)
Power	Solar array providing 6200 Watts and Three 100 Ah Lithium-Ion batteries
Propulsion	Bi- propellant System
Launch date	November 11, 2015
Launch site	Kourou, French Guiana
Launch vehicle	Ariane-5 VA-227
Orbit	Geostationary (93.5° East longitude)



Figure 3.1: GSAT-15 (picture: courtesy Google.com/pic)

The Foot print of GSAT-15 taken from www.satstar.com are given below.

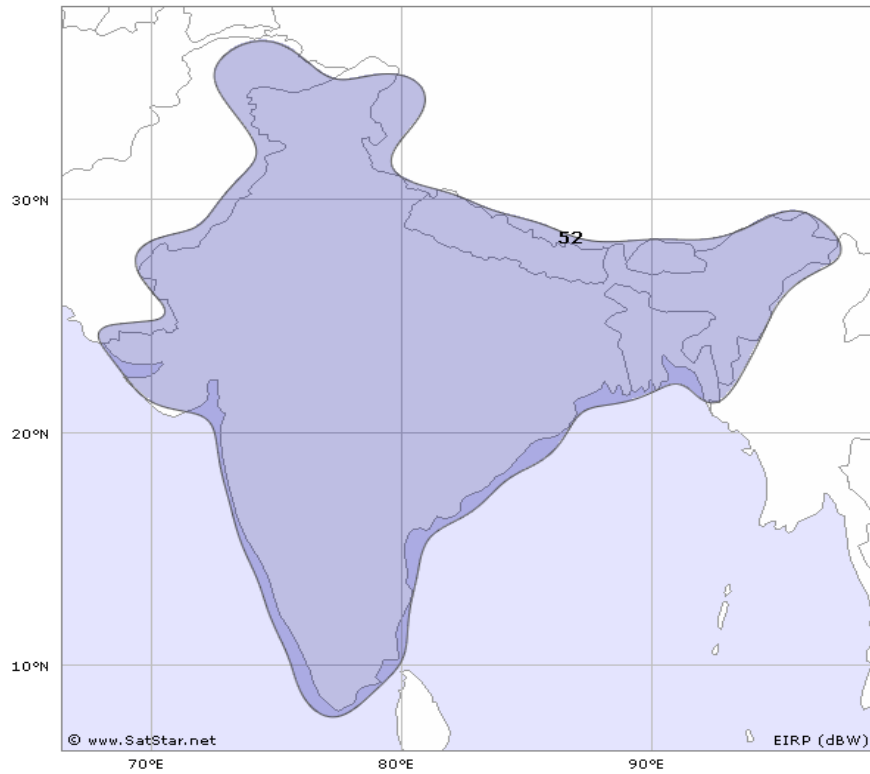


TABLE 3.2: DISH SIZE ESTIMATE BASED ON EIRP (DBW)

EIRP (DBw)	Dish size estimate (Ku-band)												
	<30	30	32	34	36	38	40	42	44	46	48	50	>50
Min (cm)	>535	475	380	300	240	190	150	120	95	75	60	50	50
Max (cm)		600	475	380	300	215	190	150	120	95	75	60	



Figure 3.2: Foot print of GSAT- 15 (source: Satstar.net)

Ku band signal of DD free dish (DTH) was being uplinked from Doordrshan Delhi

Earth station at Todapur with following parameters

TABLE 3.3: UPLINK SIGNAL PARAMETERS AND VALUES

Parameters	Values
Uplink frequency	14.140
Symbol rate	29.5
FEC	3/4

The signal uplinked from the Doordrashan Delhi earth station is uplinked to geostationary Satellite GSAT-15 at a height of 35786 Km from the surface of earth. Geostationary satellites are in geostationary orbit that can be achieved at an altitude of 35786 Km and keeps the satellite fixed over one longitude at the equator. The antenna meant for UP linking the signal is highly directional parabolic disk antenna (PDA) with following parameters

TABLE 3.4: DIAMETER, ELEVATION ANGLE, AND AZIMUTH ANGLE

Parameters	Values
Diameter of uplink PDA	8.2 m
Elevation angle of PDA	57.6°
Azimuth angle of PDA	176.2°

The signal up linked is received by the transponder of GSAT-15 satellite the signal goes through a series of signal processing modules and its frequency is down converted to 11.09 GHz and then the signal is beamed back to earth from the directional antenna panel installed at the satellite.

3.2.1 Calculation of Look Angle:

For a receive Earth station antenna Look angles are the angle at which antenna points or look at the satellite to receive the signal, angle of polarisation, angle of elevation and angle of azimuth are the look angle.

The down link signal was received at our site through a PDA which was installed at Doordrashan Kendra, Durtlang Aizawl. The first step was to calculate the look angle of receive PDA, which were calculated in following steps.

$$\text{Longitude of Satellite } (long_{SAT}) = 93.5^\circ E$$

$$\text{Longitude of earth station } (long_{ES}) = 92.7307^\circ E$$

$$\text{Latitude of earth station } \phi = 23.7779^\circ N$$

$$\text{Radius of earth } R_E = 6378 \text{ km}$$

$$\text{Altitude of satellite } R_0 = 35786 \text{ km}$$

Step 1: Calculation of angle of polarization (τ)

$$\tau = \tan^{-1} \left[\frac{\sin |(long_{ES}) - (long_{SAT})|}{\tan \phi} \right] \quad (1)$$

Substituting the parameter defined earlier the angle of polarization (τ) was calculated to be 1.74°

Step 2: Calculating the angle of elevation

The angle of elevation was calculated using the expression

$$\theta = \tan^{-1} \left[\cos \omega - \frac{\left(\frac{R_E}{R_E - R_0} \right)}{\sqrt{1 - \cos \omega}} \right] \quad (2)$$

The angle of elevation (θ) was found to be 55.2°

Step 3: Calculating the angle of Azimuth (γ)

The angle of azimuth is obtained using the expression

$$\cos \gamma = \cos \phi \cos[(long_{SAT}) - (long_{ES})]$$

Defining angle a as

$$a = |(long_{SAT}) - (long_{ES})|$$

Hence angle s could be defined as

$$s = 0.5(a + \phi + \gamma)$$

Now the azimuth angle (γ) is calculated as

$$azimuth = 180 + 2 \tan^{-1} \left[\frac{\sin(s - \gamma) \sin(s - \phi)}{\sin(s) \sin(s - a)} \right]^2 \quad (3)$$

The azimuth was calculated to be 221.3 °

After determining the look angle for GSAT-15 from the location of our experimental site the PDA was set to receive the GSAT-15 down link signal. The vertically polarised RF signal from the PDA with an offset parabolic antenna of 1.2 meter diameter is down converted to L band signal by a low noise block converter (LNBC) having noise temperature of 15 K. This signal was then fed back to Anritsu site master S332 E Spectrum analyser for further recording and processing of signal.



Figure 3.3: Tektronix RSA306B spectrum Analyser

3.2.2 Spectrum analyser

The spectrum analyser is Tektronix RSA 306 B, covering a frequency band of 9 KHz to 6.2 GHz. The RSA 306B comes with a Tektronix signal VU-PCTM RF signal analysis software and provide real time spectrum analysis. In the following paragraphs the key performance specification and key features of the RSA306B spectrum analyser as provided in their technical manual are quoted.

Key features of the spectrum analyser

1. 9 kHz to 6.2 GHz frequency range covers a broad range of analysis needs
2. +20 dBm to -160 dBm measurement range
3. Mil-Std 28800 Class 2 environmental, shock and vibration specifications for use in harsh conditions

4. Fast sweeps (2 sweep per second) over entire 6.2 GHz span for quick detection of unknown signals
5. Acquisition bandwidth of 40 MHz enables wideband vector analysis of modern standards
6. Minimum signal duration as short as 15 μ s captured with 100% probability of intercept
7. Key Features
8. Full-featured spectrum analysis capability with included Tektronix SignalVu-PC™ software
9. 17 spectrum and signal analysis measurement displays enable dozens of measurement types
10. Options for mapping, modulation analysis, WLAN, LTE, and Bluetooth standards support, pulse measurements, playback of recorded files, signal survey, and frequency/phase settling
11. EMC/EMI pre-compliance and troubleshooting - CISPR detectors, predefined standards, limit lines, easy accessory setup, ambient capture, failure analysis, and report generation
12. DataVu-PC software enables multi-unit recording in variable bandwidths
13. Real time Spectrum/Spectrogram display to minimize time spent on transient and interference hunting
14. Application programming interface (API) included for Microsoft Windows and Linux environments
15. MATLAB instrument driver for use with Instrument Control Toolbox
16. Streaming capture records long-term events

3.3 Rain Data collection source:

Rainfall data used in current work was purchased/collected from the following sources.

3.3.1 Indian Metrological department, Regional centre Guwahati

Hourly rainfall data for the experimental site for the period 2015-2019 was purchased from the IMD, regional centre Guwahati.

3.3.2 State Metrological Centre, Directorate of science and Technology, Government of Mizoram

Monthly rainfall data for the period 1986-2015 was collected from State Metrological centre, Govt. of Mizoram

3.3.3 Indian Metrological Department, New Delhi

Monthly rainfall data for the period 1901-2017 was taken from IMD.

3.4 Statistical Tools for analysis:

Analysing rain attenuation requires a large number of datasets. This data includes a geographical data of the location, historical weather for more than 30 years, RF data regarding the signal. To test any attenuation prediction model with our recorded data there are a number of statistical tests such as goodness of fit test, least square method test, etc. In our analysis we have used following statistical tools

- Bilinear interpolation for determining the zero-degree isotherm height at our location.
- Goodness of fit test for model verification
- Chi square test for model verification

- Least square test

3.4.1 The Chi-square (χ^2) test:

In this section we briefly introduce the notion of the χ^2 test adapted from the related literatures (Harding, 1985; Kemp et al., 1991). Let us assume X_1, X_2, \dots, X_n to be a sample of size n . The range space of X is distributed into k mutually exclusive intervals A_1, A_2, \dots, A_k . Let N_i be the number of X_j 's falling into A_i , $i = 1, 2, \dots, k$. The observed probabilities from measured data P_i are given by

$$\text{Observed } P(A_i) = \frac{N_i}{n} \quad (4)$$

Whilst, the theoretical probabilities $P(A_i)$ can be obtained from the hypothesized distribution denoted by

$$\text{Theoretical } P(A_i) = p_i \quad i = 1, 2, \dots, k$$

A logical selection of a statistic giving a measure of deviation can be defined as

$$D = \sum_{i=1}^k \frac{n}{p_i} \left[\frac{N_i}{n} - p_i \right]^2 \quad (5)$$

Which is the natural least-square type deviation measure. If taking $c = n/p_i$, then the equation above can be rewritten as

$$D = \sum_{i=1}^k \left[\frac{N_i - np_i}{np_i} \right]^2 \quad (6)$$

$$D = \sum_{i=1}^k \frac{N_i^2}{np_i} - n \quad (7)$$

Where D is a statistic since it is a function of NL . The distribution of statistic D approaches a χ^2 distribution with $(k - 1)$ degrees of freedom as n . If the significance level α is defined as

$$P(D > \chi^2_{k-1,\alpha}) = \alpha$$

Then the χ^2 test suggests that the proposed distribution is rejected whenever

$$d = \sum_{i=1}^k \frac{N_i^2}{np_i} - n > \chi^2_{k-1,\alpha} \quad (8)$$

and is accepted otherwise. d the sample value of D based on the sample values $X_i = 1, \dots, n$.

We then performed the χ^2 test based on the recommended procedure. Listed below is the recommended step-by-step procedure for carrying out the χ^2 tests when the distribution of X is completely specified.

1. Divide range space of X into k mutually exclusive and numerically convenient intervals A_i , where $i = 1, 2, \dots, k$. Let n_i be the number of sample values falling into A_i . As a rule, if the number of sample values in any A_i is less than five, combine the interval A_i with either A_{i-1} or A_{i+1}
2. Compute the theoretical probabilities ($A_j = p_j = 1, 2, \dots, k$) by means of the hypothesised distribution.
3. Construct as given by equation

4. Choose a value of α and determine from table for the χ^2 distribution of $(k - 1)$ degrees of freedom the value of $\chi^2_{k-1,\alpha}$
5. Reject the hypothesis distribution if $d > \chi^2_{k-1,\alpha}$. Otherwise accept the hypothesis distribution

3.4.2 Bilinear Interpolation

Bilinear interpolation is a method for a two-dimensional interpolation on a rectangle, The method is used in image processing and is suggested by International Telecommunication Union (ITU) in calculation of height of zero-degree isotherm at any location across the globe (ITU-R, 2001). Suppose we have a value of some unknown function at four points that form a rectangle. Let these points be $(x_1, y_1), (x_1, y_2), (x_2, y_1), (x_2, y_2)$ and the values of function are the following

the value at (x_1, y_1) is Q_{11}

the value at (x_1, y_2) is Q_{21}

the value at (x_2, y_1) is Q_{12}

the value at (x_2, y_2) is Q_{22}

By using bilinear interpolation, we can determine this function's value at any point inside the rectangle. Let the value of unknown variable be P .

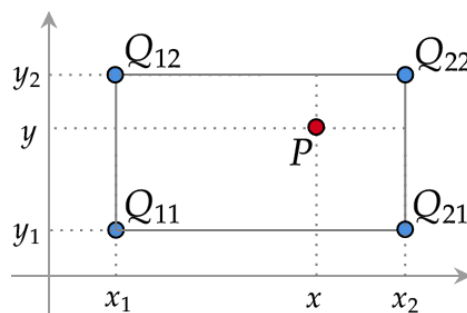


Fig 3.4: Bilinear interpolation

This interpolation scheme is widespread and has many applications, in particular in computer vision and image processing. It is based on a much simpler and widely used procedure of linear interpolation.

The data required for bilinear interpolation is often collected in the form of the following table.

TABLE 3.5: TABULAR DATA TO CALCULATE BILINEAR INTERPOLATION

	x_1	x	x_2
y_1	Q_{11}		Q_{21}
y		P	
y_2	Q_{12}		Q_{22}

Bilinear interpolation formula

The general idea of the bilinear interpolation method is the following

Start by performing two linear interpolations in the x -direction (horizontal): first at (x, y_1) , then at (x, y_2) . Next, perform linear interpolation in the y -direction (vertical): use the interpolated values at (x, y_1) and (x, y_2) to obtain the interpolation at the final point (x, y) .

Steps in simplification of the problems

1. We find the linear interpolation of function f at (x, y_1) using the values of f at (x_1, y_1) and (x_2, y_1) which are Q_{11} and Q_{21} respectively

$$R_1 = \frac{(x_2 - x)}{(x_2 - x_1)} Q_{11} + \frac{(x - x_1)}{(x_2 - x_1)} Q_{21} \quad (9)$$

2. We find the linear interpolation of f at (x, y_2) using the values of f at (x_1, y_2) and (x_2, y_2) which are Q_{12} and Q_{22} respectively

$$R_2 = \frac{(x_2 - x)}{(x_2 - x_1)} Q_{12} + \frac{(x - x_1)}{(x_2 - x_1)} Q_{22} \quad (10)$$

3. Finally, we find the linear interpolation at (x, y) using the interpolated values of f at (x, y_1) and (x, y_2)

$$P = \frac{(y_2 - y)}{(y_2 - y_1)} R_1 + \frac{(y - y_1)}{(y_2 - y_1)} R_2 \quad (11)$$

Finally, we rewrite the above expression for P to get rid of the intermediate values R_1 and R_2 .

Substituting the expressions for R_1 and R_2 from Steps 1 & 2, we get the following formula for P

$$P = \frac{(y_2 - y)}{(y_2 - y_1)} \frac{(x_2 - x)}{(x_2 - x_1)} Q_{11} + \frac{(y_2 - y)}{(y_2 - y_1)} \frac{(x - x_1)}{(x_2 - x_1)} Q_{21} \\ + \frac{(y - y_1)}{(y_2 - y_1)} \frac{(x_2 - x)}{(x_2 - x_1)} Q_{12} + \frac{(y - y_1)}{(y_2 - y_1)} \frac{(x - x_1)}{(x_2 - x_1)} Q_{22}$$

Using vectors and matrices, we can rewrite the above bilinear interpolation formula for P into the following form

$$P = \frac{1}{(x_2 - x_1)(y_2 - y_1)} [x_2 - x \quad x - x_1] \begin{bmatrix} Q_{11} & Q_{12} \\ Q_{21} & Q_{22} \end{bmatrix} \begin{bmatrix} y_2 & -y \\ y & -y_1 \end{bmatrix} \quad (13)$$

3.4.3 Statistical test and analysis

The signal measured in the wireless communication system shows wide variations with topology, with no clear-cut relationship. Hence a large number of a dataset are required for the statistical inference. In actual signal measurement, the results that we can draw are the overall experiment's probable outcome. To further evaluate the performance of the models theorized or proposed, statistical analysis tools are also required.

There are different evaluation methods available. However, there are common statistical analysis methods in the communication system that remain indispensable for evaluating a model's performance. We mentioned these tools as under

3.4.3.1 Least square method

The method of least square is a standard approach in regression analysis to approximate the solution of over determined systems. Suppose we have a set of observed data points and trying to fit a particular model to our observed data distribution. The difference of observed data values and those obtained by fitting the model is known as residual ε

$$\varepsilon = \text{observed}(Y_i) - \text{predicted}(Z_i)$$

In regression form, if the predictor variable is (X_i) then its relationship with the dependent variable (Z_i) is expressible as

$$Z_i = A + BX_i$$

Where A and B denote the regression parameters. The error term is expressible in the form

$$\sum_{i=1}^n \varepsilon = \sum_{i=1}^n (Y_i - (A + BX_i))^2 \quad (14)$$

It follows from the least-square principle that the estimators' A and B are the respective values of α and β , which minimizes the error (ε) for a given observation. This minimum rate is obtained by equating the first-order derivative of ε w.r.t α and β to zero.

For the alpha coefficient

$$\frac{\partial}{\partial \alpha} \sum_{i=1}^n \varepsilon^2 = 2 \sum_{i=1}^n (Y_i - \alpha - \beta X_i)(-1) = 0 \quad (15)$$

$$-\sum_{i=1}^n Y_i + \sum_{i=1}^n \alpha + \beta \sum_{i=1}^n X_i = 0$$

$$\sum_{i=1}^n Y_i = \sum_{i=1}^n \alpha + \beta \sum_{i=1}^n X_i$$

$$\sum_{i=1}^n Y_i = n\alpha + \beta \sum_{i=1}^n X_i$$

Where $n\alpha = \sum_{i=1}^n \alpha$

For the beta coefficient

$$\frac{\partial}{\partial \beta} \sum_{i=1}^n \varepsilon^2 = 2 \sum_{i=1}^n (Y_i - \alpha - \beta X_i)(-X_i) = 0$$

$$-\sum_{i=1}^n Y_i X_i + \alpha \sum_{i=1}^n X_i + \beta \sum_{i=1}^n X_i^2 = 0$$

$$\sum_{i=1}^n Y_i X_i = \alpha \sum_{i=1}^n X_i + \beta \sum_{i=1}^n X_i^2$$

Equation and are the Normal equations, where α and β are the point estimators of A and B

$$\sum_{i=1}^n Y_i = n\alpha + \beta \sum_{i=1}^n X_i$$

$$\sum_{i=1}^n Y_i X_i = \alpha \sum_{i=1}^n X_i + \beta \sum_{i=1}^n X_i^2$$

Rearranging the above Normal equation in matrix form and solving for α and β

$$\begin{pmatrix} n & \sum X_i \\ \sum X_i & \sum X_i^2 \end{pmatrix} \begin{pmatrix} \alpha \\ \beta \end{pmatrix} = \begin{pmatrix} \sum Y_i \\ \sum X_i Y_i \end{pmatrix}$$

$$\alpha = \frac{\sum Y_i - \beta \sum X_i}{n} \quad (15)$$

$$\beta = \frac{n \sum X_i Y_i - \sum X_i \sum Y_i}{n \sum (X_i)^2 - (\sum X_i)^2} \quad (16)$$

For the predicted value (Z_i), we assume α as a constant and β as the changing variable (Jawhly & Tiwari, 2020).

Experimental data have shown that the propagation channel influences majority of the signal variations. Keeping this in view, we obtain each site's elevation (above sea level) and vegetation profile. However, we classified the vegetation cover into four categorical types based on their influences on the signal.

3.4.3.2 Root Mean Squared Error (RMSE)

The Root Mean Squared Error (RMSE) is the standard statistical performance metric used in meteorology and climate research studies. The advantage of the RMSE is that it does not use absolute value and shows a clear difference in model performance comparison (Kasuya, 2019). The mathematical RMSE expression is

$$RMSE = \sqrt{\frac{\sum(L_{ob} - L_{pr})}{N}} \quad (17)$$

In **Error! Reference source not found.** L_{ob} is the observed loss and L_{pr} is the model predicted loss, while N is the total number of observations.

3.4.3.3 Correlation coefficient

The correlation coefficient is a measure of the linear relationship between two variables, \bar{x} and \bar{y} , which is denoted by r or R . It is also called Pearson's correlation coefficient (Kasuya, 2019), where r is defined as

$$r = \frac{\sum_{i=1}^n (x_i - \bar{x})(y_i - \bar{y})}{\sqrt{\sum_{i=1}^n (x_i - \bar{x})^2} \sqrt{\sum_{i=1}^n (y_i - \bar{y})^2}} \quad (18)$$

Here x_i and y_i denotes the variable values of the i^{th} position, \bar{x} and \bar{y} denote the mean of x and y , and n indicate the sample size. The correlation coefficient value ranges from 0 to 1, and a value closer to 1 represents a better linear relationship.

Although we did not mention this statistical tool in our work, this correlation coefficient helps determine the observed signal relationship's initial analysis with the different parameters associated. The coefficient of determination test provides a more solid statistical test framework for model analysis.

3.4.3.4 Coefficient of Determination

One of the tools widely used to measure the strength of the regression relationship is the coefficient of determination or the R -squared analysis. It is denoted by r^2 or R^2 and is expressed as (Cornell, 1987)

$$R^2 = 1 - \frac{SS_{residual}}{SS_{total}} \quad (19)$$

$$SS_{residual} = \sum (x - \hat{x})^2 \quad (20)$$

$$SS_{total} = \sum (x - \bar{x})^2 \quad (21)$$

Where \hat{x} represents the predicted data, \bar{x} denotes the mean of the observed data, and x represents the empirical data.

R^2 is a statistical measure representing the variance proportion for a dependent variable explained by an independent variable or the variables in regression model. Similar to the correlation coefficient the R^2 value ranges from 0 to

1, and the coefficient of determination or the R^2 value closer to 1 indicates a stronger regression relationship.

3.5 Data analysis software

Following programs and software were used for the analysis of data.

TABLE 3.6: Software/Programme used

Software/Programs	Manufacturer/Developer	Address
Microsoft Excel	Microsoft Corporation	Albuquerque, New Mexico, United States
MatlabR2018a	Math work	United States Natick Massachusetts

In completion of this teases a lot of recommendations and research papers of ITU were used. It is worthwhile to add few pages regarding ITU, its history and its working.

3.6 International Telecommunication Union Organisation:

ITU was founded in Paris in 1865 as the international telegraph union. It took its present name in 1932 and in 1947 became a specialized agency of united nation organization. On 15 November 1947, an agreement between ITU and the newly created United Nations recognized the ITU as the specialized agency for global telecommunications. This agreement entered into force on 1 January 1949, officially making the ITU an organ of the United Nations. Although its first area of expertise was telegraph, the work of ITU now cover the entire ICT sector, from digital

broadcasting to internet, from mobile technologies to 3D TV. An organization of public private partnership since its inception, ITU currently has a membership of 193 countries and some 700 private entities. Headquarter of ITU is in Geneva, Switzerland and has twelve regional and area office around the world. (itu.int/history/pages)

Purpose

The constitution of international telecommunication union cites the following purpose for the union.

- To maintain and extend international cooperation between all members of the union for the improvement and rational use of telecommunication of all kinds
- To promote and to offer technical assistance to developing countries in the field of telecommunications.
- To promote the development of technical facilities and their efficient operation.
- To promote the extension of the benefits of the new telecommunication technologies to all the world's inhabitant.
- To harmonize the actions of members in the attainment of these ends.
- To promote at the international level the adoption of a broader approach to telecommunication issues, an approach that includes other world and regional organization and nongovernmental organization concerned with telecommunication

3.7 ITU Sectors

The ITU comprises three Sectors, each managing a different aspect of the matters handled by the Union, as well as ITU Telecom. The sectors were created during the restructuring of ITU at its 1992 Plenipotentiary conference. Three pillars or sector of ITU are

- 1: Radio Communication Sector (ITU-R)
- 2: The Telecommunication Standardization Sector (ITU-T)
- 3: The Development sector (ITU-D)

3.7.1 Radio communication (ITU-R)

Established in 1927 as the International Radio Consultative Committee or CCIR (from its French name *Comité consultatif international pour la radio*), this Sector manages the international radio-frequency spectrum and satellite orbit resources. In 1992, the CCIR became the ITU-R.

3.7.2 Standardization (ITU-T)

Standardization was the original purpose of ITU since its inception. Established in 1956 as the International Telephone and Telegraph Consultative Committee or CCITT (from its French name *Comité consultatif international téléphonique et télégraphique*), this Sector standardizes global telecommunications (except for radio). In 1993, the CCITT became the ITU-T. The Standardization work is undertaken by Study Groups, such as Study Group 13 on Networks and Study Group 16 on Multimedia, and Study Group 17 on Security. The parent body of the

Study Groups is the quadrennial World Telecommunication Standardization Assembly. New work areas can be developed in Focus Groups, such as the Focus Group on Machine Learning for 5G and the ITU-WHO Focus Group on Artificial Intelligence for Health.

3.7.3 Development (ITU-D)

Established in 1992, this Sector helps spread equitable, sustainable and affordable access to information and communication technologies (ICT). It also provides the Secretariat for the Broadband Commission for Sustainable Development

3.7.4 ITU Telecom

ITU Telecom organizes major events for the world's ICT community.

3.8 ITU Recommendations:

Following recommendation and research paper of ITU were consulted during the analysis of both rain fall and signal attenuation.

3.8.1 ITU - R.P 839-4 (09-13)

This recommendation of ITU deals with Rain height model for prediction methods

the mean annual rain height above mean sea level, h_R , may be obtained from the zero-degree isotherm as

$$h_R = h_0 + 0.36 \text{ km}$$

For areas of the world where no specific information is available, the mean annual zero-degree isotherm height above mean sea level, h_0 , is an integral part of this

Recommendation and is available in the form of a digital map provided in the (ITU-R, 2013)

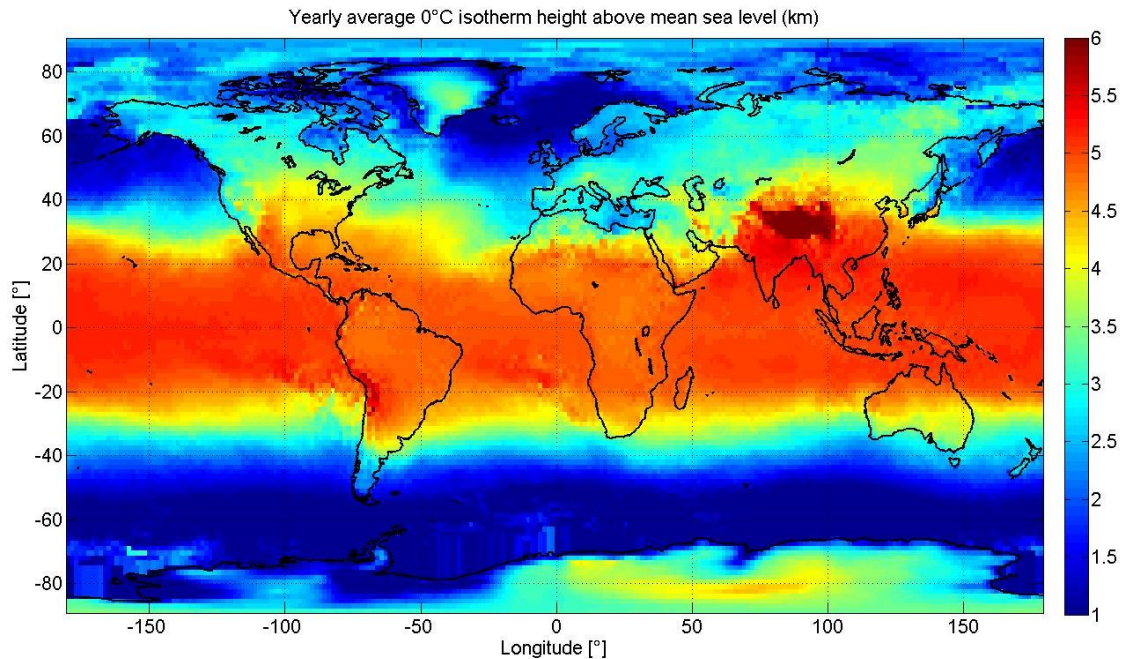


Figure 3.5: Yearly average zero-degree isotherm height

In addition to this digital map zero-degree isotherm height the recommendation also provided three more files h_0 .jpg, lat.txt and log.txt. These files contain data regarding latitude and longitude across the earth and the height of zero-degree isotherm. The data is provided from 0° to 360° in longitude and from $+90^\circ$ to -90° in latitude. For a location different from the grid points, the mean annual 0°C isotherm height above mean sea level at the desired location can be derived by performing a bilinear interpolation on the values at the four closest grid points.

For Aizawl we calculated the average zero-degree isotherm height for our experimental site by using bilinear interpolation and the h_0 was calculated to be

$$h_0 = 4.857 \text{ km}$$

3.8.2 ITU R-REC-P.837-7

The International Telecommunication Union 837-7 series of recommendation deals with characteristics of precipitation for propagation planning. These are the latest in series of recommendation that came out in 2017, earlier recommendations in the series came out in years 1992, 1997, 1999, 2001, and 2013.

The recommendation provides insight into the conversion of rain rate from higher integration time to 1 minute integration time.

The annual rainfall rate data exceeded for 0.01% of an average year, $R_{0.01}$ (mm/hr), is also an integral part of this Recommendation and are available as digital maps. The latitude grid is from -90° N to $+90^\circ$ N in 0.125° steps, and the longitude grid is from -180° E to $+180^\circ$ E in 0.125° steps. These digital maps are available in the ITU recommendation P.837-7 (ITU-R, 2017a).

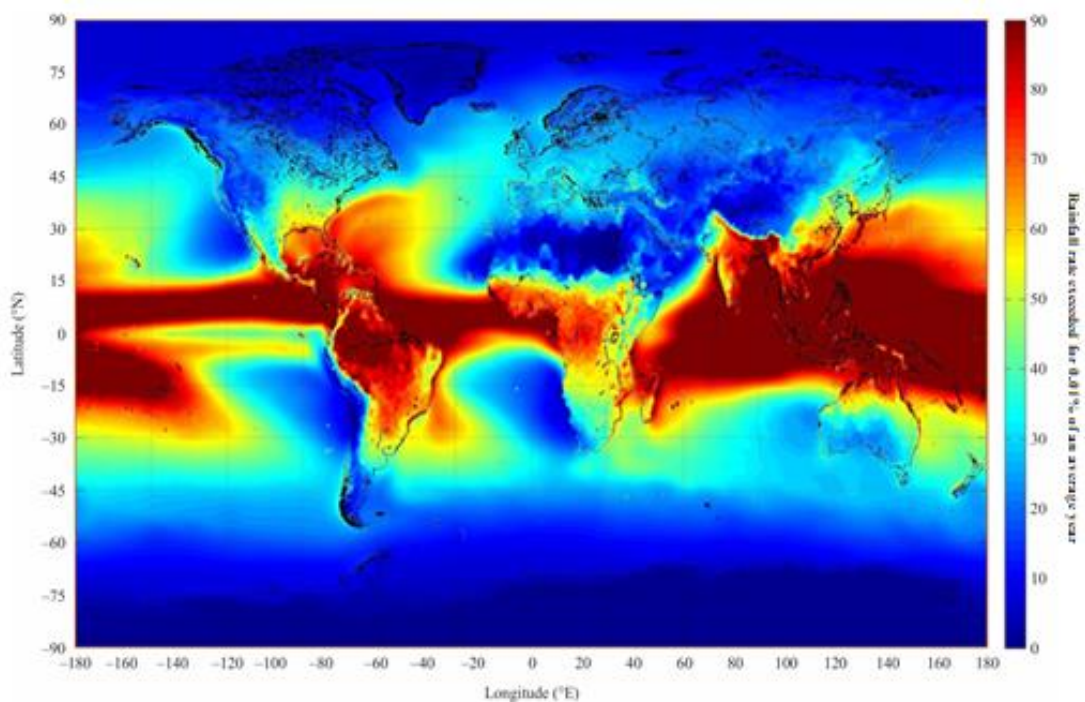


Figure 3.6: ITU digital map for $R_{0.01}$ rate for the globe

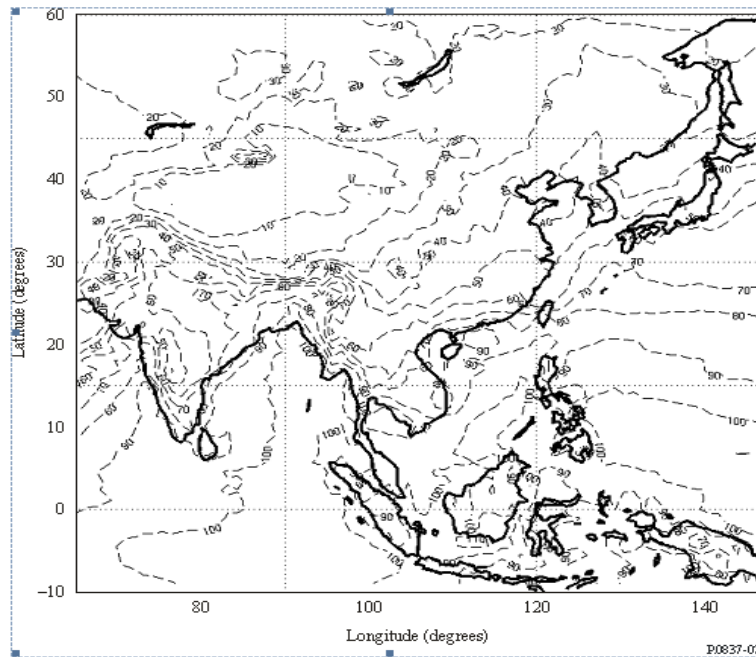


FIGURE 3.7:A picture from the earlier recommendation P.837-6 (ITU-R, 2012) showing region of India. Respective $R_{0.01}$ rate is as shown in the figure

3.8.3 Recommendation ITU-R-618-13

This series of recommendation deals with Propagation data and prediction methods required for the design of Earth-space telecommunication systems. The ITU-R 618-13 (ITU-R, 2017b) is the latest in the series of recommendation that came out in 2017, earlier recommendation are given in the year 1986, 1990, 1992, 1994, 1995, 1997, 2001, 2003, 2007, 2009, and 2015. This series contain the methodology of applying ITU model for rain fall attenuation.

3.9 MATLAB Programme

Matlab was used for calculating rain attenuation using Crane and ITU-R model.

3.9.1 Crane Model

Cranerainpl is the matlab function to calculate rain attenuation of RF signal using the Crane model.

Syntax:

```
L=cranerainpl (range, freq, rainrate)
```

```
L=cranerainpl (range, freq, rainrate, elev)
```

```
L=cranerainpl (range, freq, rainrate, elev, tau)
```

L=cranerainpl(range, freq, rainrate) returns the signal attenuation L, due to rain based on Crane rain model signal attenuation is a function of signal path length, range, the signal frequency and the rain rate. The rain rate is defined as the long-term statistical rain rate. The attenuation model applies only for frequencies from 1 GHz to 1000 GHz. The crane model accounts for the cellular nature of rain.

L= cranerainpl (range, freq, rainrate, elev) also specifies angle of elevation.

L=cranerainpl(range, freq, rainrate, elev, tau) also considers the angle of polarization.

The specific function

```
L=cranerainpl (range, freq, rainrate, elev, tau)
```

is frequently used our analysis of rain attenuation by crane model.

3.9.2 ITU Model

Matlab function `rainpl` calculate the rain attenuation of RF signal due to ITU model

Syntax

`L=rainpl(range,freq,rainrate)` (1)

`L=rainpl(range,freq,rainrate,elev)` (2)

`L=rainpl(range,freq,rainrate,elev,tau)` (3)

`L=rainpl(range,freq,rainrate,elev,tau,pct)` (4)

3.10 Conclusion:

In this chapter we discussed the important tools and method used in our study

3.11 References

- Cornell, J. A. (1987). Factors that Influence the Value of the Coefficient of Determination in Simple Linear and Nonlinear Regression Models. *Phytopathology*, 77(1), 63. <https://doi.org/10.1094/phyto-77-63>
- Harding, A. T. (1985). Probability and statistics for engineers (3rd edition), by I. Miller and J. E. Freund. Pp 530. £43. 1984. ISBN 0-13-711938-0 (Prentice-Hall). *The Mathematical Gazette*. <https://doi.org/10.2307/3617602>
- ITU-R. (2001). *Rec. ITU-R P.839-3 1 RECOMMENDATION ITU-R P.839-3*. https://www.itu.int/dms_pubrec/itu-r/rec/p/R-REC-P.839-3-200102-S!!PDF-E.pdf
- ITU-R. (2012). *R-REC-P.837-6 Recommendation ITU-R P.837-6*. https://www.itu.int/dms_pubrec/itu-r/rec/p/R-REC-P.837-6-201202-S!!PDF-

E.pdf

ITU-R. (2013). *Rec. ITU-R P.839-4 RECOMMENDATION ITU-R P.839-4.*

https://www.itu.int/dms_pubrec/itu-r/rec/p/R-REC-P.839-4-201309-I!!PDF-

E.pdf

ITU-R. (2017a). *R-REC-P.837-7-201706 RECOMMENDATION ITU-R P.837-7.*

https://www.itu.int/dms_pubrec/itu-r/rec/p/R-REC-P.837-7-201706-I!!PDF-

E.pdf

ITU-R. (2017b). *R-REC P.618-13 Recommendation ITU-R P.618-13.*

https://www.itu.int/dms_pubrec/itu-r/rec/p/R-REC-P.618-13-201712-I!!PDF-

E.pdf

Jawhly, T., & Tiwari, R. C. (2020). The special case of Egli and Hata model optimization using least-square approximation method. *SN Applied Sciences*.

<https://doi.org/10.1007/s42452-020-3061-0>

Kasuya, E. (2019). On the use of r and r squared in correlation and regression.

Ecological Research, 34(1), 235–236. <https://doi.org/10.1111/1440-1703.1011>

Kemp, C. D., Kemp, A. W., Scheaffer, R. L., McClave, J. T., Ott, L., Mendenhall,

W., Keller, G., Warrack, B., Bartel, H., & Healey, J. F. (1991). Probability and

Statistics for Engineers. *Biometrics*. <https://doi.org/10.2307/2532538>

Suryanarayana Rao, K. N. (2007). GAGAN - The Indian satellite based augmentation system. *Indian Journal of Radio and Space Physics*.

Chapter

4

Results and Discussion

CHAPTER 4: RESULTS AND DISCUSSIONS

CHAPTER 4: RESULTS AND DISCUSSIONS

4.1: Analysis of Rainfall data:

Rainfall intensity or rainfall rate is one of the most critical meteorological parameters that causes severe degradation of satellite-Earth communications above 10 GHz. At frequencies above 10 GHz rain strongly attenuates and depolarizes radio waves and constitutes a major Impediment to satellite link performance (Stutzman et al., 1986). Therefore, an understanding of the statistical characteristics of rainfall intensity is extremely crucial for the planning of any microwave or millimetre-wave telecommunication systems, especially in the heavy rainfall regime of tropical regions.

The characteristics of the rainfall in tropical regions must be investigated in every design of communication links through this region in order to meet the system's operational reliability. It is common knowledge that rainfall rate cumulative distributions vary greatly from region to region. High rainfall rates and the consequent high rain induced attenuation in the tropical regions is arguably the greatest constraint to the usability of the Ku-bands and above in the tropics

This chapter deals with the analysis of rainfall data of Aizawl Mizoram. Aizawl is the capital city of Mizoram and the Latitude and Longitude of Durtlang, the place where experimental set up for gathering of attenuation data was installed is at Latitude $23.779^{\circ}N$ and Longitude $92.7307^{\circ}E$. The average height of the place is

1384 meter above mean sea level. The state of Mizoram lies between Latitude of 22 degree and 25 degrees north.



Figure 4.1: Map of Mizoram

Weather of Aizawl is classified as semi tropical with mean temperature of 26 degree Celsius and mean humidity of 69.8 %. The mean humidity and temperature variation at Aizawl throughout the year are shown below.

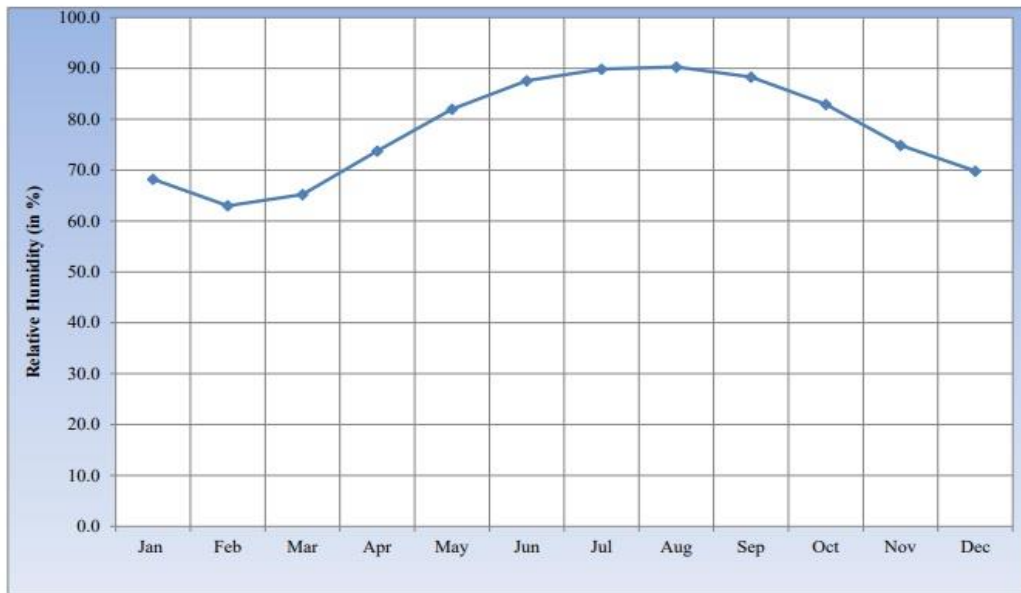


Figure 4.2: Average monthly relative humidity of Aizawl (1986-2015)

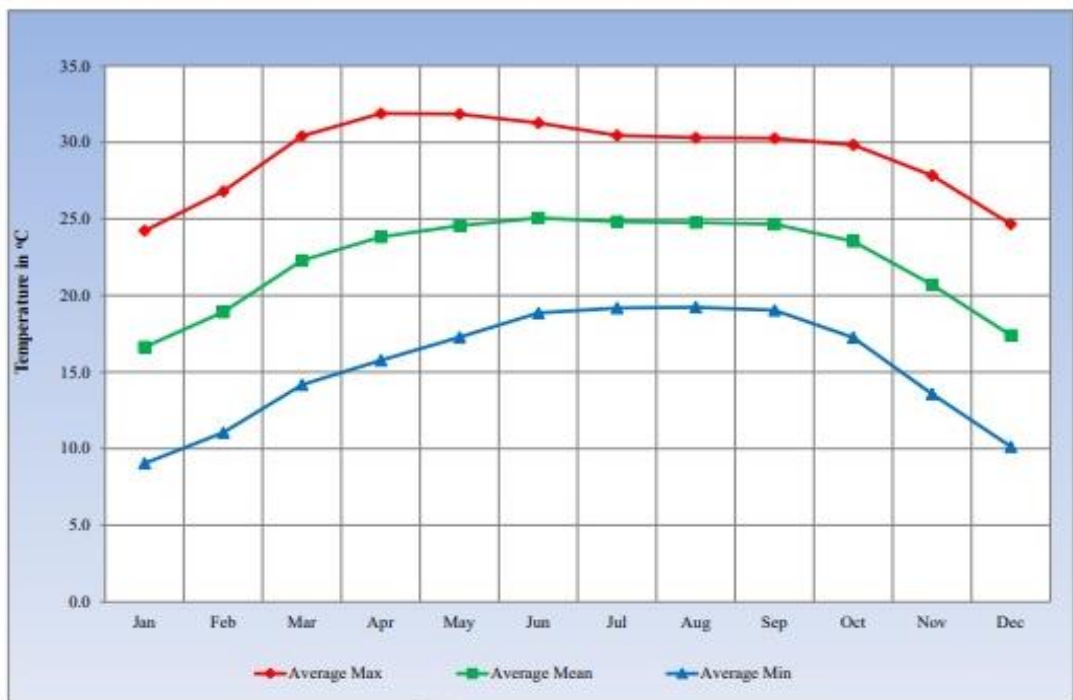


Figure 4.3: Monthly Avg., Minimum and Maximum Temperature of Aizawl

4.1.1 Source of Rainfall data:

Rainfall data for the region was collected/purchased from the following sources.

1: Indian Metrological department, Regional centre Guwahati

2: State Metrological centre, Directorate of science and Technology, Government of Mizoram, Aizawl

3: Indian Metrological department, Ministry of Earth science Government of India, New Delhi.

Hourly rainfall data for the period 2015-2019 were purchased from IMD regional centre Guwahati. Monthly rainfall data for the period 1986-2015 was taken from state metrological centre, Government of Mizoram. Historical Monthly rainfall data for the period 1901-2017 were taken from the Indian metrological department, Government of India.

4.2 Rain data analysis:

From the analysis of rainfall data from 1986 to 2015, Aizawl has an average yearly rainfall of 2743 mm with monsoon months (JJAS) having on average 78 percent of total yearly rain. We regard these months as worst months for the RF attenuation analysis.

TABLE 4.1: YEAR-WISE RAINFALL AND MONSOON MONTHS RAINFALL

Year	Yearly rainfall (mm)	Monsoon month (JJAS) rainfall (mm)	% JJAS of yearly rainfall
1986	2702.3	1801	66.65
1987	2679	2040	76.15
1988	2719.4	2057.3	75.65
1989	2695.5	2074.9	76.98
1990	2934.9	1837.3	62.60

1991	2502.8	1904.7	76.10
1992	2580.7	1958	75.87
1993	2739.8	2199.7	80.29
<hr/>			
1994	2278.4	1676.7	73.59
1995	3185.9	2397	75.24
1996	2868.5	2139.4	74.58
1997	2943.6	2368.9	80.48
1998	2730.6	2137.6	78.28
1999	2994.9	2633.1	87.92
2000	2903.8	2100.6	72.34
2001	2810.2	2133.5	75.92
2002	2788.5	2247.9	80.61
2033	2970.6	2409.6	81.11
2004	3108.2	2508.6	80.71
2005	2436.4	1853.9	76.09
2006	2717.3	2496.2	91.86
2007	3375.4	2661.1	78.84
2008	2330.1	1962.9	84.24
2009	2047.4	1631.6	79.69
2010	3012.5	2221.1	73.73
2011	2577.5	2213.9	85.89
2012	2938.5	2146.2	73.04
2013	2708.2	2449.2	90.44
2014	2283.6	2029.3	88.86
2015	2731.4	2053.6	75.18
<hr/>			
Average	2743.20	Average	78.30
<hr/>			

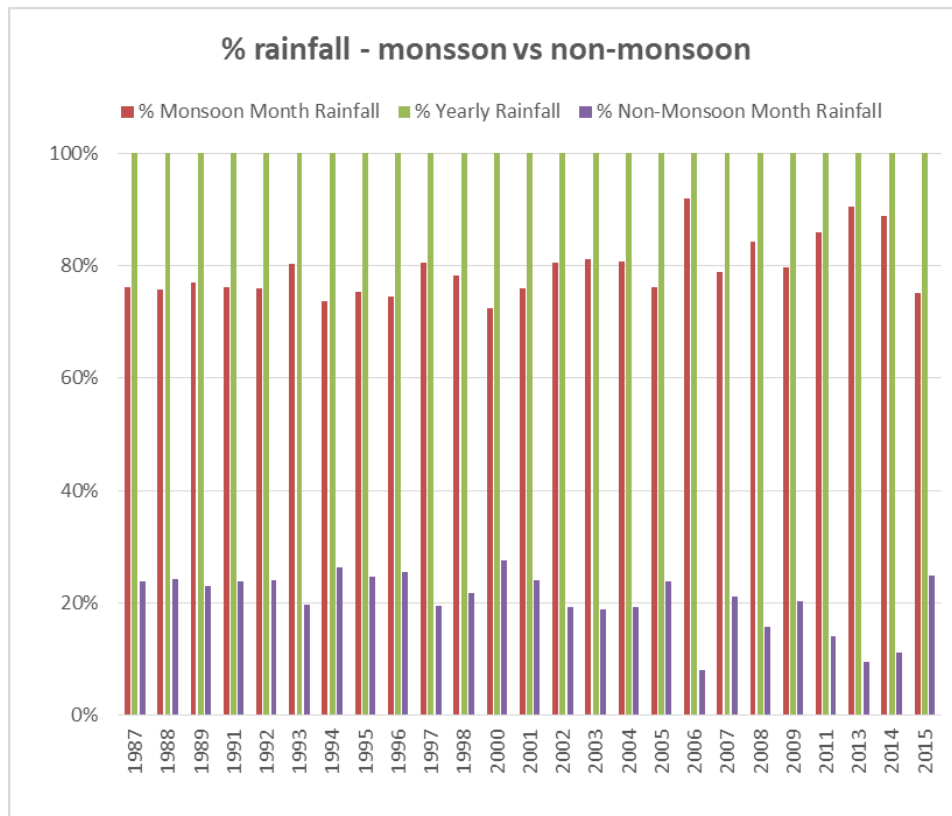


Figure 4.4: Percentage of rainfall. Monsoon vs non-monsoon month

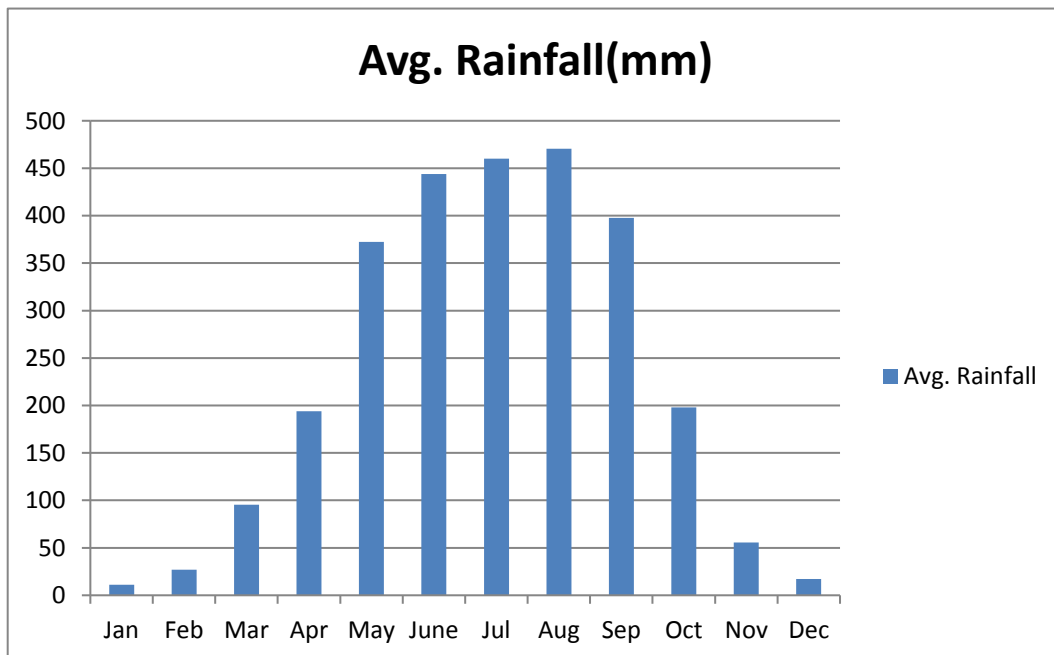


Figure 4.5: Average rainfall (mm) per month

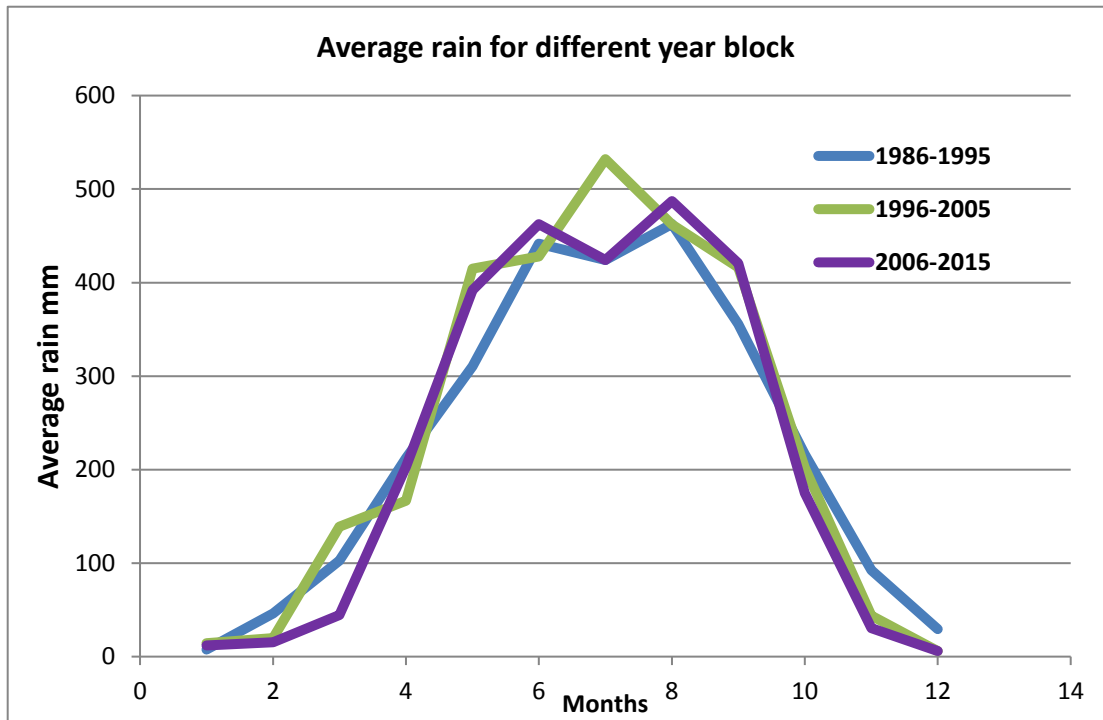


Figure 4.6: Average rain-rate for different year blocks

4.2.1 Point rainfall rate Statistics:

The implementation of high-frequency radio-link networks requires the understanding of signal propagation in rainy media, because microwave systems are especially hampered by rain effects. To successfully estimate a future link margin, annual point rainfall rate statistics must be available in the location where the radio communication link has been planned. Rain rate data within an average year allow the estimation of the percentage of time during which attenuation due to rain is significant. Unfortunately, long-term rainfall rate data covering the whole distributions are not always available everywhere.

An integration time of 1-minute is selected by the ITU as a compromise between experimental accuracy and the amount of rainfall data collected. In many

countries all over the world, long-term rain statistics are only available for long integration time of perhaps one hour or more. Since rainfall rate data at higher than 1-minute integration time are more readily available than 1-minute integration time data, methods for the conversion of rainfall rate distribution with variable integration time to the equivalent 1-minute would be very helpful. This is because most rain induced attenuation prediction methods available (to name a few; the ITU-R model (ITU-R, 2017b) , the DAH model (Dissanayake & Allnutt, 1997), the Crane models (Crane, 1980; Crane & Shieh, 1989) utilize the 1-minute rainfall rate data for a certain range of time percentage.

The Rainfall rate is normally determined for a particular blackout rate. This rate is typically 0.01% of a normal year. The blackout rate is characterized as a factual computation that is utilized to anticipate the level of time that rain attenuation surpasses a specific limit. On the off chance that level of surpassed time is 100%, it implies it rains intensely each of the 365 days or 8760 hour and connection is fizzled for every one of the 8760 h. Correspondingly, in the event that it is 1%, it implies down-pour surpasses for 87.60 h in a year causing link failure, in the event that it is 0.01%, it implies link fails for 0.876 h or 52.56 min in a year. Practically all models are determined for 0.01% rainfall exceedance. A wide range of terms are utilized for indicating the percent of time variable. This incorporates outage percentage, blackout rate, exceedance rate, accessibility, reliability or dependability. If P is probability of link not being available for certain percent of time in a year, at that point $(100-P)$ is the connection accessibility or link reliability. Hence an exceedance probability of 0.01% means an expected outage of 0.01% or 53 min per year and it denotes a link availability of 99.99%. For rainfall estimation we consider exceedance probability

rather than the non-exceedance probability. Exceedance probability(p) gives the probability that certain rainfall or higher will occur in a given year.

Thus, the long-term behaviour of rain rate is described by what is called a cumulative distribution or exceedance curve. If our microwave communication is designed to take care of link budget margin at 0.01 percentage of year rain rate it means outage time per year will not be more than 53 minutes. Thus, for a design engineer working in higher frequency communication system design rain rate at exceedance 0.01 percent is very important. The following table gives the connection between percent times as used in higher frequency communication network design

TABLE 4.2: RELATION BETWEEN PERCENTAGE TIME AND ABSOLUTE TIME

Percentage time	Absolute time out of one year
0.1	8.76 Hours
0,01	52.56 Minutes
0.001	5.26 Minutes
0.0001	0.53 Minutes

For broadcasting microwave communication systems rain exceedance rate at 0.01 percent of time will suffice because it ensures system outage time less than 53 minutes in an average year but for a design engineer catering to Navigation or Telemedicine sector system must be designed to take care of 0.0001 percent rain rate exceedance. A communication link outage of 53 minutes in an average year for telemedicine sector cannot be allowed.

For any stochastic event such as rain fall there is another term recurrence interval or return period T .

$$\text{Return period } T = \frac{1}{p} \quad (1)$$

where p = exceedance probability of event.

Return period is the term more used in Hydrology. Design engineers in hydrology are also concerned with the extreme rainfall events obviously the longevity of their project like dams and bridges depends upon how robust are their structure to withstand the extreme rainfall events.

4.2.2 Rainfall IDF Curves:

The rainfall intensity–duration–frequency (IDF) curves are graphical representations of the probability that a given average rainfall intensity will occur within a given period of time (Dupont, 2006). Providing mathematical relationship between the rainfall intensity I , the duration D , and the return period T (or equivalent to the annual frequency of exceedance p), the IDF curves allow for the estimation of the return period of an observed rainfall event or conversely of the rainfall intensity corresponding to a given return period. IDF curve provides a method to establish the relationship between the magnitude of a hydrological variable and its frequency.

For our given work IDF curve were drawn for the historical rain data of Aizawl for the duration 1986 to 2015 a period of 30 years.

Following procedure was used to derive IDF curve

Step 1:

- Yearly rainfall data is arranged in descending order of magnitude.
- First data at top is assigned rank 1 next rank 2 and so on.
- The last data will have a rank n equal to total data point in sample.
- Exceedance probability is calculated using Weibull's method.

- If m is the rank of a data point and n is the number of data then exceedance probability that random variable X is greater than or equal to x_m is given by

$$P = P(X \geq x_m) = \frac{m}{n+1} \quad 1)$$

- Return period is calculated as inverse of exceedance probability.

Plot the exceedance curve with probability or return period along axis of x and ordinate as value of random variable.

Applying the above method, the annual exceedance curve is obtained as shown below.

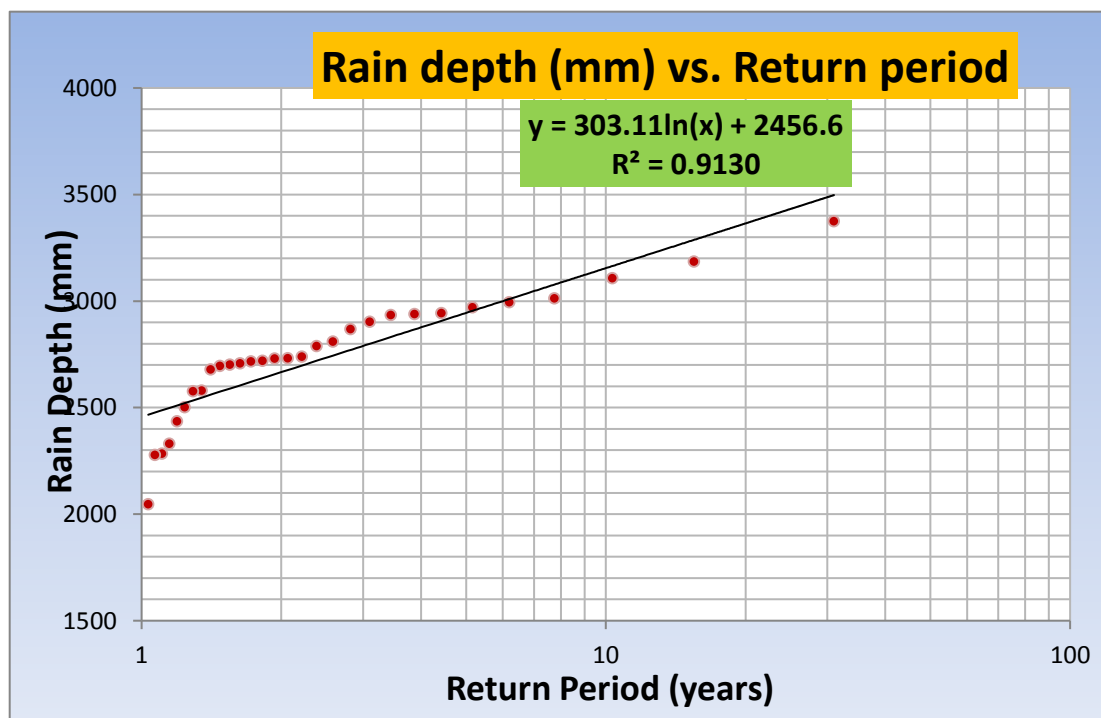


Figure 4.7: Annual rainfall depth Exceedance curve for the district Aizawl Mizoram

The annual rainfall depth Y and the return period T are related by the equation

$$Y = 303.011 \log_e(T) + 2456.6 \quad mm \quad (2)$$

Return period T is the inverse of exceedance probability.

4.2.3 Rain depth Exceedance curve for integration time 24 hours:

Rain depth (mm) exceedance curve with integration time 24 hours were obtained as follows.

- Rainfall data of particular month is arranged in descending order giving highest rainfall rank 1 and so on.
- Monthly data is converted to daily data by simple averaging technique.
- Exceedance probability of all ranks is calculated using Weibull's method.

$$p = P(X \geq x_m) = \frac{m}{n + 1}$$

- Return period is calculated as inverse of exceedance probability.
- Exceedance curve is plotted with return period or exceedance probability on axis of x and rain depth on axis of y.

Exceedance curve is shown below.

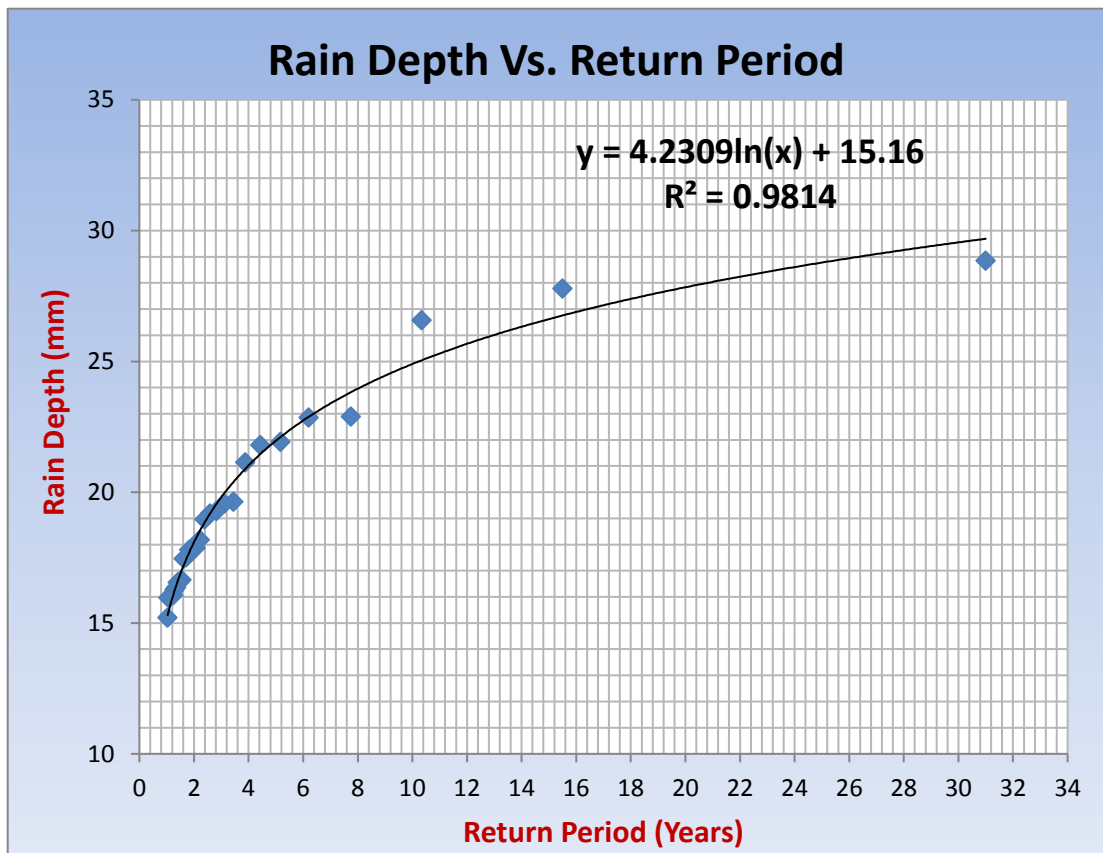


Figure 4.8: Rain depth exceedance curve with integration time 24 hours

From logistic regression analysis the 24 hours rain depth (mm) R_{24} and return period T are related by the equation.

$$R_{24} = 4.2309 \log_e (T) + 15.16 \quad (3)$$

To calculate the rainfall intensity in mm/hour we used the IDE equation developed by Kothyari and Garde (Kothyari & Garde, 1992). Kothyari and Garde utilizing the rain data of 78 rain gauge station from all over India developed an equation for the calculation of annual rainfall intensity (mm/hr.). This equation is widely used across the country for hydrologic, hydraulic and water resource system.

The Kothyari and Garde equation is given below.

$$L_t^T = C \left(\frac{T^{0.20}}{t^{0.71}} \right) (R_{24}^2)^{0.33} \quad (4)$$

The value of C for different geographical region of India is given in table below

TABLE 4.3: C VALUE FOR DIFFERENT REGION OF INDIA

Geographical region	Zone	C
Northern India	1	8.0
Central India	2	7.7
Western India	3	8.3
Eastern India	4	9.1
Southern India	5	7.1

Where

T = return period

t = duration of rain in hour

R_{24}^2 = 24 hour 2 year return period annual rain depth

L_t^T = rain intensity in mm/hour

If we choose $t = 1$ hour the above equation can give rain intensity for any exceedance value for one hour integration time. The value of R_{24}^2 for Aizawl can be calculated by using equation (3) developed by us for the Aizawl region.

Using equation (3) by putting $T = 2$ years the value of annual rain depth for 2 years return period was calculated and then and then by utilizing Kothyari and Garde equation (4) the rain rate (mm/hr) exceeded for different percentage of time was obtained for 1 hour integration time. The values obtained are given in table below.

TABLE 4.4: EXCEEDANCE RAIN RATE (MM/HOUR) WITH INTEGRATION TIME ONE HOUR.

Percentage time	Absolute time out of one year in minutes	Rain rate R (mm/hr) exceeded with integration time 60 mins
0.5	2628	20.67
0.3	1576	22.90
0.2	1051	24.82
0.1	526	28.51
0.05	263	32.72
0.03	158	36.78
0.02	105	39.88
0,01	53	45.19
0.0005	26	53.15
0.0002	11	63.67
0.0001	3	71.62

4.2.4 Experimental Data:

Five year daily rain data (2014- 2018) for the experimental location with integration time one hour was obtained from regional IMD centre Guwahati. From the data we calculated the cumulative statistics of rainfall by Weibull's method and obtained the rainfall rate with integration time one hour with different exceedance probability.

The result obtained is shown in table below:

TABLE 4.5: Measured Rain Rate vs. Exceedance

Exceedance probability	0.5	0.3	0.2	0.1	0.05	0.03	0.02	0.01	0.005	0.002	0.001
Rain rate (mm/hr)	19.12	20.6	23.8	27.5	31.2	37.22	38.32	44.3	52.01	64.12	70.21

4.2.5 Comparison of Experimental Data with Historical Data:

The measured rain rate with integration time one hour was compared with the one hour integration time rain rate obtained from historical rain data. The two rain rates one observed during the experimental period and the other derived from historical data were compared. The comparison is shown graphically below.

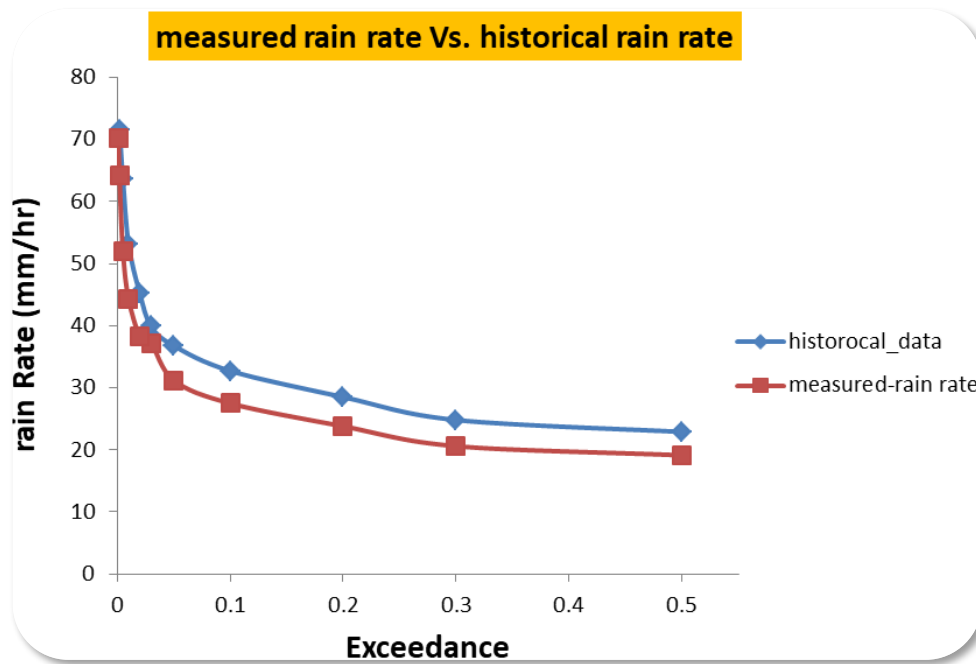


Figure 4.9: Measured and Historical rain rates with integration time one hour.

The sample data and the population data are showing nice agreement. The MAE, MSE and RMSE for the data were obtained as follows.

Table 4.6: Table of comparison metrics

MAE	MSE	RMSE
-1.0455	1.721	1.206

The coefficient of Determination R^2 was found to be

$$R^2 = 0.973 \quad (5)$$

Hence it can be concluded that the sample data is in perfect agreement with the population data.

4.3 Conversion of rain rate from 60 Minute to one minute integration time

Now we have exceedance rain rate with one hour integration time. To convert this rain rate to rain rate with one minute integration time a MATLAB based statistical conversion method provided by ITU in their recommendation ITU-R P.837.7 (ITU-R, 2017a) was used. The inputs required to be given to software are

- The latitude and Longitude of the place
- T-minute integrated $P(R)$: percentage exceedance value between (0–100%).
- T-minute integrated $P(R)$: rain rate values (mm/h)
- Both the percentage Exceedance value and rain rate values are to be input by comma separation.
- Source integration time. In our case it is 24 hours.

The GUI of ITU-R.P837.7 with Latitude and Longitude of Durtlang is shown below.

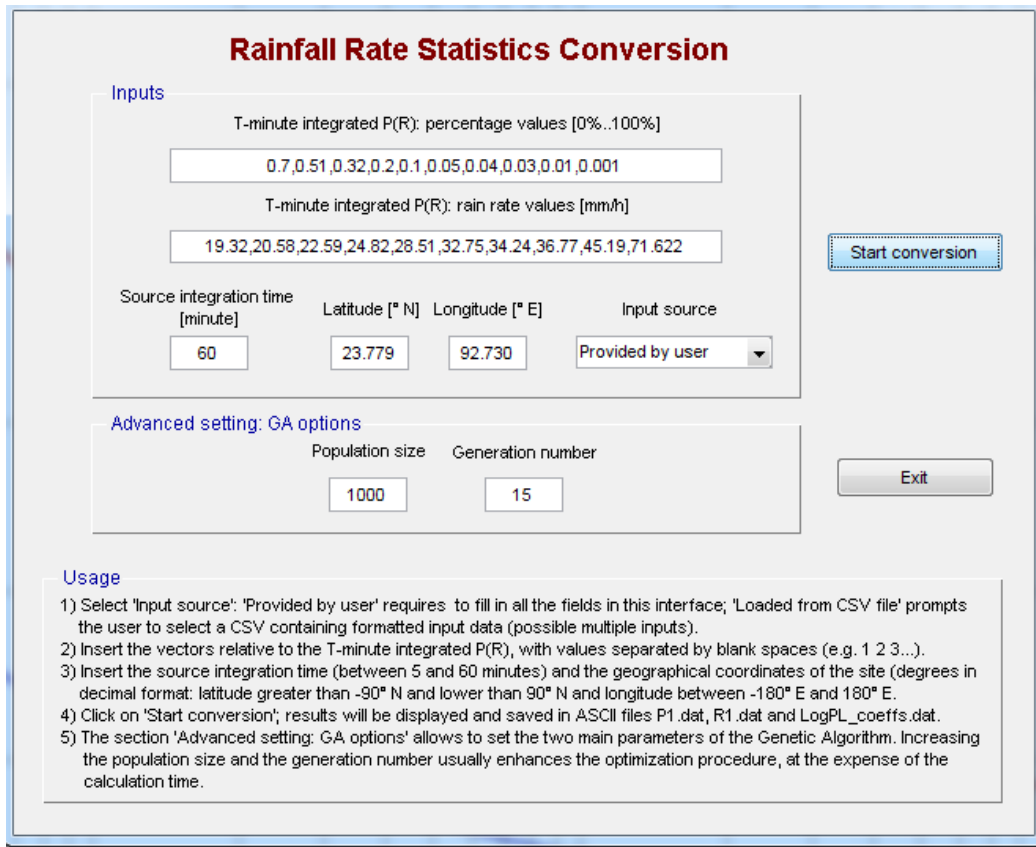


Figure 4.10: GUI of ITU-R P.837.7

After providing the inputs to GUI the conversion was run in MATLAB and it produced the graph depicting the input one-hour integration time rain rate in blue and the converted 1 minute integration time rain rate in red for different exceedance percentage. The graph is shown below

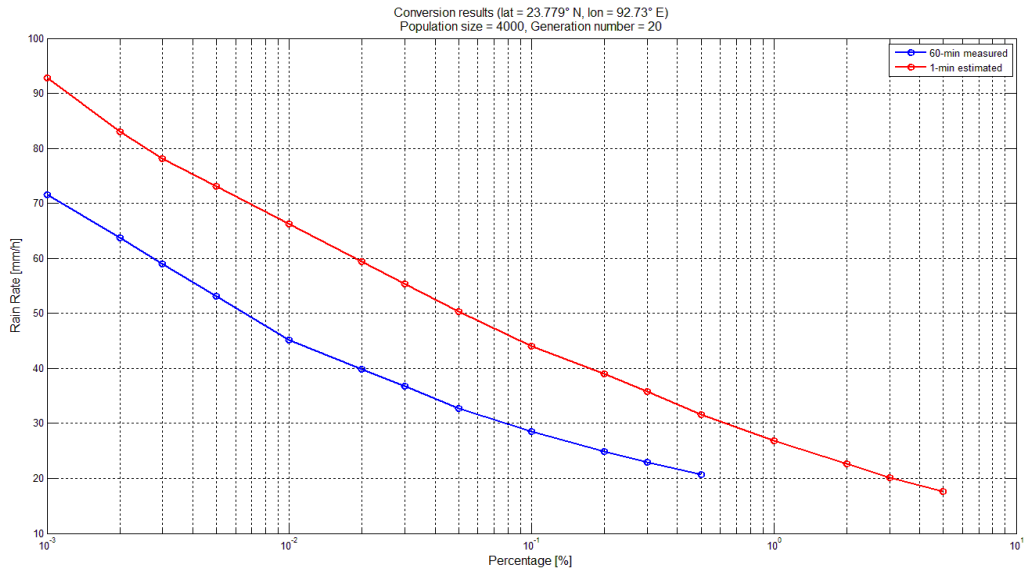


Figure 4.11: Exceedance rain-rate conversion from integration time one hour to 1 minute

The software also generates data files $P_1.dat$ and $R_1.dat$ that generates respectively the probability and rain rate vectors of the estimated 1 min integrated $P(R)$, and data file $log_PL_coeffs.dat$ that contains the values of power law expression defining the estimated 1 min integrated $P(R)$. This GUI software is very useful since it gives the corresponding 1 min integrated rainfall rate from 60 min measured values. The 1 min integrated rain rate values are always required to be provided to different models for correct rain attenuation estimations. The importance of 1 min integration rain rate values is that some rainfall maybe of very small durations but of very high intensities. Thus, we have obtained the estimated exceedance rain rate with one minute integration time. The conversion is summarized in table below.

Table 4.7: Conversion of rain rate from integration time 60 Minute to 1 Minute

Exceedance probability	Rain rate (mm/hour) Integration time 60 Minute	Rain rate(mm/hour) Integration time1 minute
0.5	20.67	31.25
0.3	22.9	36.72
0.2	24.28	39.32
0.1	28.51	44.67
0.05	32.72	50.12
0.03	36.78	54.82
0.02	39.88	59.92
0.01	45.19	66.12
0.005	53.15	71.32
0.002	63.67	85.12
0.001	71.62	94.62

It can be observed from the table as the integration time is decreased rain intensity increases. At exceedance of 0.01 percent of an average year the rain rate at 60 minute integration time was 45.19 mm per hour but at 1 minute integration time it becomes 66.12 mm per hour.

The conversion is shown below in form of graph.

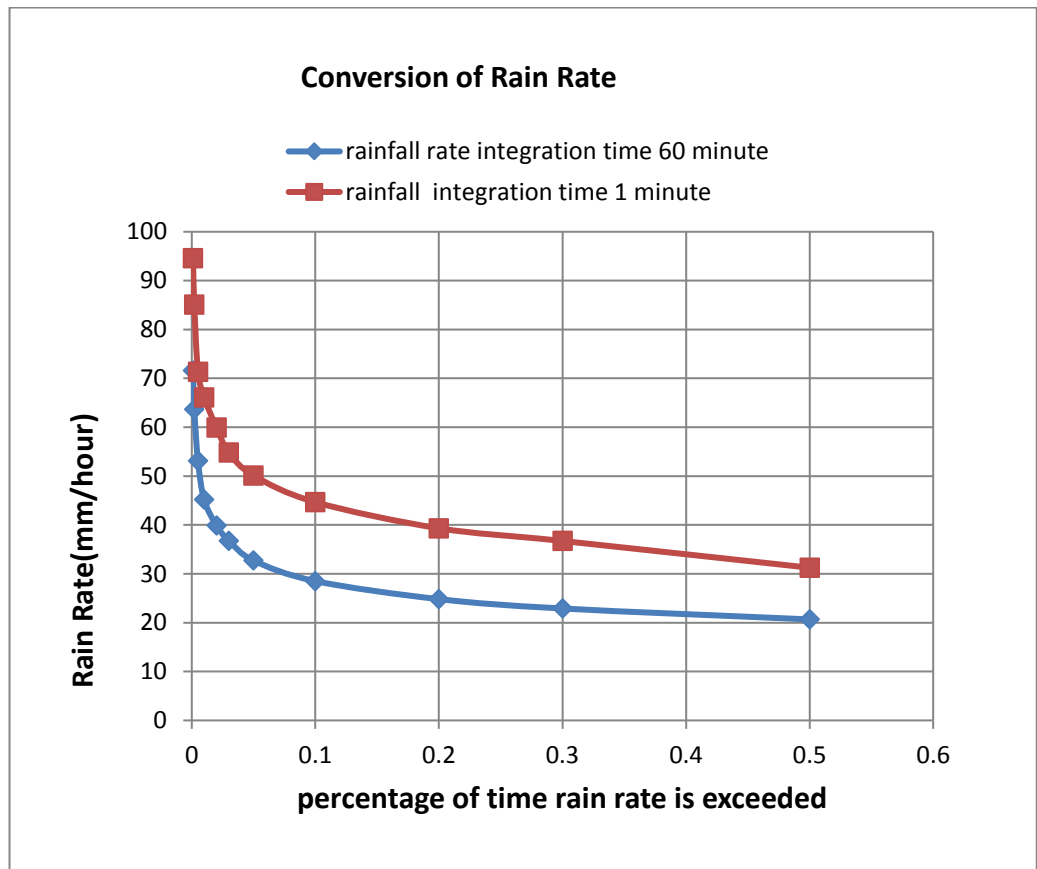


Figure 4.12: Rain rate conversion

4.4 Proposed Regression based rain rate model:

By the logistic analysis of rain rate as response variable and exceedance probability as explanatory variable we propose following two model for Aizawl region to relate rain rate R and exceedance probability (p).

4.4.1 Rain Rate integration time one minute:

Using logistic regression the rain rate with integration time one minute can be related to exceedance probability. The equation obtained by applying logistic regression connecting the exceedance rain rate with one minute integration time R_1 in mm/hour with the exceedance probability p in percentage time is given as.

$$R_1(\text{Model}) = -9.933 \log_e(p) + 27.368 \quad (6)$$

The above equation is a good fit as verified by R^2 value of 0.98 can be used for deriving exceedance rain rate with integration time of one minute for the entire Aizawl region. The regression analysis is shown graphically below.

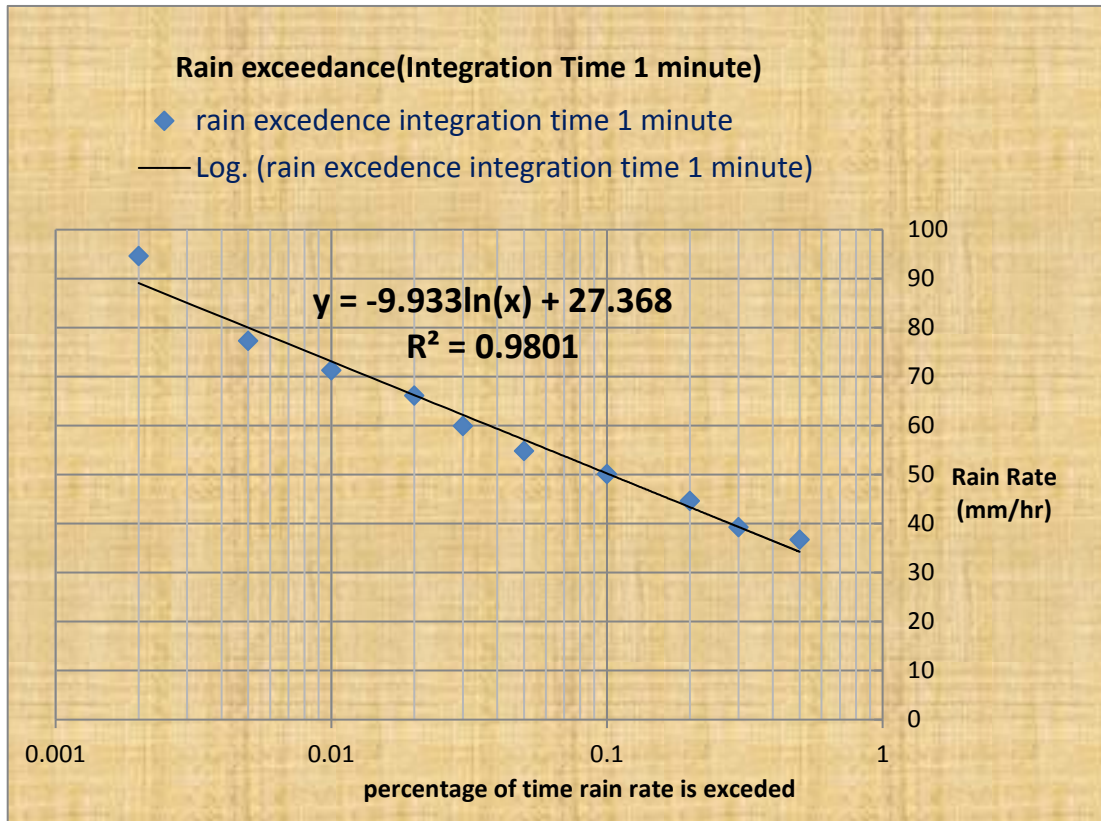


Figure 4.13: Estimated exceedance with rain-rate (mm/hour) integration time 1 minute

4.4.2 Rain Rate integration time 60 Minute:

Similarly, the regression equation obtained for exceedance rain rate with one hour integration time can be used as a reference equation by future researcher or microwave communication system design engineer.

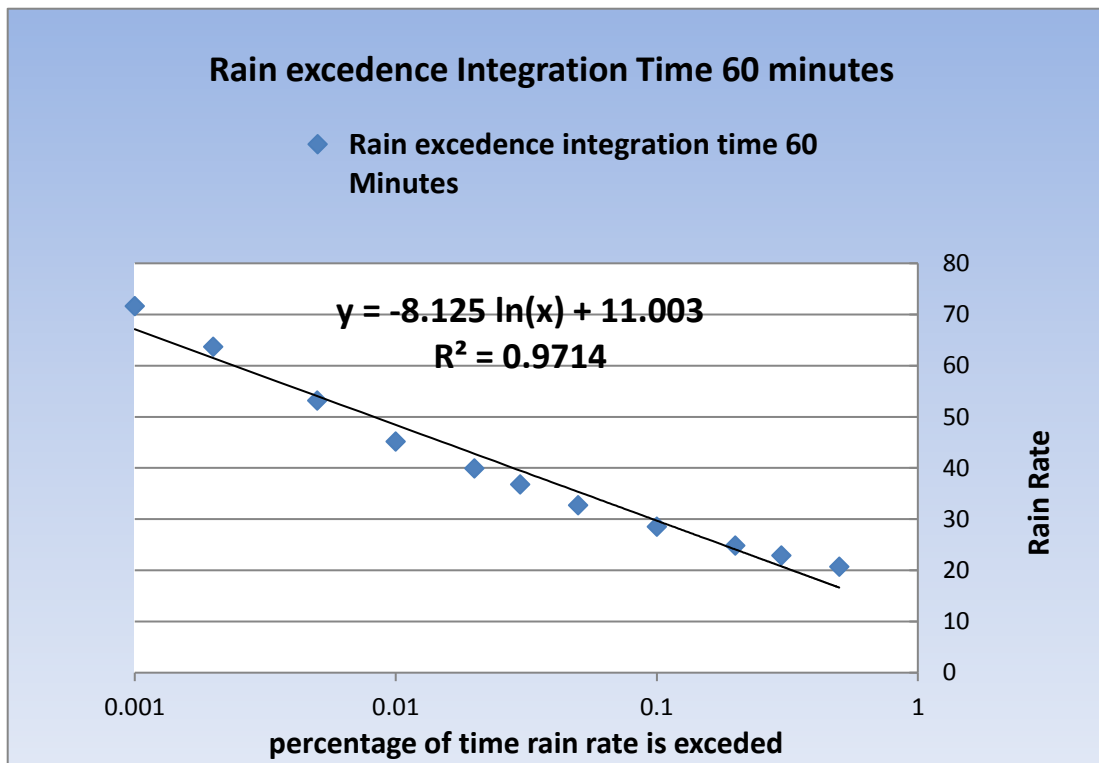


Figure 4.14: Exceedance rain rate with integration time one hour or 60 minutes

The equation derived by applying logistic regression connecting exceedance rain rate with one hour integration time with exceedance probability p may be used for entire Aizawl region.

$$R_{60}(\text{Model}) = -8.135 \log_e(p) + 11.003 \quad (7)$$

This equation is an excellent fit as verified by a R^2 value of 0.9714.

4.5 Comparison with other models:

4.5.1 Mopfouma Model:

Mopfouma (Moupfouma et al., 1990) proposed a model for cumulative rain rate which approximates a lognormal distribution at low rain rates and a gamma distribution at high rain rate. This model is widely applicable both in temperate as well as tropical climates. Estimated exceedance rain rate with one hour integration

time were used to calculate the exceedance rain rate with one minute integration time using Moupfouma model.

$$p(R \geq r) = 10^{-4} \left(\frac{R_{0.01}}{r + 1} \right)^b e^{u(R_{0.01} - r)} \quad (8)$$

$R_{0.01}$ = rain rate exceeded during 0.01% of time in average year

r = Rain rate exceeded for a fraction of time in average year

Where parameter b is given by

$$b = \left[\frac{r - R_{0.01}}{R_{0.01}} \right] \log_e \left(1 + \frac{r}{R_{0.01}} \right) \quad (9)$$

Parameter u is given by

$$u = \left[4 \log_e \left(\frac{10}{R_{0.01}} \right) \right] e^{-\gamma(r/R_{0.01})^\beta}$$

$$\beta = 0.214$$

$$\gamma = 1.066$$

$$R_{0.01} = \alpha M^\delta$$

α, δ are regression coefficient

M = mean annual rainfall intensity $\left(\frac{mm}{hour} \right)$

$$\alpha = 12,2903, \quad \delta = 0.2973$$

Estimated exceedance rain rate with one hour integration time were used to calculate the exceedance rain rate with one minute integration time using equations mentioned above by Moupfouma model. The comparison with our estimated rain rate with one minute integration time is shown below by the scatter plot.

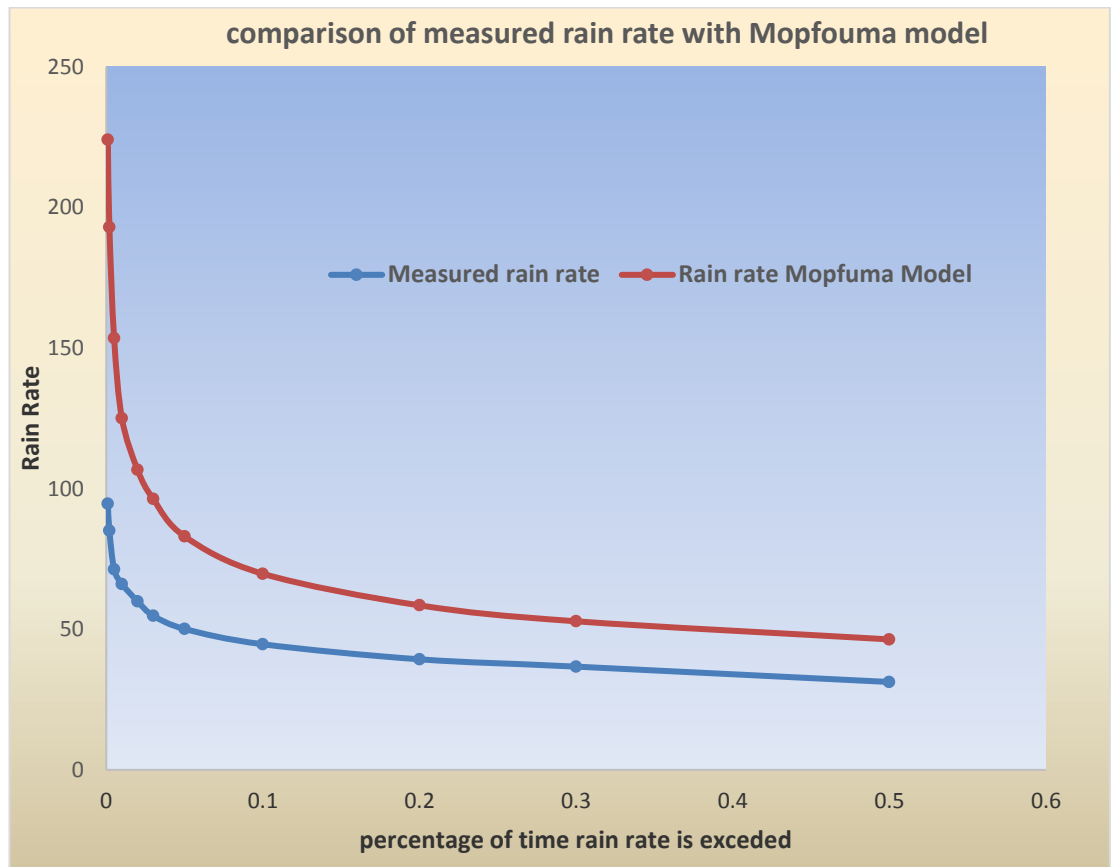


Figure 4.15: Comparison of the data with Mopfouma Model.

At low rain rates the estimated values are close to the values predicted by Moupfouma model but at high rain rates the Moupfouma model overestimates the rain rates. Predicted rain rate by Mopfouma Model does not match with our experimental data as evident from the above graph.

4.5.2 Segal Model:

The power law relationships can be utilized to approximate the association between the rainfall rate at 1-minute integration time and that obtained at other integration times. One method (Segal, 1986) to convert rainfall data with finite integration time to equivalent 1-minute integration time is expressed as the following

$$R_1(P) = aP^b R_t(P) \quad (10)$$

Where,

$R_1(P)$: rain rate with integration time 1 minute for exceedance probability p

$R_t(P)$: rain rate with integration time t minutes

a and b are regression coefficient.

4.5.3Burgueno Model:

Based on 49 years of rainfall rate data measured in Barcelona, Spain, investigators (Burgueño et al., 1988) suggested that the relationship could be expressed as

$$R_1(P) = a R_t(P) \quad (11)$$

Where $R_1(P)$ and $R_t(P)$ are the rainfall rates exceeded with equal probability P for integration time of 1 minute and t minutes respectively. The parameter of a and b for the conversions from x -minute to 1-minute rainfall rate statistics is given in the table below.

TABLE 4.8: PARAMETERS FOR SEGAL AND BURGUENO METHOD

t (mins)	Segal's method		Burgueno's method	
	a	b	a	b
5	1.156	0	1.28	0.98
10	1.263	0	1.69	0.94
30	1.569	-0.015	1.32	1.06
60	1.759	-0.054	0.92	1.24

4.5.4 Comparison with Segal and Burgueno Model:

Exceedance rain rate with one minute integration time predicted by both the models and were compared with our estimated rates. The comparison is summarized in scatter diagram below.

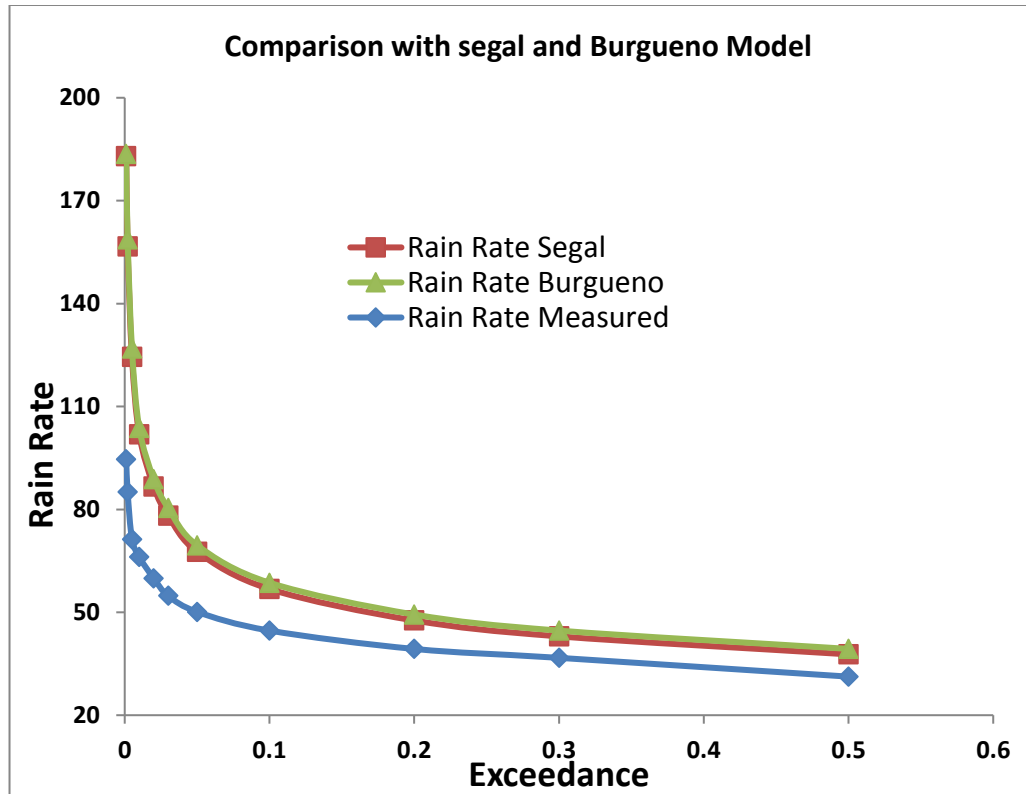


Figure 4.16: Comparison of measured rain rate with Segal and Burgueno Model

It can be concluded from the graph that both the Segal And Burgueno Model overestimates the measured the rain rate. Both these models are regression based model developed from the measurements in temperate climate.

4.6 Proposed Power Regression Model For rain Rate Conversion:

We propose a power law, based on power regression analysis of rain rate conversion data obtained in table 8 for conversion of Rain Rate from integration time of 60 Minute to 1 minute for Aizawl region. We did an power regression analysis of rain rate with integration time 60 minute as explanatory variable and rain rate with one

minute integration time as response variable and obtained following power law relation between them.

$$R_1 = A(R_{60})^B \quad (12)$$

A, B are regression coefficient

$$A = 2.6142$$

$$B = 0.8418$$

The power regression analysis is shown graphically in figure below.

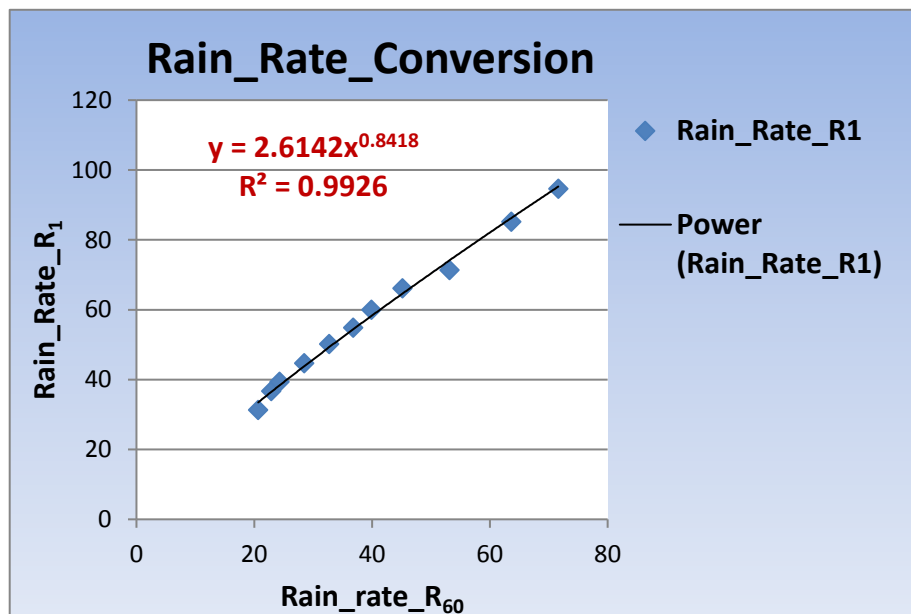


Figure 4.17: Proposed Rain Rate Conversion Model

4.7 Rain Attenuation Analysis:

4.7.1 Introduction:

The explosive growth in demand of satellite communication network has already congested the currently available spectrum in C band and Ku band and urgent need is being felt among the system designers in microwave to shift to higher frequency band beyond 20 GHz. Higher frequency band ensures higher availability of frequency spectrum smaller size of electronics just to give few examples of advantage of using higher frequency bands. However, the advantage that we get from using higher frequency comes with a gross disadvantage. Rain attenuation of the signal increases exponentially as higher and higher frequencies are used. So, the signal suffers strong fade as the wavelength approaches the drop size of rain. Thus, to design a communication system for high frequency satellite channel proper link budget planning is to be done to take adequate care of fade margins at the critical exceedance rate.

Rain induced attenuation is given as probabilistic value because of the statistical variation in rainfall rates. This is often expressed as attenuation or signal loss exceeded for certain percentage of time such as perhaps 0.1% of the year. Rainfall is a serious cause of attenuation for radio wave propagation at frequency bands above 10GHz. It is important to accurately predict the fading outage due to rain. A reliable prediction of attenuation by rain is necessary for a system designer to realistically determine link availability, establish the link margin and provide means to combat network outage.

4.8 Prediction of rain attenuation models:

4.8.1 ITU model (ITU-R P.618-13, 2017):

International Telecommunication union (ITU) is a united nation organization dealing with radio communication standards all over the world. The ITU radio communication sector (ITU-R) is one among the three divisions of the International Telecommunication Union (ITU) which is responsible for radio communication. It manages the international radio- frequency spectrum and satellite orbit resources and also enhances standards for radio communication systems with the objective of ensuring the effective use of the spectrum.

The ITU-R provides global rain statistics by dividing the earth into rain regions and assigning a rain rate to each region along with the probability of that rain rate being exceeded [6]. This model uses the rain rate at 0.01% probability level for the estimation of attenuation and then applies an adjustment factor to the predicted rain fade depth for other probabilities. It can be used for the frequencies from 4 - 55 GHz and 0.001 - 5% percentage probability range. It is based on log-normal distribution and both rain intensity and path attenuation distribution conform to the same log-normal distribution. Inhomogeneity in rain in both horizontal and vertical directions is considered in the prediction [13].

The Experimental set up for RF measurement for the current study was set up at Doordrashan Kendra Durtlang Aizawl. The project site has the following geographical parameters.

TABLE 4.9: GEOGRAPHICAL LOCATION OF THE PROJECT SITE

Parameters	Values
Latitude	23.7779 °N
Longitude	92.7307 °E
Altitude above mean sea level	1384 m

Ku Band signal of DD free dish from the geostationary satellite G-SAT 15 at parking slot of 93.5 °E with the following RF parameters were used for the experimental study.

TABLE 4.10: RF PARAMETERS FOR THE EXPERIMENTAL SET-UP

Parameters	Values
Down Link Frequency	11.09 GHz
Down link Polarization	Vertical
Symbol rate	29.5 MSPS
Receive PDA elevation angle	55.2 °
Receive PDA azimuth angle	221.3 °
Receive PDA diameter	1.2 m

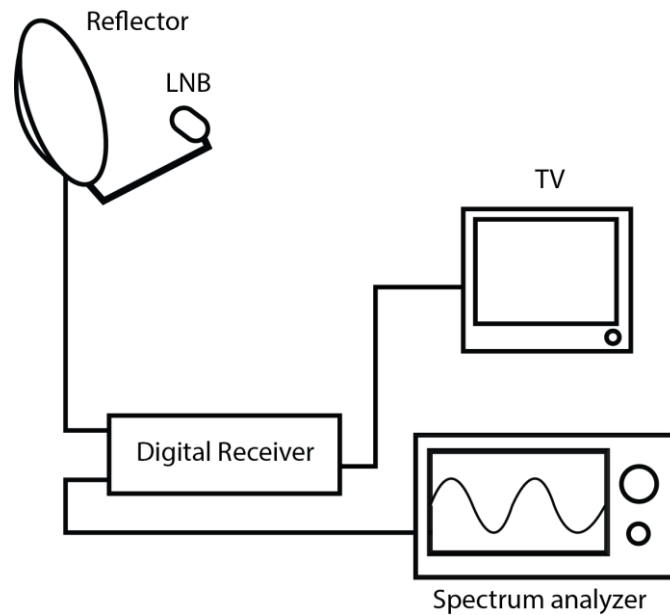


Figure 4.18: The experimental set up

The satellite signal was received with an offset parabolic antenna of diameter 1.2 meter. The vertically polarized Ku band signal was down converted to an L band signal by a LNBC of noise temperature 15K. The down converted signal is fed into a digital receiver and BNC output of digital receiver is fed to Tektronix spectrum analyser having a post detection bandwidth of 10 Hz. The output of spectrum analyser is recorded and stored in a data logger.

4.8.1.1 Calculations of rain attenuation using ITU model

Figure below show the schematic space earth path for the calculation of attenuation by the ITU model.

height of the earth station above mean sea level (h_s) = 1.348 km

h_R = rain height

elevation angle (θ) = 55.2°

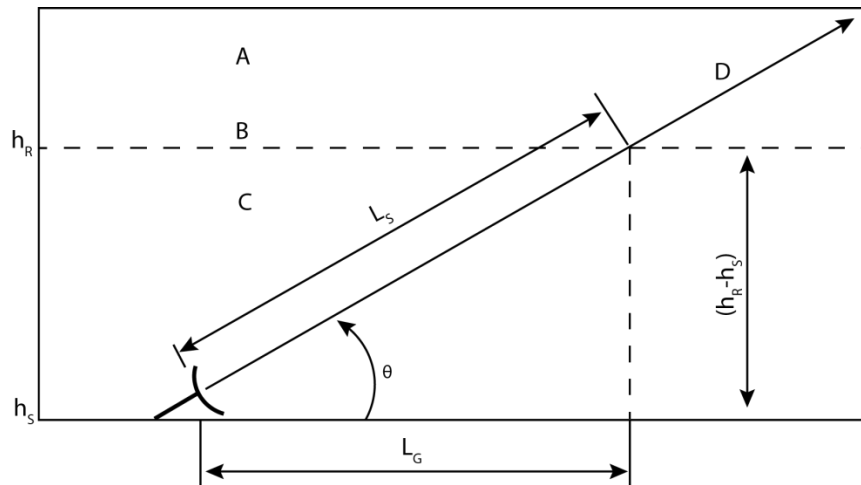


Figure 4.19: Space earth signal path (courtesy ITU)

The following procedure provides estimates of the long-term statistics of the slant-path rain attenuation at the site location for frequencies up to 55 GHz. The following parameters are required

$R_{0.01}$: point rainfall rate for the location for 0.01% of an average year (mm/h)

R_E : effective radius of the Earth (8500 km)

h_s : height above mean sea level of the earth station (km)

θ : elevation angle

ϕ : latitude of the earth station (degrees)

f : frequency (GHz)

Step 1:

Firstly, we calculated the rain height h_R from the ITU recommendation ITU-R P. 839. Rain height h_R is given by the relation.

$$h_R = h_0 + 0.36 \text{ km}$$

where h_0 is the height of zero-degree isotherm at the location. We calculated The value of h_0 from the location data file provided by ITU. The data is

provided for the location from 0 degree to 360 degrees longitude and -90 to +90 latitude. Since the location of our site was not the grid point the data file was loaded into MATLAB and h_0 for the location was calculated by employing the technique of bilinear interpolation using four nearest grid points around the location. The value of h_0 was calculated as

$$h_0 = 4.857 \text{ km}$$

$$h_R = 0.36 + 4.857 = 5.217 \text{ km}$$

Step 2:

The slant path length L_S , below the rain height was calculated as follows

For $\theta \geq 5^\circ$

$$L_S = \frac{(h_R - h_S)}{\sin \theta} \text{ km} \quad (13)$$

For $\theta < 5^\circ$, the following formula is used

$$L_S = \frac{2(h_R - h_S)}{\left(\sin^2 \theta + \frac{2(h_R - h_S)}{R_E}\right)^{\frac{1}{2}} + \sin \theta} \text{ km} \quad (14)$$

The value of L_S was calculated, where $L_S = 4.6681 \text{ km}$

Step 3:

In this step we calculated the horizontal projection of the slant path length from

$$L_G = L_S \cos \theta$$

L_G was calculated, where $L_G = 2.665 \text{ km}$

Step 4:

As a fourth step we were required to calculate rainfall rate $R_{0.01}$, exceeded for 0.01 % of an average year with an integration time of 1 minute. This rate we have already calculated for our experimental site and it was

$$R_{0.01} = 66.12 \text{ mm/hour}$$

Step 5:

In this step we calculated the specific attenuation γ_R , using the frequency dependent coefficients given in recommendation ITU-RP.838 and $R_{0.01}$ by using the power law relation

$$\gamma_R = k (R_{0.01})^\alpha \quad \text{dB/km} \quad (15)$$

Values for the coefficients k and α are determined as functions of frequency (GHz), in the range from 1 to 1000 GHz, from the following equations, which have been developed from curve-fitting to power-law coefficients derived from scattering calculations

$$\log_{10} k = \sum_{j=1}^4 \left(a_j \exp \left[- \left(\frac{\log_{10} f - b_j}{c_j} \right)^2 \right] \right) + m_k \log_{10} f + c_k \quad (16)$$

$$\alpha = \sum_{j=1}^5 \left(a_j \exp \left[- \left(\frac{\log_{10} f - b_j}{c_j} \right)^2 \right] \right) + m_\alpha \log_{10} f + c_\alpha \quad (17)$$

Where

f = frequency (GHz)

k = either k_H or k_V

α = either α_H or α_V

H And V stands for the state of polarization either horizontal (H) or vertical (V)

TABLE 4.11: COEFFICIENT FOR k_H

j	a_j	b_j	c_j	m_k	c_k
1	-5.33980	-0.10008	1.13098		
2	-0.35351	1.26970	0.45400		
3	-0.23789	0.86036	0.15354		
4	-0.94158	0.64552	0.16817		

TABLE 4.12: COEFFICIENT FOR k_V

j	a_j	b_j	c_j	m_k	c_k
1	-3.80595	0.56934	0.81061		
2	-3.44965	-0.22911	0.51059		
3	-0.39902	0.73042	0.11899		
4	0.50167	1.07319	0.27195		

TABLE 4.13: COEFFICIENT FOR α_V

j	a_j	b_j	c_j	m_α	c_α
1	-0.14318	1.82442	-0.55187		
2	0.29591	0.77564	0.19822		
3	0.32177	0.63773	0.13164		
4	-5.37610	-0.96230	1.47828		
5	16.1721	-3.29980	3.43990		

TABLE 4.14: FREQUENCY-DEPENDENT COEFFICIENTS FOR ESTIMATING SPECIFIC RAIN ATTENUATION USING EQUATIONS (16), (17) AND (15)

f (GHz)	k_H	α_H	k_V	α_V
4	0.0001071	1.6009	0.0002461	1.2476
4.5	0.0001340	1.6948	0.0002347	1.3987
5	0.0002162	1.6969	0.0002428	1.5317
5.5	0.0003909	1.6499	0.0003115	1.5882

f (GHz)	k_H	α_H	k_V	α_V
6	0.0007056	1.5900	0.0004878	1.5728
7	0.001915	1.4810	0.001425	1.4745
8	0.004115	1.3905	0.003450	1.3797
9	0.007535	1.3155	0.006691	1.2895
10	0.01217	1.2571	0.01129	1.2156
11	0.01772	1.2140	0.01731	1.1617
12	0.02386	1.1825	0.02455	1.1216
13	0.03041	1.1586	0.03266	1.0901
14	0.03738	1.1396	0.04126	1.0646
15	0.04481	1.1233	0.05008	1.0440
16	0.05282	1.1086	0.05899	1.0273
17	0.06146	1.0949	0.06797	1.0137
18	0.07078	1.0818	0.07708	1.0025
19	0.08084	1.0691	0.08642	0.9930
20	0.09164	1.0568	0.09611	0.9847
21	0.1032	1.0447	0.1063	0.9771
22	0.1155	1.0329	0.1170	0.9700
23	0.1286	1.0214	0.1284	0.9630
24	0.1425	1.0101	0.1404	0.9561
25	0.1571	0.9991	0.1533	0.9491
26	0.1724	0.9884	0.1669	0.9421
27	0.1884	0.9780	0.1813	0.9349
28	0.2051	0.9679	0.1964	0.9277
29	0.2224	0.9580	0.2124	0.9203
30	0.2403	0.9485	0.2291	0.9129
31	0.2588	0.9392	0.2465	0.9055
32	0.2778	0.9302	0.2646	0.8981
33	0.2972	0.9214	0.2833	0.8907
34	0.3171	0.9129	0.3026	0.8834
35	0.3374	0.9047	0.3224	0.8761
36	0.3580	0.8967	0.3427	0.8690
37	0.3789	0.8890	0.3633	0.8621
38	0.4001	0.8816	0.3844	0.8552
39	0.4215	0.8743	0.4058	0.8486
40	0.4431	0.8673	0.4274	0.8421

f (GHz)	k_H	α_H	k_V	α_V
41	0.4647	0.8605	0.4492	0.8357

For our set up downlink frequency was 11.09 GHz and polarization was vertical

The value of k and α were calculated as

$$k = 0.01731$$

$$\alpha = 1.1617$$

Value of specific attenuation was calculated from the relation

$$\gamma_R = k(R_{0.01})^\alpha \quad (18)$$

$$\gamma_R = 2.251 \text{ dB/km} \quad (19)$$

Step 6:

Further we calculated the horizontal reduction factor, $r_{0.01}$, for 0.01% of the time by the equation

$$r_{0.01} = \frac{1}{1 + 0.78 \sqrt{\frac{L_G \gamma_R}{f}} - 0.38(1 - e^{-2L_G})} \quad (20)$$

The value we calculated was

$$r_{0.01} = 1.4148 \quad (21)$$

Step 7:

Now we calculated the vertical adjustment factor, $v_{0.01}$, for 0.01% of the time as

$$\sigma = \tan^{-1} \left(\frac{h_R - h_S}{L_G r_{0.01}} \right) \text{ degrees} \quad (22)$$

σ Was calculated to be 1.017 degrees

For $\sigma > \theta$,

$$L_R = \frac{L_G r_{0.01}}{\cos \theta} \text{ km}$$

Else

$$L_R = \frac{(h_R - h_S)}{\sin \theta} \text{ km}$$

Since in our case else condition was true we calculated L_R by the later equation

And its value was calculated to be

$$L_R = 4.6679 \text{ km}$$

If $|\phi| < 36^\circ$,

$$\chi = 36 - |\phi| \text{ degree}$$

Else,

$$\chi = 0 \text{ degree}$$

Since latitude ϕ in our case was less than 36° , the value of χ was calculated to be

$$\chi = 12.223 \text{ degrees}$$

Value of $v_{0.01}$ was calculated using the formulae given below

$$v_{0.01} = \frac{1}{1 + \sqrt{\sin \theta} \left[31 \left(1 - e^{-\left(\frac{\theta}{1+\chi}\right)} \right) \frac{\sqrt{L_R Y_R}}{f^2} - 0.45 \right]} \quad (23)$$

Value of $v_{0.01}$ comes out to be

$$v_{0.01} = 0.8442$$

Step 8: Effective path length is given by the relation

$$L_E = L_R v_{0.01} \quad (24)$$

$$L_E = 3.9408 \text{ km}$$

Step 9: The predicted attenuation exceeded for 0.01% of an average year is obtained using the relation

$$A_{0.01} = \gamma_R L_E \quad (25)$$

$$A_{0.01} = 8.871 \text{ dB} \quad (26)$$

Step 10: The estimated attenuation to be exceeded for other percentages of an average year, in the range 0.001% to 5%, is determined from the attenuation to be exceeded for 0.01% for an average year by the relation

$$A_p = A_{0.01} \left(\frac{p}{0.01} \right)^{-(0.655+0.033 \ln(p)-0.045 \ln(A_{0.01})-\beta(1-p) \sin \theta)} \quad (27)$$

Where the value of β was determined as follows

$$\text{If } p \geq 1\% \text{ or } |\phi| \geq 35^\circ \quad \beta = 0$$

$$\text{If } p < 1\% \text{ and } |\phi| < 36^\circ \text{ and } \theta \geq 25^\circ \quad \beta = 0.005(|\phi| - 36)$$

$$\text{Otherwise} \quad \beta = 0.005(|\phi| - 36) + 1.8 - 4.2$$

Attenuation for other exceedance percentage were calculated and summarized in the graph bellow.

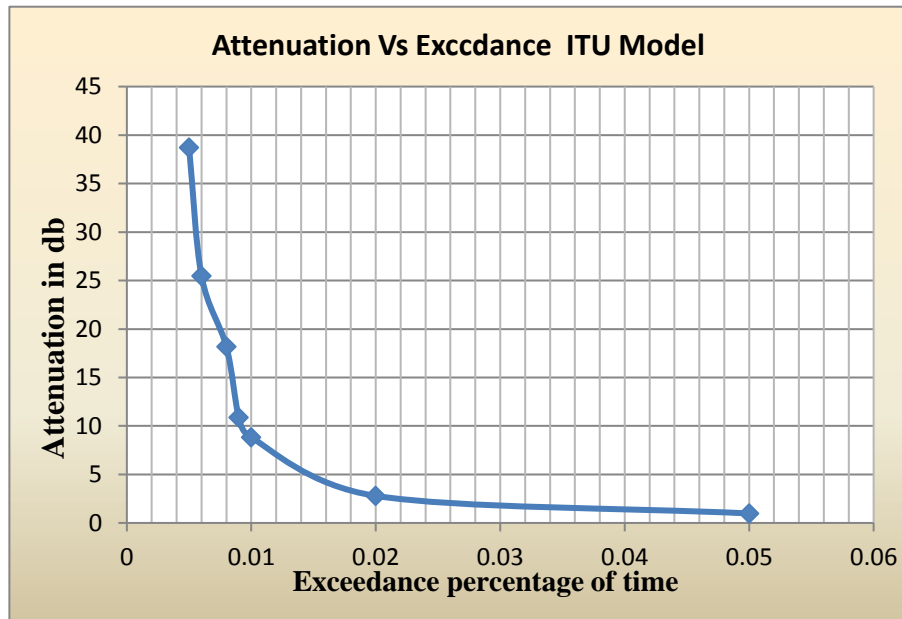


Figure 4.20: Attenuation vs. exceedance (ITU model)

4.8.2 SAM model

This model is known as the Simplified Attenuation Model (SAM), proposed by Strutzman and Dishman (Stutzman & Dishman, 1982). It is one of the most extensively used rain attenuation prediction model. We computed the rain attenuation according to the SAM model in the following steps.

Step 1: The height of zero-degree isotherm in SAM model depends upon the geographical location of earth station (Earth station latitude λ)

$$H_0 = 4.8 \text{ km} \quad \text{for } |\lambda| < 30^\circ$$

$$H_0 = 7.8 - 0.1 \lambda \quad \text{for } |\lambda| > 30^\circ$$

For our study area $\lambda < 30^\circ$

$$H_0 = 4.8 \text{ km}$$

Step 2: Effective rain height in SAM model is dependent on rain rate R mm/hr

$$H_e = H_0 \quad \text{for } R < 10 \text{ mm/hr}$$

$$H_e = H_0 + \log_{10} \left(\frac{R}{10} \right)$$

Step 3: Path length L for elevation angle θ is given by

$$L = H_e - H_0 / \sin \theta$$

Step 4: Rain attenuation in SAM model is given by

$$A(R) = aR^b \frac{1 - \exp \left[-b\gamma \log_e \left(\frac{R}{10} \right) L \cos \theta \right]}{\gamma b \log_e \left(\frac{R}{10} \right) \cos \theta} \quad (28)$$

Where a and b are given by

$$a = 4.21 \times 10^{-5} f^{2.42} \quad \text{for} \quad 2.9 < f < 54 \text{ GHz}$$

$$a = 4.09 \times 10^{-2} f^{2.42} \quad \text{for} \quad 54 < f < 180 \text{ GHz}$$

$$b = 1.41 f^{-0.0779} \quad \text{for} \quad 8.5 < f < 54 \text{ GHz}$$

$$b = 2.63 f^{-0.272} \quad \text{for} \quad 25 < f < 164 \text{ GHz} \quad \text{for} \quad 2.9 < f < 54 \text{ GHz}$$

$$\gamma = 1/22$$

Attenuation corresponding to different time rate was calculated applying the above-mentioned steps and the results are given in TABLE 7 with the graphical result.

TABLE 4.15: ATTENUATION (dB) WITH RAIN RATE BASED ON SAM MODEL

Exceedance	Rain rate	Attenuation (dB)
0.5	31.25	6.5
0.1	44.67	10.01
0.03	54.82	12.748
0.01	66.12	15.89
0.005	71.32	17.37
0.002	85.12	21.38

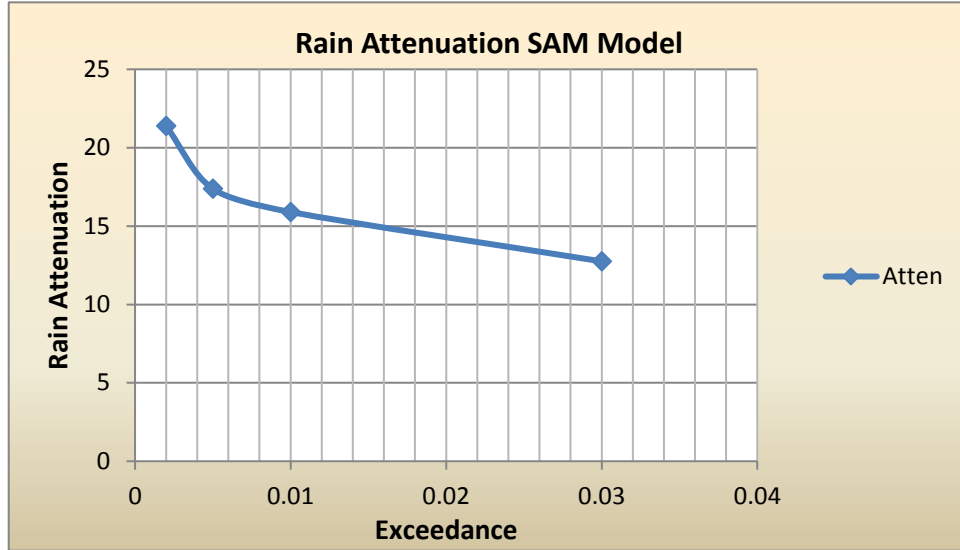


Figure 4.21: Rain attenuation vs exceedance

4.8.3 DAS model

Height of Earth station location above sea level (H_0) = 1.3841 km

Latitude of the study area (λ) = 23.779 km

Elevation angle (θ) = 55.2

Step 1: The rain height H_R in this model is calculated by the relation

$$H_R = 5.1 - 2.15 \log_{10} \left(1 + 10^{\frac{\lambda-27}{25}} \right) \text{ km} \quad (29)$$

The height for our location was calculated to be $H_R = 4.581$ km

Step 2: The slant path length of signal L_S is calculated from the relation

$$L_S = (H_R - H_0) / \sin \theta$$

The value was calculated to be $L_S = 3.8933$

Step 3: To take into account the spatial nonuniformity of the rain rate, path length reduction factor was introduced in this model. The path length reduction factor Γ_p is related to horizontal projection of slant path and is given by

$$\Gamma_p = \frac{90}{(90 + 4L_0)} \quad (30)$$

Where $L_o = L_S \cos \theta$

The path reduction factor was calculated to be $\Gamma_p = 0.9101$ km

Step 4: Rain attenuation exceeded for 0.01% of average year $A_{0.01}$ was calculated according to the equation

$$A_{0.01} = a(R_{0.01})^b L_S \Gamma_p \quad \text{dB} \quad (31)$$

Where $R_{0.01}$ is the rain rate exceeded 0.01 percent of an average year

Step 5: The attenuation value predicted for any other percentage of time was calculated by the equation

$$A_p = A_{0.01} \left(\frac{p}{0.01} \right)^{-\beta} \quad (32)$$

Where $\beta = 0.33$ for $0.01 \geq p \geq 0.01$

The attenuation obtained is summarized in TABLE 8

TABLE 4.16: EXCEEDANCE AND ATTENUATION (dB)

Exceedance	Attenuation (dB)
0.1	6.285611
0.05	9.013285
0.03	11.75559
0.02	14.51483
0.01	20.81361

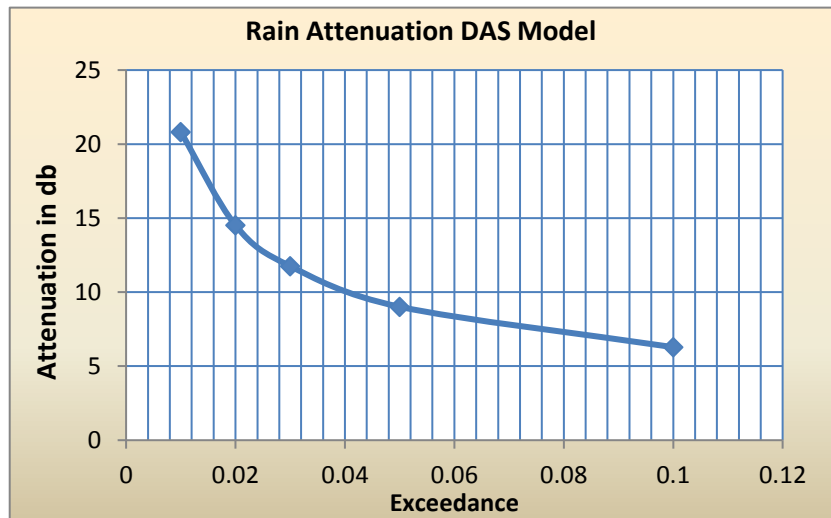


Figure 4.22: Exceedance vs Attenuation DAS Model

4.8.4 Crane model

The Crance model calculates the attenuation of RF signal that propagates through the region of rainfall. This model was developed by Crane for use on earth-space propagation which is one of the most commonly used method of determining rain attenuatin. This model is based on the obsevation of rain rate, rain structure, and the vertical temperature varition of temperature in the atmosphere.

The ITU and Crane models are very similar but have some differences. The ITU and Crane rain attenuation models both requires statistical annual rainfall rates and utilizes an effective path length reduction factor to account for the cellular nature of atoms. The 0.01% rainfall rates tables provided by Crane and ITU are different. The Crane rainfall zones are similar to the ITU zones but more zones are defined in the US than in the ITU model.

We implemented the Crane model for our data in Matlab using Matlab function `cranerainpl`. `Cranerainpl` is the Matlab function to calculate rain attenuation of RF signal.

Syntax

```
L=cranerainpl(range,freq,rainrate)
```

```
L=cranerainpl(range,freq,rainrate,elev)
```

```
L=cranerainpl(range,freq,rainrate,elev,tau)
```

`L=cranerainpl(range,freq,rainrate)` returns the signal attenuation L , due to rain based on Crane rain model. Signal attenuation is a function of signal path length, r mage, the signal frequency and the rain rate. The rain rate is defined as the long term statistical rain rate. The attenuation model applies only for the frequencies from 1 GHz to 1000 GHz. The Crane model also accounts for the cellular nature of rain.

`L=cranerainpl(range,freq,rainrate,elev)` also specifies the angle of elevation

`L=cranerainpl(range,freq,rainrate,elev,tau)` also considers the angle of polarization.

`L=cranerainpl(range,freq,rainrate,elev,tau)` is frequently employed our analysis of rain attenuation by

The parameters given to the argument of function were our data

Frequency = 11.09 GHz

Angle of elevation (elev) = 55.2 °

angle of polarization (τ) = 1.74°

rainpath (range) = 4.6679 km

The results obtained are given in TABLE 9.

TABLE 4.17: RAIN ATTENUATION FROM CRANE MODEL

Rain exceedance (% of time)	Attenuation (dB)
0.5	5.2891
0.3	6.1815
0.2	6.6033
0.1	7.4668
0.05	8.3407
0.03	9.0901
0.02	9.8984
0.01	10.8766
0.005	11.6921

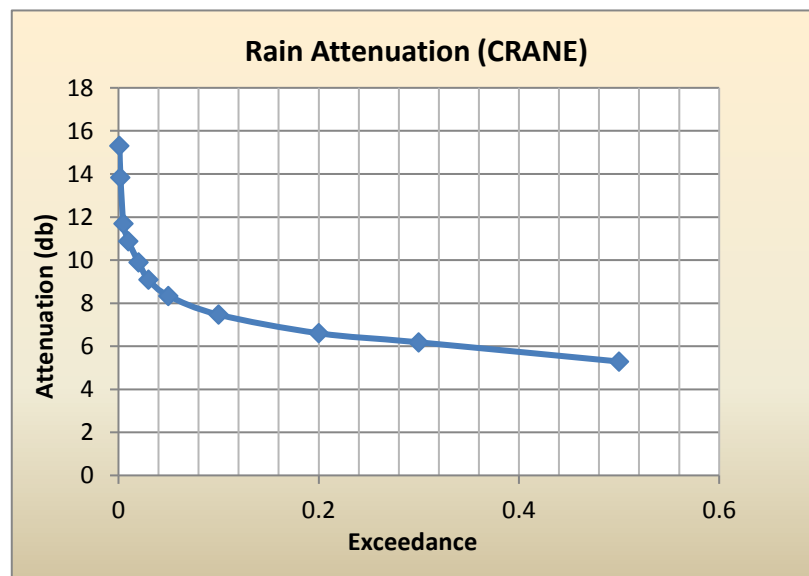


Figure 4.23: Rain exceedance vs. attenuation (Crane model)

For different frequencies the rain attenuation using Crane model was calculated where the results are summarized in TABLE 10

TABLE 4.18: RAIN EXCEEDANCE AND ATTENUATION AT DIFFERENT FREQUENCIES

Rain Exceedance	Attenuation				
	11.09 GHz	20 GHz	30GHz	40 GHz	50 GHz
0.5	5.289	15.523	28.370	40.087	49.156
0.3	6.181	17.762	32.060	44.842	54.572
0.2	6.603	18.804	33.764	47.021	57.040
0.1	7.466	20.910	37.178	51.361	61.935
0.05	8.340	23.008	40.547	55.610	66.700
0.03	9.090	24.782	43.375	59.153	70.654
0.02	9.898	26.675	46.370	62.885	74.801
0.01	10.876	28.935	49.420	67.283	79.666
0.005	11.692	30.798	52.828	70.865	83.613
0.002	13.837	35.620	60.279	79.969	93.585
0.001	18.300	38.847	65.212	85.944	100.087

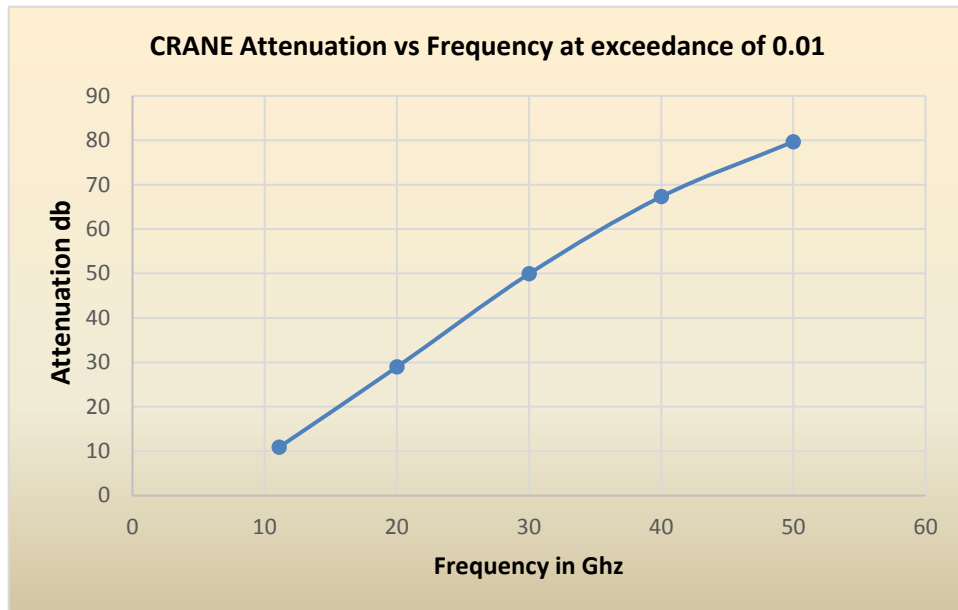


Figure 4.24: Rain attenuation at different frequencies (Crane model)

The figure 7 graph clearly shows that as the frequency of the signal increases the severity of attenuation also increases. At frequency 11.09 GHz rain attenuation is around 10 dB but at frequency 50 GHz it increases to 80 dB.

- Predicted attenuation at various frequencies by Crane model at different exceedance is shown below in graph.

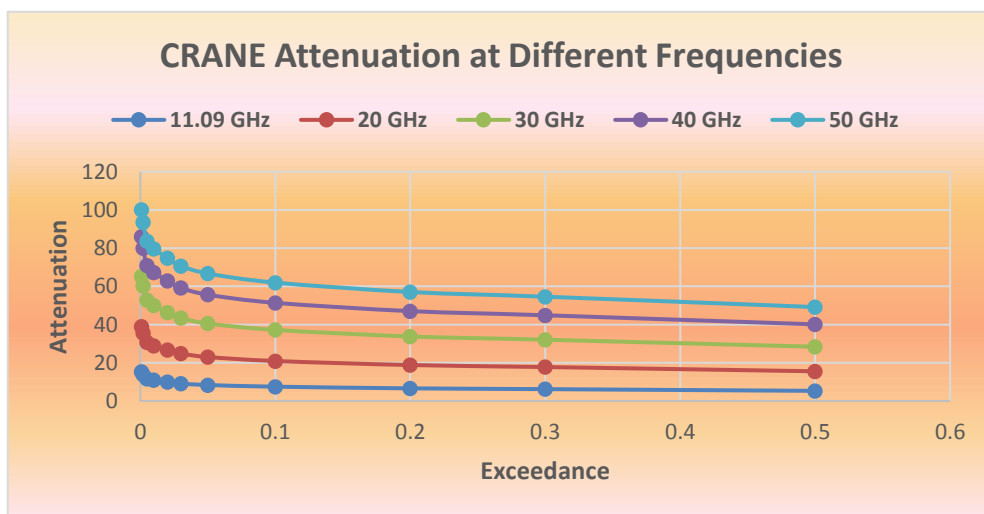


Figure 4.25: Predicted attenuation at different frequencies by Crane Model.

4.8.5 ITU Model with MATLAB:

Using Matlab function `rainpl`, we calculated the attenuation using the ITU model
Matlab function `rainpl` calculates the rain attenuation of RF signal due to the ITU
model

Syntax

```
L=rainpl(range,freq,rainrate)
L=rainpl(range,freq,rainrate,elev)
L=rainpl(range,freq,rainrate,elev,tau)
L=rainpl(range,freq,rainrate,tau,pct)
```

The results obtained are provided in TABLE 26 and in Figure 24

TABLE 4.19: RAIN ATTENUATION FROM ITU MODEL

Rain Exceedance (% of time)	Attenuation (dB)
0.5	4.304
0.3	5.167
0.2	5.5425
0.1	6.3182
0.05	7.1122
0.03	7.7999
0.02	8.5489
0.01	9.4631
0.005	10.2328
0.002	12.2872
0.001	13.716

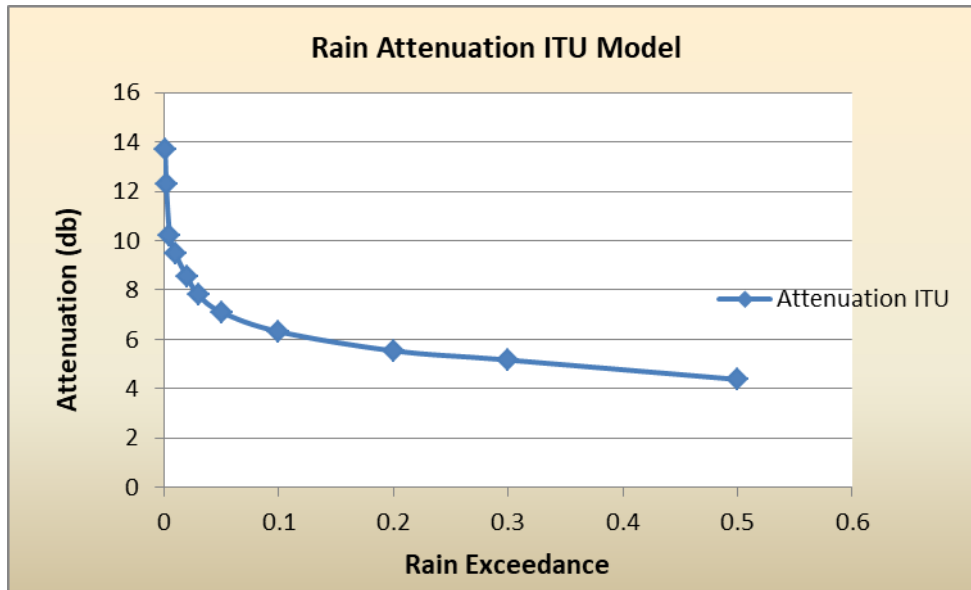


Figure 4.26: Rain attenuation vs. exceedance ITU model

Using the ITU model the attenuation prediction at various frequencies were also calculated the results are provided in Table 12 and in Figure 9

TABLE 4.20: PREDICTED RAIN ATTENUATION AT DIFFERENT FREQUENCIES

Rain Exceedance	Attenuation				
	11.09 GHz	20 GHz	30GHz	40 GHz	50 GHz
0.5	4.304	12.137	21.176	29.1183	34.922
0.3	5.167	14.010	24.133	32.8346	39.070
0.2	5.5425	14.890	25.511	34.5523	40.976
0.1	6.3182	16.684	28.295	38.0016	44.785
0.05	7.1122	18.4891	31.071	41.4121	48.288
0.03	7.7999	20.031	33.422	44.2805	51.661
0.02	8.5489	21.690	35.933	47.3256	51.971
0.01	9.4631	23.688	38.934	50.9434	58.887
0.005	10.232	25.350	41.414	53.9139	62.087
0.002	12.287	29.708	47.846	61.5545	70.266
0.001	13.716	32.669	52.167	66.6381	75.669

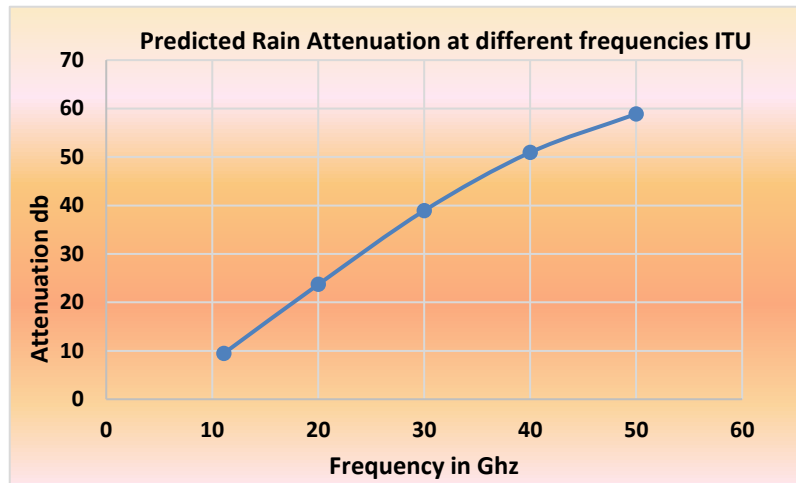


Figure 4.27: Attenuation vs., frequency ITU model

- Attenuation predicted at various frequencies by ITU model at various frequencies is shown graphically below.

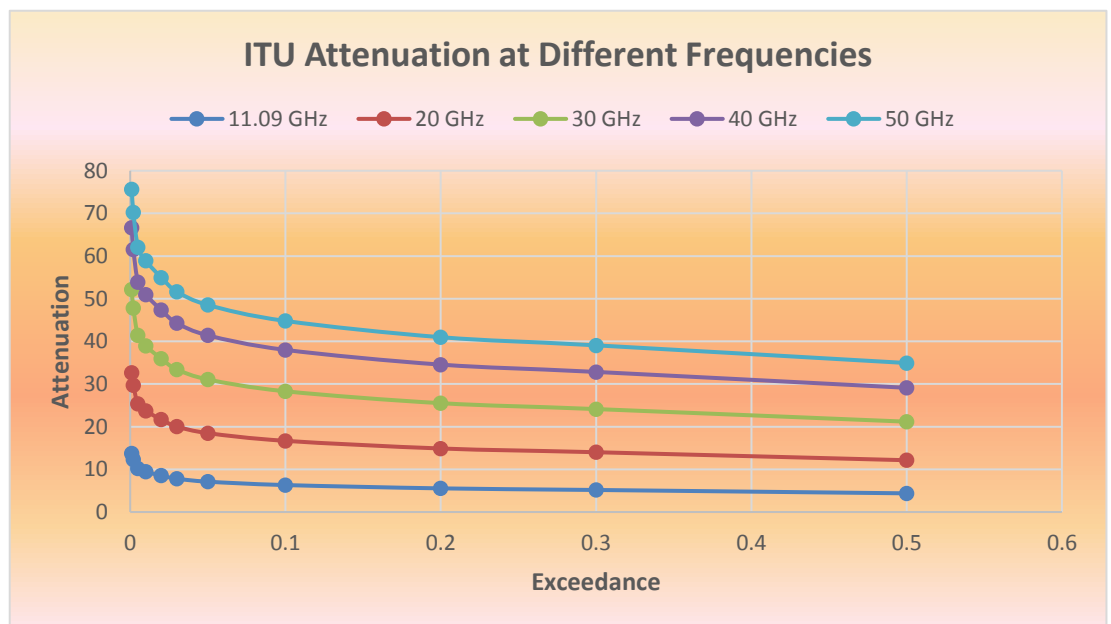


Figure 4.28: ITU Attenuation at different frequencies

4.8.6 Measured attenuation

For our study area the measured attenuation at different rain rate exceedance, that occurs for percentage of time) is given in Table 12 and presented in graphical plot as shown in Figure

TABLE 4.21: MEASURED RAIN ATTENUATION

Rain exceedance (% of time)	Attenuation (dB)
0.5	3.98
0.3	4.89
0.2	5.32
0.1	6.18
0.05	6.94
0.03	7.32
0.02	7.75
0.01	8.72
0.005	9.23
0.002	10.82
0.001	12.43

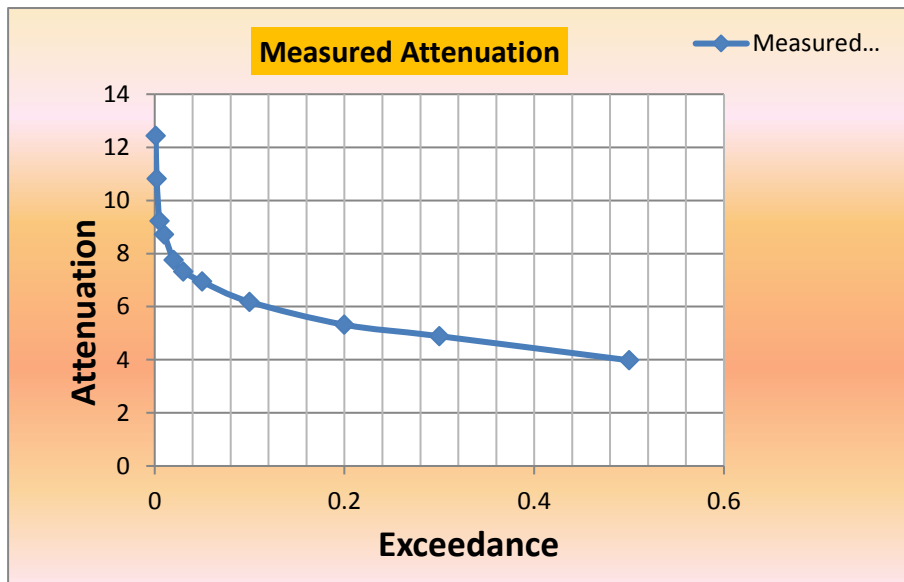


Figure 4.29: Exceedance vs. attenuation, Measured

4.9 Comparison of Measured attenuation with predicted Attenuation:

4.9.1 Comparison with SAM and DAS Model:

Comparison between measured attenuation and predicted attenuation by SAM and DAS Model is shown graphically below.

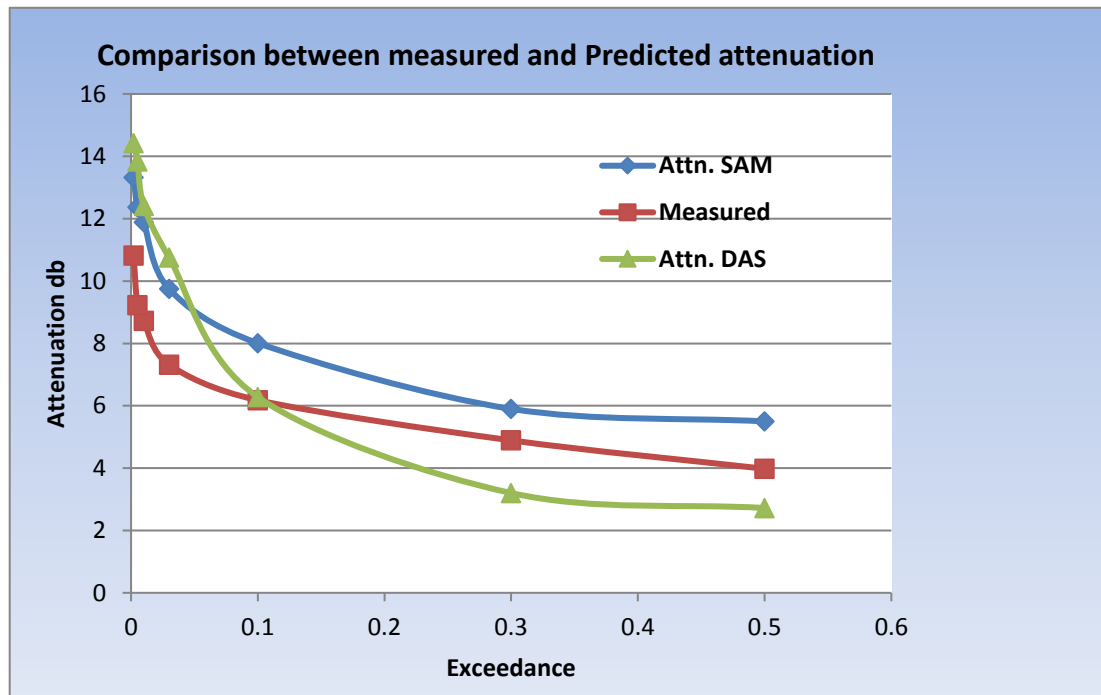


Figure 4.30: Measured attenuation Vs. Predicted attenuation SAM and DAS Model

- At all exceedance percentage predicted attenuation from SAM model is higher than measured attenuation. It can be concluded that SAM model overestimates the attenuation.
- Predicted attenuation by DAS model is lesser than the measured attenuation at higher exceedance or lower rain intensity but predicted attenuation is higher than the measured attenuation at low exceedance or higher rain intensity. Thus, we can conclude that at lower rain intensities DAS model underestimates the attenuation whereas at higher rain rate it overestimates the attenuation.

4.9.2 Comparison with ITU and Crane model:

Comparison between measured attenuation and attenuation predicted by ITU and Crane model is shown graphically below.

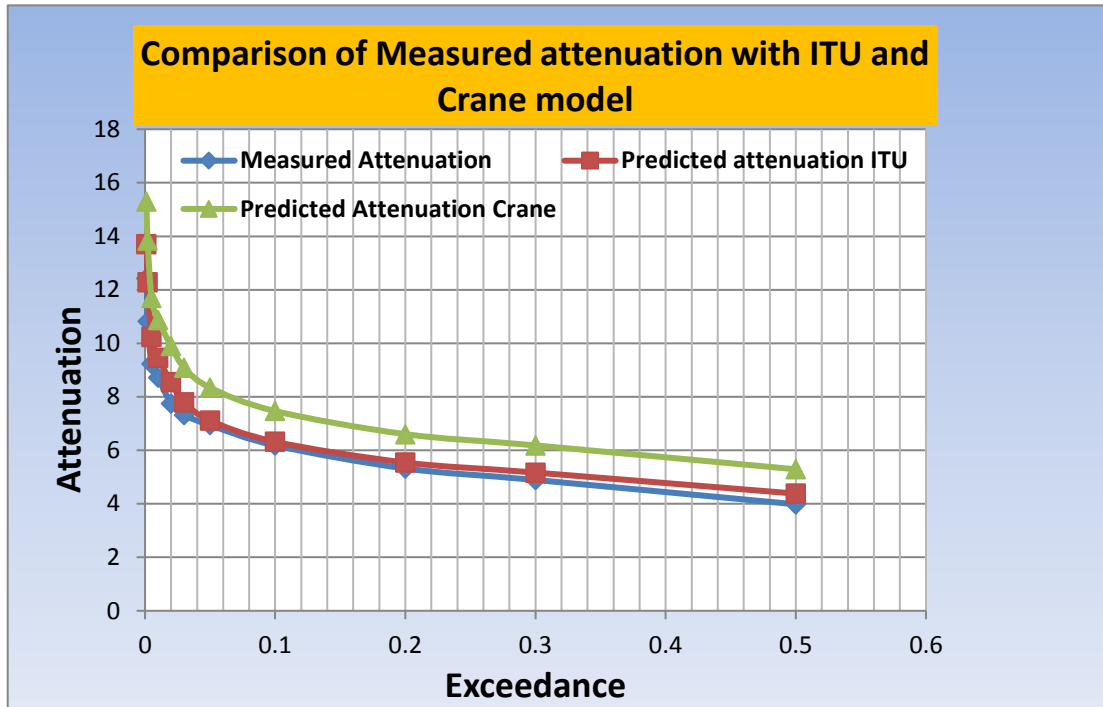


Figure 4.31: Comparison of measured attenuation with ITU and Crane model

- Attenuation predicted by Crane model is slightly higher than the measured attenuation, However shape of both the curve, the measured attenuation and predicted by Crane is almost identical.
- Attenuation predicted by ITU model matches perfectly with the measured attenuation.
- In the figure below comparison of predicted attenuation between ITU and Crane model is shown.

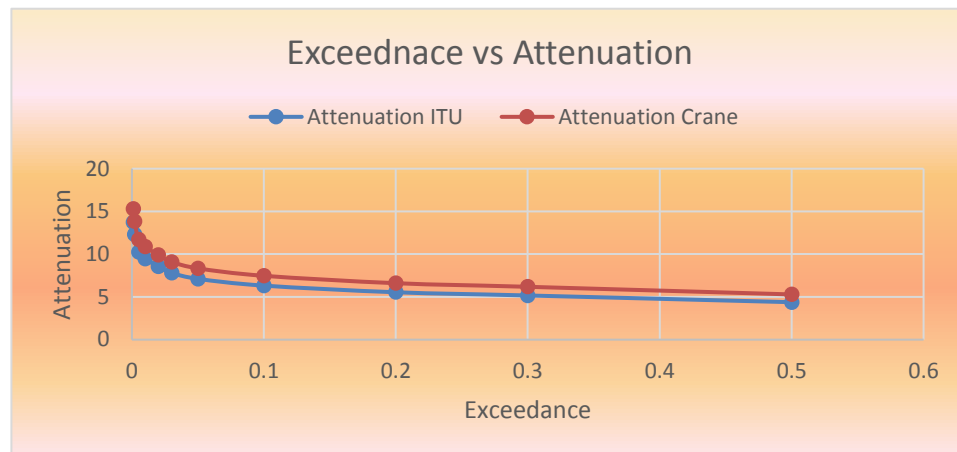


Figure 4.32: Exceedance vs. attenuation for ITU and Crane model

4.9.3 Evaluation of models in terms of Comparison Metrics:

MAE, MSE and RMSE are the metrics in evaluating different models with the measured data. We calculated the mean absolute error (MAE), mean squared error (MSE) and root mean squared error (RMSE) for the four models, namely, SAM, DAS, ITU, and Crane model with the measured data. The result is summarized in table below.

Table 4.22: Comparison metrics

	SAM Model	DAS Model	Crane Model	ITU Model
MAE	- 2.54967	- 2.24798	- 1.9091	- 0.634919
MSE	6.455514	10.68351	4.04246	0.59615
RMSE	2.59966	3.06465	1.90901	0.51882

- It can be concluded from the table that both SAM and DAS model with large MSE and RMSE errors, does not match with measured attenuation.
- Crane model with low MAE and RMSE values but high MSE value matches better compared to SAM and DAS model.
- ITU model with low values on all the three metrics matches very well with the measured attenuation.
- Thus it can be concluded that ITU and up to some extent Crane Model matches with the measured data. SAM and DAS model are not suitable for rain attenuation prediction for Aizawl Region

To further evaluate the Crane and ITU Model with The measured attenuation the value of coefficient of Determination was calculated for ITU and Crane model.

The value of R^2 for ITU and Crane model is given below.

$$R^2 = 0.90333 \quad \text{For ITU Model}$$

$$R^2 = 0.52514 \quad \text{For Crane Model}$$

High value of R^2 for ITU model confirms that ITU model fits the measured attenuation very well. Hence it can be concluded that ITU model performs very well in Aizawl climate.

4.10 Regression analysis of Measured and ITU predicted attenuation:

Regression Analysis of measured attenuation A_M and exceedance p gave the following equation

$$A_M = -1.243 \log_e(p) + 3.164 \quad (32)$$

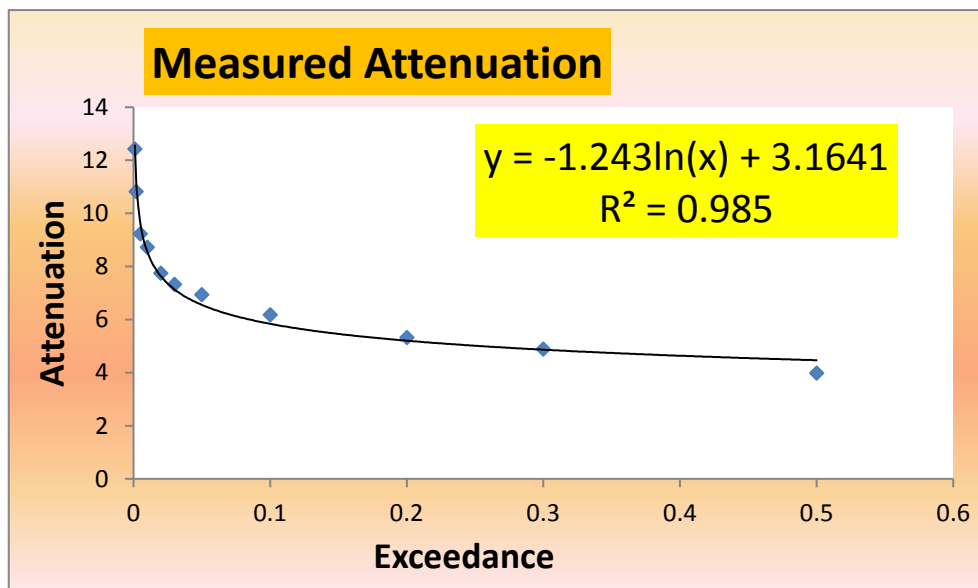


Figure 4.33: Measured Attenuation vs. Rain exceedance

Regression analysis of predicted ITU attenuation A_{ITU} and Exceedance gave the following Equation.

$$A_{ITU} = -1.443 \log_e(p) + 3.084 \quad (33)$$

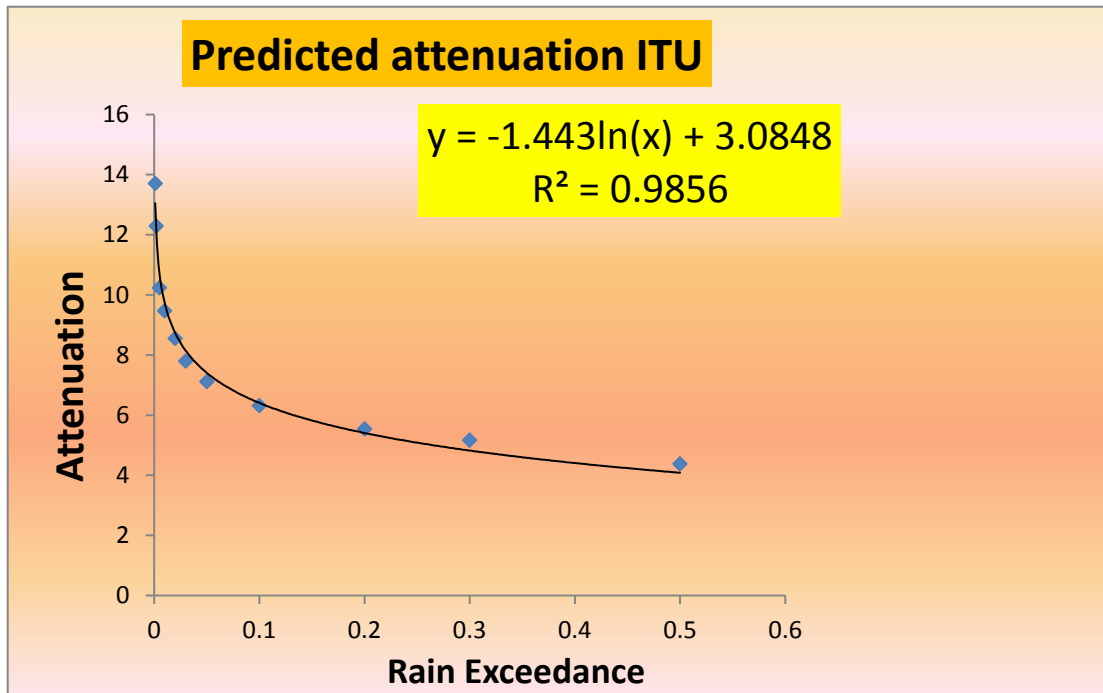


Figure 4.34: Exceedance vs. attenuation for ITU model

From our analysis we can conclude that ITU model of rain attenuation closely matches with the measured attenuation data while Global Crane model overestimates the attenuation measurement at our site. Therefore, the ITU model or variations of the same model will be the best performing existing model for our study area.

4.11 Proposed Rain attenuation model:

From the power regression analysis of the available rain attenuation data we propose following rain attenuation models for the rain attenuation.

4.11.1 Single component rain attenuation model:

From the power regression analysis of rain attenuation, A , as response variable and rain rate (mm/hour) R with one minute integration time as explanatory variable we propose following power law relationship between the two.

$$A(\text{Model}) = \alpha R^\beta \quad (34)$$

α, β are regression coefficients

$$\alpha = 0.1465$$

$$\beta = 0.9744$$

The regression analysis is shown graphically below. With value of coefficient of determination R^2 given by

$$R^2 = 0.9933$$

The value of R^2 shows that the model is excellent fit.

Regression analysis is shown graphically below.

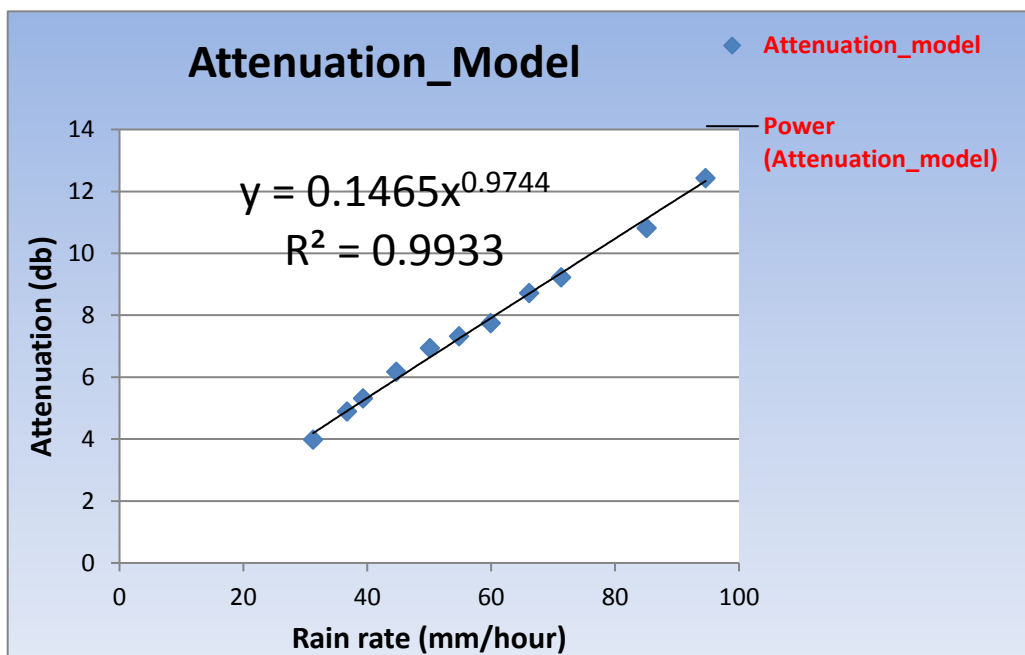


Figure 4.35: Proposed single Component Model for Rain Attenuation Ku Band

4.11.2 Two Component Rain Attenuation Model:

Since limited data is available for Ku band frequencies. To optimize the single component model we propose a two component rain attenuation model for Ku Band.

First Component:

First component is applicable for rain rate (one minute integration time) R satisfying the following relation

$$R \leq 60 \frac{\text{mm}}{\text{hour}} \quad (35)$$

The regression equation connecting the response variable attenuation A and explanatory variable rain rate (integration time 1 minute) is given by the following power law equation

$$A (\text{model}) = \delta R^\gamma \quad (36)$$

Where δ , and γ are regression constants

$$\delta = 0.118$$

$$\gamma = 1.0328$$

The regression analysis is shown graphically below

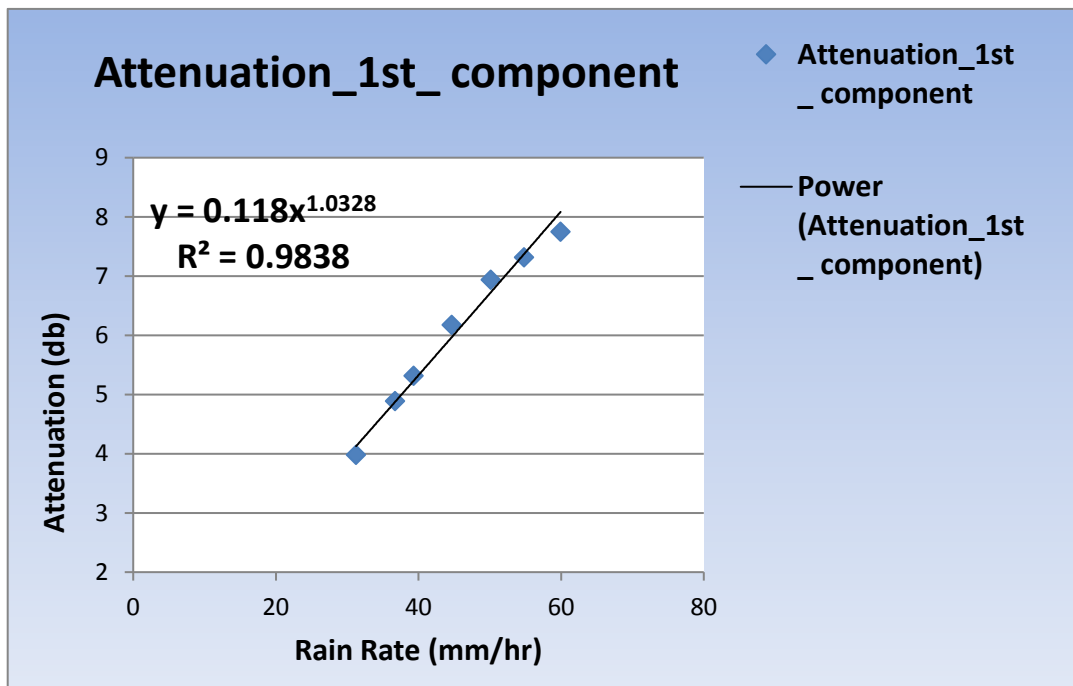


Figure 4.36: 1st component of proposed two components Attenuation Model

2nd Component:

2nd component of the model is applicable for rain rate R satisfying

$$R > 60 \text{ mm/hour}$$

Attenuation A for 2nd component is related with rain rate R by the relation

$$A (\text{Model}) = b R^d \quad (37)$$

where b and c are regression coefficient

$$b = 0.1441$$

$$d = 0.9763$$

The regression analysis is shown graphically below.

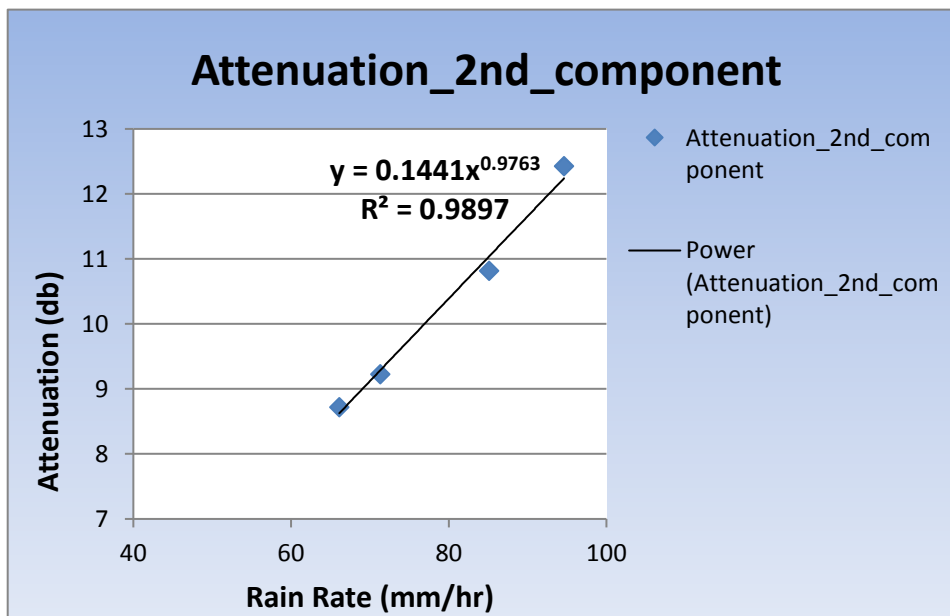


Figure 4.37: 2nd component of the proposed two component attenuation model

4.11.3 Proposed Rain Attenuation Model for Different Frequencies:

From the power regression analysis of ITU predicted rain attenuation for different frequencies (Table 12), we propose a rain attenuation model for $A_{0.01}$ for different higher frequencies. $A_{0.01}$ refers to the level of rain attenuation that is exceeded for 0.01 percent of time in an average year for a specific location, and is used as a metric

to evaluate the performance of satellite communication system. $A_{0.01}$ gives the value of attenuation that is exceeded only for 0.01 percent of time cumulatively over an entire year, in other words for the rest 99.99 % of time attenuation will be below this value. Therefore if we know $A_{0.01}$ and keep this value as the rain margin in our communication system, we are sure that 99.99 percent of time , the aforesaid margin will be able to compensate the fade.

The power law relationship between frequency 'f' of signal as explanatory variable and rain attenuation $A_{0.01}$ as response variable is given by the relation.

$$R_{0.01}(Model) = a f^b \quad (38)$$

a, b are regression coefficient

$$a = 0.5434$$

$$b = 1.271$$

Power regression analysis is shown graphically below.

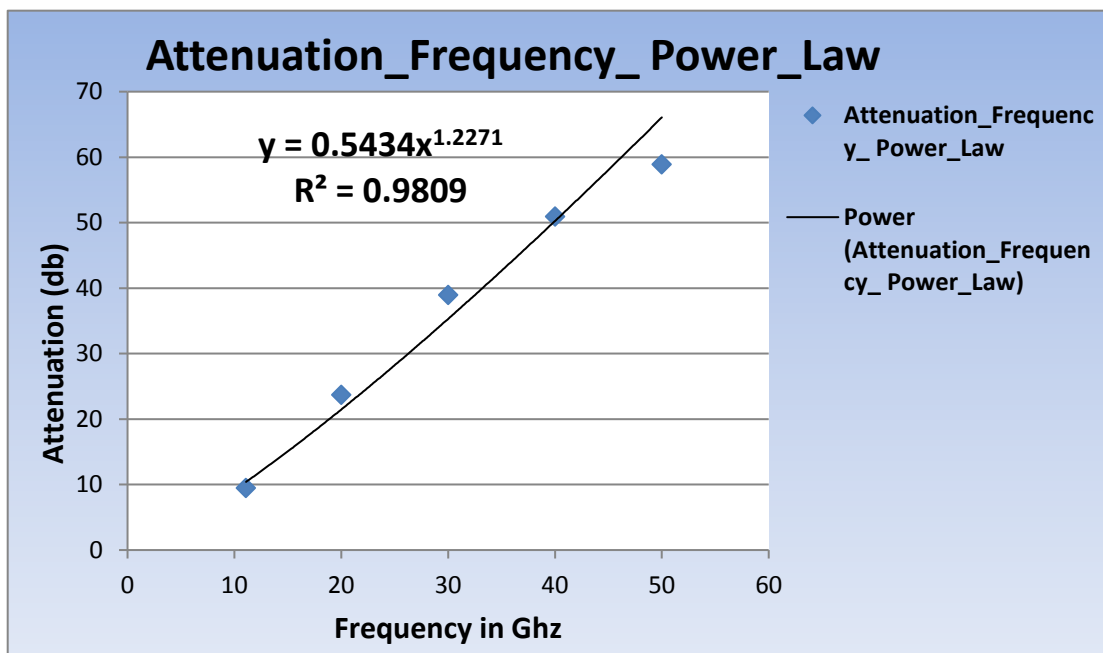


Figure 4.38: Proposed Attenuation frequency Model.

R^2 value of 0.9809 suggests the power law relationship is good fit.

4.12 Fade Mitigation Technique: Satellite communication channels can experience fading due to various reasons such as atmospheric conditions, antenna misalignment, and free space loss and signal destruction. Fading could lead to a decrease in signal quality and can even result in a complete loss of communication link. Therefore, various techniques are used to mitigate the effect of fading in satellite channel including static and adaptive fade mitigation.

4.12.1 Static Fade Mitigation: static fade mitigation technique involves the use of fixed power margin in the link budget, which are pre-determined on the expected fading characteristics of the channel. Example of static fade mitigation includes forward error correction (FEC), diversity technique and power control. FEC involve adding redundant data to the transmitted signal, which allow for the recovery of lost data at the receiver, Diversity technique involve transmitting the same signal through multiple paths and then receiver combines the received signal to improve the overall signal quality. Power control involves adjusting the transmitted power based on expected signal strength at the receiver.

4.12.2 Adaptive Fade Mitigation: Adaptive fade mitigation uses dynamic parameters that are adjusted in real time based on the current fading characteristics of the channel. Example of adaptive fade mitigation includes adaptive modulation and coding (AMC), adaptive power control, and adaptive antenna beam forming. AMC adjusts the modulation and coding scheme based on the channel conditions to maximise the data rate while maintaining a certain level of error rate. Adaptive power control involves adjusting the transmitted power in real time, based on the

current signal strength at the receiver. Adaptive antenna beam forming dynamically adjusts the antenna beam direction to maximise the receive signal strength.

For signals above 10 GHz frequency and for the tropical regions where rain is ample and intense, the amount of rain fade is enormous and cannot be compensated just by adding fixed margin, static fade mitigation techniques are not useful. This is because there is a limitation on the amount of additional power that can be provided to link. Further, this would lead to drainage of power and saturation of satellite transponder when the atmospheric conditions are fadeless. Real time adaptive FMT is used in such scenario to effectively tackle the situation. Adaptive techniques, since they are invoked only when there is a large fade in excess of static margin that need compensation. The action taken to combat the impairment is in accordance with the real time fading experienced by the signal. The link resources in such case are adaptively allocated so that data transfer remains unaffected. Adaptive Fade Mitigation, therefore, can be formally defined as an arrangement through which a satellite link is sustained against possible atmospheric fades, occurring to a signal by judicious and optimal redistribution available resources, thus compensating or avoiding the impairment (Castanet et. al., 2009).

The typical Adaptive Fade Mitigation Technique (AFMT) arrangement achieve the mitigation objective by performing four major task, which are, Measure, Predict, Decide, and act. The schematics of a AFMT control loop is shown Below.

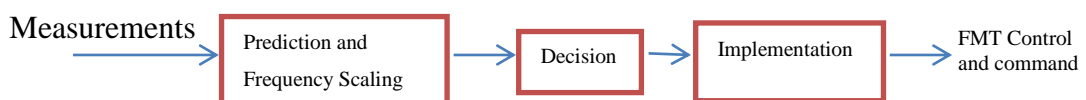


Figure 4.39: Schematics of Adaptive FMT loop

The Adaptive FMT loop consists of three independent module, prediction module, decision module and implementation module. Input to the loop is the measured value of fade while the output is FMT command. A good FMT technique should have minimum drainage of resources and lowest probability of signal outage at the receiver. The prediction should not fall below the actual attenuation and the amount of overestimation should be minimum.

4.13 FMT concepts:

4.13.1 Measurements:

The input to adaptive FMT comes from two modules

1: Signal quality monitor: This module is responsible for monitoring the quality of received signal. It measures key parameters such as signal strength, signal to noise ratio, bit error ratio. The signal quality monitor provides the necessary feedback to the AFMT loop to trigger adjustments when the signal quality falls below a predetermined threshold.

2: Fading Detector: This module detects the onset of fading by analysing the variation in received signal strength over time.

4.13.2 Prediction:

The prediction of fade is the most important part of the control loop. It predicts the upcoming fade values from the current time series of fade by using a complex algorithm. The two important feature of prediction algorithm are necessary, first the process should provide no under-prediction of attenuation and second the instances of over-prediction must be minimum. Further, the controllers require a small but finite reaction time for activating the mitigation technique. Hence the prediction should be made over interval which can provide a comfortable time margin in

advance so that the implementation of compensation may take place simultaneously with the fade.

Following types of prediction technique are usually adopted for the purpose may be broadly classified into the following, but non exhaustive, classes (Roy et.al,2012).

4.13.3 Statistical approach of Prediction:

Use of statistical parameters for rain fade is a very commonly used prediction method. The log- normal stationary distribution of rain attenuation along with appropriate and pre- defined dynamic properties is used from which the rain attenuation may be obtained (Masseng and Bakken, 1981). Some other models use a weighted average of fade slopes over the past samples for prediction of samples ahead (Kastamonitis, et.al. 2003). A near real time fade prediction algorithm based on the two-sample model (Bolea- Alamanc. Et.al. 2003., Van de Kamp,2002) has also been found to perform well.

4.13.4 Regression based predictor:

First order linear regression (Dossi, 1990) has been used to calculate the fade slope over previous samples with increasing added bias in favour of most recent sample, which are then utilized for predicting fade. Prediction based on Auto regressive moving average (ARMA) equations with a moving window of samples of recent past is also popular (Gremont, et.al., 1999). An algorithm that switches between integrated auto regressive integrated moving average and generalised autoregressive conditional heteroscedasticity (ARIMA / GARCH) slope model for short term fade prediction (De Montera, et.al.,2008) is also used for prediction.

4.13.5 Artificial neural network (ANN) method:

ANN has been extensively used to predict tropospheric attenuation and was deployed for the decision making block of controller (Malygin et.al, 2002). Adaptive form of the neural network is used in both linear (Chambers and Otung, 2005) and non-linear form (Roy, et.al.,2012) for prediction. Few hybrid prediction technique combining both the ARMA and Adaptive linear neuron (ADALINE) algorithm has also been proposed (Chambers and Otung, 2008).

4.13.6 Decision:

The decision blocks address to following questions in FMT process. These are

- 1: Whether any FMT is needed or not at any instant of time.
- 2: If FMT is needed then how much fade compensation is required?
- 3: which type of FMT can be used?

4.13.7 Mitigation Technique:

Various standard FMT's are applied depending upon the extent of attenuation (Castanet, et.al., 2002) and are usually implemented by the control system. These controllers have the ability of detecting and predicting the actual level of total attenuation in the path of satellite link. The control system, depending upon the predicted attenuation level, takes a decision and activates a suitable type of FMT to compensate the probable loss. Broadly the FMT's can be divided into two categories on the basis of its approach of mitigation (Rajat Acharya, Satellite signal Propagation, Impairments and Mitigation, *Academic press, 2017 Elsevier Ltd.*).

- 1: Compensation Type FMT: These are the technique which attempt to compensate the effects due to fade by modifying the link and signal parameters.

2: Avoidance type FMT: Those Technique which attempt to avoid the effects of fade by rerouting the link through change in link path, frequency, time of transmission etc.

4.13.8 Compensation Type FMT:

The signal parameter energy per bit to noise density, $\frac{E_b}{N_0}$, is a measure of signal quality received at the receiver.

$$\frac{E_b}{N_0} = \left(EIRP - L_{fs} - L_A + \frac{G_R}{T} + G_c - k \right) - R \text{ dBHz} \quad (39)$$

EIRP = Effective isotropic radiated power transmitted by the source

L_{fs} = free space loss

L_A = Atmospheric loss

$\frac{G_R}{T}$ = ratio of receive antenna gain to noise temperature, Figure of merit for receiver

G_c = FEC coding gain

k = Boltzmann's constant

R = data rate

When large L_A tries to pull down E_b / N_0 at the receiver, the same can be restored by modifying any of the controllable parameter on the right hand side of equation (39).

4.13.9 EIRP Control:

Uplink power control and downlink power control are two EIRP control Technique

Uplink power control (ULPC): In this technique the output power of a transmitting earth station is enhanced to compensate the fade in uplink signal. It is, therefore, an earth station EIRP control. The ULPC aims to keep a constant level of all the carriers at the transponder of satellite. The transmitter power is increased during the fade

condition to counteract it and again decreased when favourable propagation conditions are restored. However, only minimum power variation is implemented. This ensures the minimum drainage of power and the possibility of driving transponder amplifier of satellite into non linear region.

The main drawback of ULPC is the problem of adjacent channel interference. A satellite transponder carries a number of channels which are placed adjacently in frequency or time separated by guard band or time. If the power of a channel is sufficiently increased compared to the other channel, the latter being not under fade condition, a part of the energy of the affected channel falls into adjacent channel and may lead to adjacent channel interference.

Since the ULPC requires adjustment in the earth station resource which are readily available, Therefore, it can be implemented in a very flexible way. Despite the drawback of adjacent channel interference, ULPC constitute an effective counter measure against signal fading.

Downlink power control (DLPC):

In DLPC, the on board channel output power is changed to compensate the downlink attenuation. However, since the satellites have very limited power resources, DLPC is implemented with limited power levels. Also since satellite coverage area is usually large, and only a part of it is affected at any point of time by rain, while for remaining coverage area the signal remains unaffected. Therefore, a large extent increase in power to address the requirement of a limited area may lead to saturating the signal in unaffected area and causing non-linear effects. Thus besides the adjacent channel interference the DLPC may cause intermodulation interference, a

type of interference caused by intermodulation products generated by the non-linear amplification of multiple carriers.

On board beam shaping (OBBS):

OBSS is a technique used in satellite communication to achieve highly focussed, directional spot beams that provide high-gain signal coverage to specific areas on the earth surface.

Spot beams are small, highly focussed beams of electromagnetic radiation that are directed towards specific region on the earth surface within the foot print of satellite.

On board beam shaping technique is based on active antennas allows these spot beams gain to adapted to propagation conditions. Under fade conditions, the antenna beam width gets more concentrated on the affected regions and thus increasing the antenna gain for the affected areas. This ensures increased EIRP only for the affected areas to cater to the requirement of signal fade. The OBSS therefore consists of appropriately shaping the satellite antenna pattern so that the power received by the ground terminals remains nearly constant, even under the rain fade conditions (Panagopoulos, et.al., 2004).

4.14 Adaptive waveform Technique:

These adaptive waveform technique of AFMT, adaptively adjust the parameters of signal structure, like , coding or modulation, to maintain a desired level of reliability despite the changing channel conditions.

4.14.1 Adaptive coding (ADCOD):

Adaptive coding adjusts the coding rate of signal based on channel condition. When rain fade is high, signal to noise ratio is low, there is greater likelihood of errors in the bits received, and higher coding rate is used to improve E_b / N_0 of the signal.

Similarly when there is an improvement in channel condition, signal to noise ratio is high and there is lesser likelihood of errors in the bits received, and in such scenario lower coding rate may be used.

4.14.2 Adaptive Modulation (ADM) :

The most commonly used modulation scheme in satellite communication is PSK (phase shift keying) modulation. To obtain higher spectral efficiency, that is to transmit more bits per second without any additional bandwidth requirement, ADM employs the higher order PSK schemes like 8 PSK, 16 PSK, 64 PSK or 256 QAM etc. having higher spectral efficiencies (Livieratos and Corttis, 2001). In general as the order M of M -array PSK or M -array QAM increases the spectral efficiency of link become higher. On the other hand as the separation between adjacent amplitude and phase state is reduced, they become difficult to distinguish under noisy state and hence higher order modulation schemes become more susceptible to errors.

Adaptive modulation technique utilises higher order modulation schemes under clear sky conditions and uses more robust modulation schemes under the condition of heavy metrological impairments.

Data Rate adaptation (DRA):

DRA is a fade mitigation technique used in satellite communication to dynamically adjust the data rate of transmission based on channel conditions to maintain a desired level of reliability. DRA adjusts the data rate of the transmission based on channel conditions to maintain a desired level of reliability. When the channel conditions are good, the data rate can be increased to take advantage of the available bandwidth.

When the channel condition deteriorates due to atmospheric impairments, the data rate is decreased to maintain a desired level of reliability.

DRA uses feedback from the receiver to determine the channel conditions and adjust the data rate. The feedback may be based on a number of factors, including the received signal to noise ratio, the bit error rate or other measure of signal quality.

DRA is typically implemented using a rate adaptation algorithm that adjusts the data rate in real time based on feedback from receiver. The rate adaptation algorithm may be based on a variety of techniques, including threshold methods, statistical method or machine learning based method.

4.15 Avoidance type FMT:

Avoidance type FMT are countermeasures against rain fade or other type of impairments in which the effective link is modified or duplicated in such a manner that that the effect of the impairments on the link is avoided. A common technique to avoid is to shift the link in time, space or frequency. The action is not to modify the link budget but instead to establish a new one, such that impairments which are basically temporal and spatially bound and frequency dependent, does not influence the modified link thus established. Diversity is one of the methods to implement the avoidance type FMT.

4.15.1 Diversity:

In a satellite system diversity in the link may be established by having different locations of transmission, different locations of reception, different frequency to establish the link or even by having different time to establish the link. The objective of diversity is to reroute the information in the network so that atmospheric impairments may be avoided.

Following four type of diversity is commonly found in satellite communication.

1; Site diversity

2: Orbital diversity

3: Frequency diversity

4: Time diversity

Site diversity:

Site diversity uses two or more earth stations at different locations that can establish link with a satellite. Since regions of high rain are usually concentrated over a small geographical extent and hence two geographically separated earth station that can establish link with the same satellite with same transmitting parameters can ensure continuity of data transmission when one of the earth station is under heavy atmospheric impairments.

Orbital diversity:

Orbital diversity involve using multiple satellite in different orbit to provide redundant coverage. By using multiple satellites , the system can provide a more reliable service even in presence of atmospheric and other types of interference.

Frequency diversity:

Frequency diversity is a technique that involves the transmitting the same signal on multiple frequencies. By using multiple frequencies the system can reduce the effects of interference that is specific to one frequency band.

To implement frequency diversity we need to have payloads and ground stations equipped with two different frequencies. These frequencies must be wide apart to obtain significant gain out of this technique. When a fade is occurring, links reroute using the lowest frequency available in payload. For example, this technique may

employ the Ka band frequency during normal operation and switches over to lower band like C band during fade exceeding a certain threshold.

Apart from the dual frequency requirement, another drawback of the system is in the capacity allocation. The lower frequency band are unable to offer equally large bandwidth and the throughput of the system suffer.

Time Diversity:

The rain causing attenuation is time limited and time diversity exploits this fact. TD FMT utilizes the idea of delayed transmission of the data to avoid fade. That is the information which was supposed to be transmitted during the fade event, is stored and retransmitted after a delay comparable with rain event. Therefore, TD can be implemented in systems that can withstand data latency and in which real time operation is nor essential.

4.16 References

- Burgueño, A., Puigcerver, M., & Vilar, E. (1988). Influence of rain gauge integration time on the rain rate statistics used in microwave communications. *Annales Des Télécommunications*. <https://doi.org/10.1007/BF03011107>
- Crane, R. K. (1980). Prediction of Attenuation by Rain. *IEEE Transactions on Communications*. <https://doi.org/10.1109/TCOM.1980.1094844>
- Crane, R. K., & Shieh, H. - C. (1989). A two- component rain model for the prediction of site diversity performance. *Radio Science*. <https://doi.org/10.1029/RS024i005p00641>
- Dissanayake, A., & Allnutt, J. (1997). A prediction model that combines rain attenuation and other propagation impairments along earth-satellite paths. *IEEE Transactions on Antennas and Propagation*. <https://doi.org/10.1109/8.633864>
- Dupont, B. S. (2006). REVISION OF THE RAINFALL-INTENSITY DURATION CURVES FOR THE COMMONWEALTH OF KENTUCKY. *Transportation Research Record: Journal of the Transportation Research Board*.
- ITU-R. (2017a). *R-REC-P.837-7-201706 RECOMMENDATION ITU-R P.837-7*. https://www.itu.int/dms_pubrec/itu-r/rec/p/R-REC-P.837-7-201706-I!!PDF-E.pdf
- ITU-R. (2017b). *R-REC P.618-13 Recommendation ITU-R P.618-13*. https://www.itu.int/dms_pubrec/itu-r/rec/p/R-REC-P.618-13-201712-I!!PDF-E.pdf
- Kothyari, U. C., & Garde, R. J. (1992). Rainfall Intensity- Duration- Frequency Formula for India. *Journal of Hydraulic Engineering*. [https://doi.org/10.1061/\(asce\)0733-9429\(1992\)118:2\(323\)](https://doi.org/10.1061/(asce)0733-9429(1992)118:2(323))

- Moupfouma, F., Martin, L., Spanjaard, N., & Hughes, K. (1990). Rainfall rate characteristics for microwave systems in tropical and equatorial areas. *International Journal of Satellite Communications*. <https://doi.org/10.1002/sat.4600080307>
- Segal, B. (1986). The Influence of Rainage Integration Time, on Measured Rainfall-intensity Distribution Functions. *Journal of Atmospheric and Oceanic Technology*. [https://doi.org/10.1175/1520-0426\(1986\)003<0662:tiorit>2.0.co;2](https://doi.org/10.1175/1520-0426(1986)003<0662:tiorit>2.0.co;2)
- Stutzman, W. L., & Dishman, W. K. (1982). A simple model for the estimation of rain-induced attenuation along earth-space paths at millimeter wavelengths. *Radio Science*. <https://doi.org/10.1029/RS017i006p01465>
- Stutzman, W. L., Pratt, T., Imrich, D. M., Scales, W. A., & Bostian, C. W. (1986). DISPERSION IN THE 10-30 GHZ FREQUENCY RANGE: ATMOSPHERIC EFFECTS AND THEIR IMPACT ON DIGITAL SATELLITE COMMUNICATIONS. *IEEE Transactions on Communications*. <https://doi.org/10.1109/tcom.1986.1096515>
- Castanet, L., Bolea-Alamafiac, A., Bousquet, M., Claverotte, L., Gutierrez-Glavan, R., 2009. Performance assessment of fade mitigation Technique for the GEOCAST IST project with transparent and OBP Architecture. *Int. J. Space Communication*, 22(1),1-12.
- Castanet, L., et.al., 2002. Interference and fade mitigation technique for Ka and V band satellite communication systems. In. *Proceedings of COST 280 workshop, Noordwijk, The Netherlands*.
- Chambers, A. P., Otung, I. E., 2005. Neural network approach to short term fade prediction on satellite links. *Electron. Lett.* 41(23), 1290- 1292.

Chambers, A. P., Otung, I. E., 2008. Near optimum short term fade prediction on satellite links at Ka and V bands. *Int. J. Satell. Commun. Netw.* 26(1), 31-43.

Dossi, L., 1990. Real time prediction of attenuation for application to fade countermeasures in satellite communication. *Electron. Lett.* 26 (4), 250-25.

Gremont, B., Filip, M., Gallois, P., et.al. 1999. Comparative analysis and performance of two predictive fade detection schemes for Ka band fade countermeasures, *IEEE Sel.Areas Commun.* 17 (2), 180-192.

De Montera, L., Mallet, C., Barthe's, L., et.al., 2008. Short term prediction of rain attenuation level and volatility in Earth-to-satellite links at EHF bands. *Nonlinear process. Geophys.* 15(4). 631- 643.

Roy, B., Acharya, R., Sivaraman, M. R., 2012. Attenuation prediction for for fade mitigation using neural network with in situ learning algorithm. *Adv. Space Res.* 49, 336- 350.

Masseng, T., Bakken, P. M., 1981. A stochastic model for rain attenuation. *IEEE trans. Commun.* 29(5),600-669.

Kastamonitis, K., Gremont, B., Filip, M., 2003. Short term prediction of rain attenuation based on fade slope, *Electron. Lett.* 39(8), 687- 689.

Livieratos, S. N., Cottis, P. G., 2001, Availability and performance of single multiple site diversity satellite system under rain fades, *Eur. Trans. Telecommun.* 12 (1), 55-56.

Malygin, A., Filip, M., Vilar, E., 2002. NN implementation of a fade countermeasure controller in a Vsat link. *Int. J.Satell.Communic. Netw.* 20(2), 79-95.

Panagopoulos, A. D., Arapoglou, P. D. M., Cottis, P. G., 2004. Satellite communication at Ku, Ka and V band : Propagation impairments and mitigation Technique. *IEEE Commun. Surv. Tutorials* 6(3), 2-14.

Bolea- Alamanac, A., Bousquet, M., Castanet, L., 2003. Implementation of short term prediction model in fade mitigation technique control loops. *In: joint COST 272/280 workshop, ESA/ESTEC, Noordwijk, The Netherlands, 26- 28 May, 2003.*

Rajat Acharya, Satellite signal Propagation, Impairments and Mitigation, *Academic press, 2017 Elsevier Ltd.*

Van de Kamp, M., 2002. Rain attenuation as a Markov process, using two samples. *In: Eight Ka- Band utilization Conference, Baveno, Italy, 25- 27 September 2002.*

Chapter | **5**

Conclusion and Summary

CHAPTER 5: SUMMARY AND CONCLUSION

Based on the research problem undertaken, methodologies adopted data gathering, analysis of data and interpretations; following are the summary and conclusions of this thesis.

Chapter 1 describes a detailed introduction about the satellite communication, framework of various concepts used in the current work. Also, impact of weather on satellite communication or rain attenuation is discussed in details. The important tropospheric phenomenon affecting satellite communication system above 10GHz are Rain Attenuation or Attenuation due to precipitation; Gaseous Absorption; Cloud Attenuation; Melting Layer Attenuation; Sky Noise Increase; Signal Depolarization and Scintillation Attenuation, are also described in this chapter.

Chapter 2 discusses a detailed, systematic and relevant review of literature related to the research problem undertaken.

Chapter 3 describes a detailed methodology used by the author, experimental set up namely Spectrum Analyzer and various models used such as; ITU-R model, SAM, DAS and Crane Model.

.Chapter 4 describes a detailed analysis and interpretation of the experimental data, based on the various tools including various models. Chapter 4 is in three parts, part 1 of the chapter deals with analysis of rainfall data, part 2 of the chapter is related to rain attenuation analysis of RF data, and part three of the chapter deals with various fade mitigation techniques used in microwave communication.

5.1 Rainfall Analysis:

- From the 30 year (1986-2025) historical rainfall data gathered from state metrological department, Government of Mizoram, both long term and short

term descriptive statistics of rainfall at Aizawl were derived. The most striking feature of rainfall depth at Aizawl was that monsoon months (JJAS) are having almost 80 percent of total yearly rain.

- Cumulative statistics of annual rainfall depth (rain exceedance curve) was derived, By performing logistic regression analysis of cumulative statistics we discovered following equation connecting the annual rainfall depth Y and return period T .

$$Y = 303.011 \log_e(T) + 2456.6 \quad mm \quad (1)$$

- Rain depth (mm) exceedance curve with integration time 24 hours were derived. The logistic regression analysis of the derived data we obtained the following equation relating rain depth with 24 hours integration time R_{24} and return period T .

$$R_{24} = 4.2309 \log_e(T) + 15.16 \quad (2)$$

- Using equation 2 and Kothyari and Garde IDF equation (3) we derived rainfall intensity (mm/hour) with integration time of 60 minutes for various exceedance probabilities.

$$L_t^T = C \left(\frac{T^{0.20}}{t^{0.71}} \right) (R_{24}^2)^{0.33} \quad (3)$$

The result is shown graphically below.

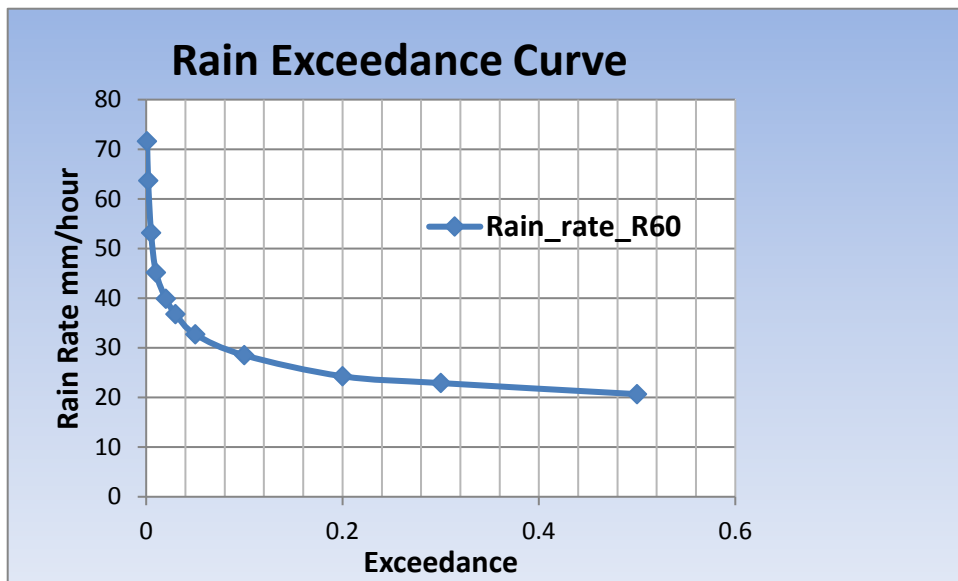


Figure 5.1 : Rain rate exceedance curve with integration time 60 Minutes

- Rain rate with 60 minute integration time was converted to 1 minute integration time using the algorithm contained in ITU-R.P. 837.7 recommendation. The result is summarized in graph below.

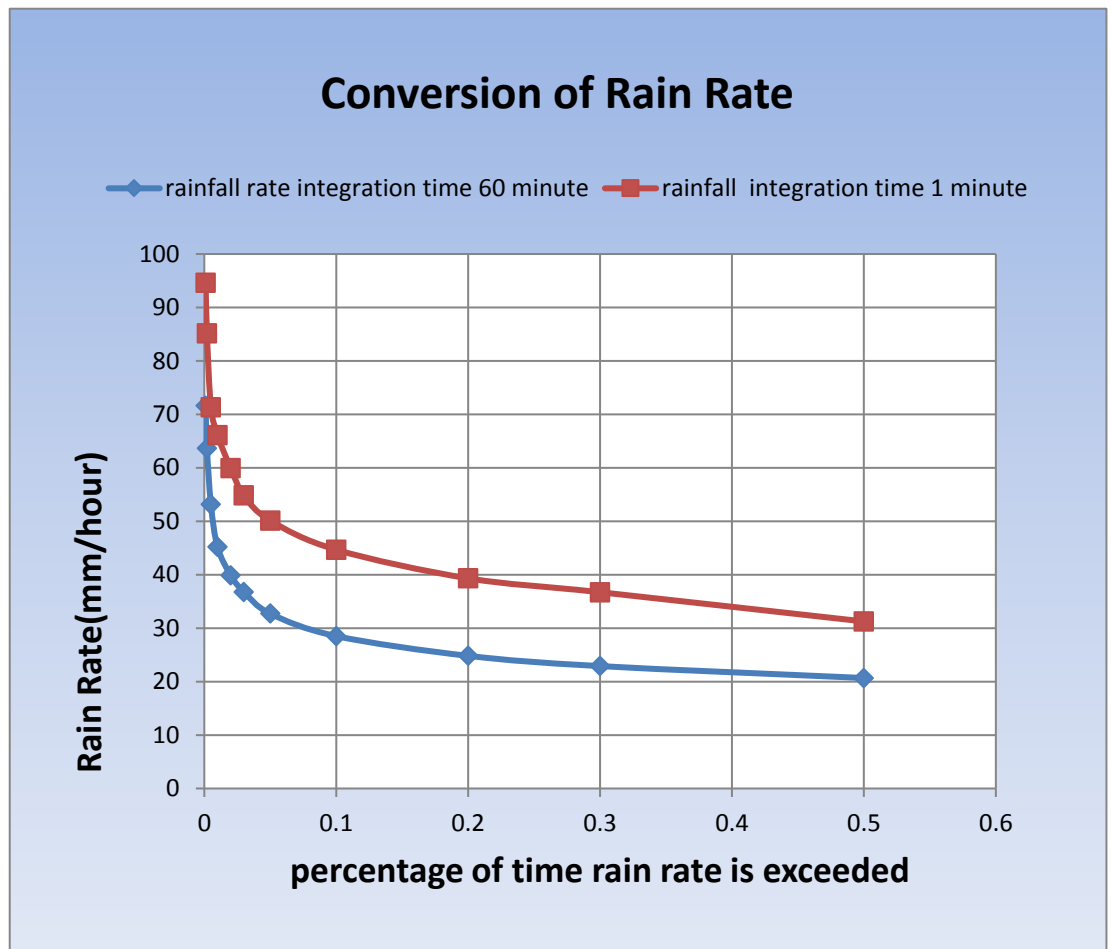


Figure 5.2: Rain rate conversion from integration time 60 minute to 1 minute.

- Using logistic regression analysis we discovered the following equation relating rain rate (mm/hour) with integration time 1 minute R_1 and exceedance probability p .

$$R_1(\text{mm/hr}) = -9.933 \log_e(p) + 27.368 \quad (4)$$

- Finally we proposed a power law rain rate conversion model for converting rain rate R_{60} from 60 minute integration time to 1 minute integration time R_1 .

$$R_1(\text{Model}) = A (R_{60})^B \quad (5)$$

where A, B are regression coefficient

$$A = 2.6142 \quad (6)$$

$$B = 0.8418 \quad (7)$$

Rain attenuation for different frequencies using Crane model was calculated and the result are summarized in following table and graph.

5.2 Rain Attenuation Analysis:

Experimental set up to gather RF data was setup at Doordrashan Kendra Aizawl, Durtlang, details of setup explained in chapter 3 and 4. Campaign for RF data gathering was run for two years (2016-2018). The measured data was compared with four rain attenuation prediction models, namely, SAM, DAS, Crane and ITU models. The results may be summarised as follows'

- We calculated the predicted rain attenuation by the four models. MATLAB was used for calculating predicted rain attenuation by Crane and ITU models, whereas, Microsoft excel was used for SAM and DAS models.
- The predicted rain attenuation from the four models was compared with the measured attenuation. The comparison metrics comprising of parameters MAE, MSE, RMSE for all four models with measured attenuation is given below.

Table 5.1: Comparison metrics

	SAM Model	DAS Model	Crane Model	ITU Model
MAE	- 2.54967	- 2.24798	- 1.9091	- 0.634919
MSE	6.455514	10.68351	4.04246	0.59615
RMSE	2.59966	3.06465	1.90901	0.51882

From the comparison metrics it can be concluded that Crane and ITU models matches well with our measured data. Further coefficient of determination for comparison of ITU and CRANE model with the measured data was calculated and we found the following result.

The value of R^2 for ITU and CRANE model is given below.

$$R^2 = 0.90333 \quad \text{For ITU Model}$$

$$R^2 = 0.52514 \quad \text{For Crane Model}$$

From the above values it can be concluded that the ITU model matches the measured attenuation nicely. Hence ITU model is the most suitable rain attenuation prediction model for the Aizawl region.

- Though our experimental RF data collection was for a single frequency 11.09 GHz, we calculated the rain attenuation for higher frequencies using ITU and Global Crane model to provide a reference data for upcoming microwave communication systems at higher frequencies in the north-eastern region. The predicted rain attenuation at various frequencies by the ITU model is given in below graph.

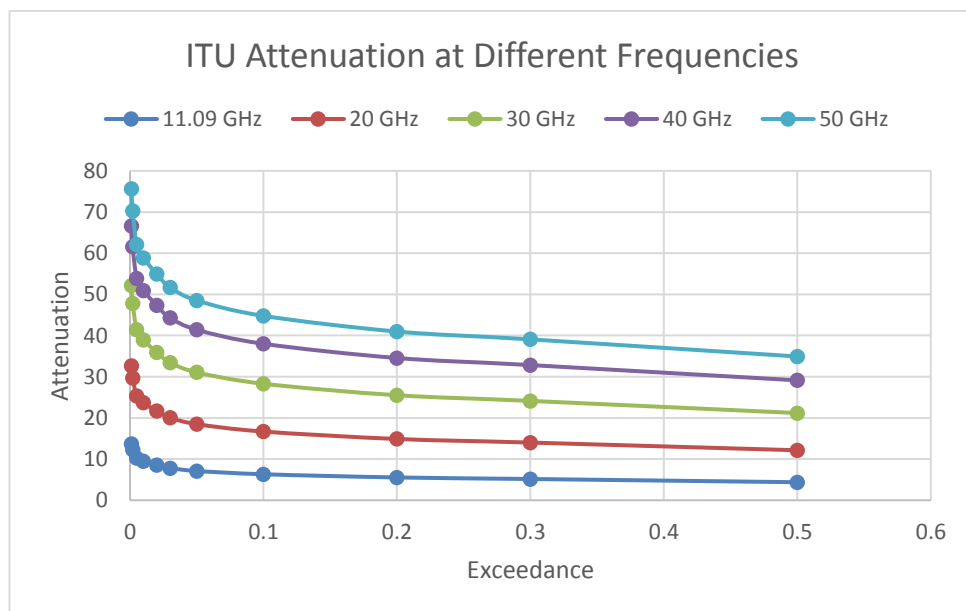


Figure 5.3: Predicted rain attenuation at different frequencies by ITU model.

It is worth observing from the graph that rain attenuation increases exponentially as the frequency of operation is increased.

The graph below shows the severity of rain attenuation with the increase of

frequency.

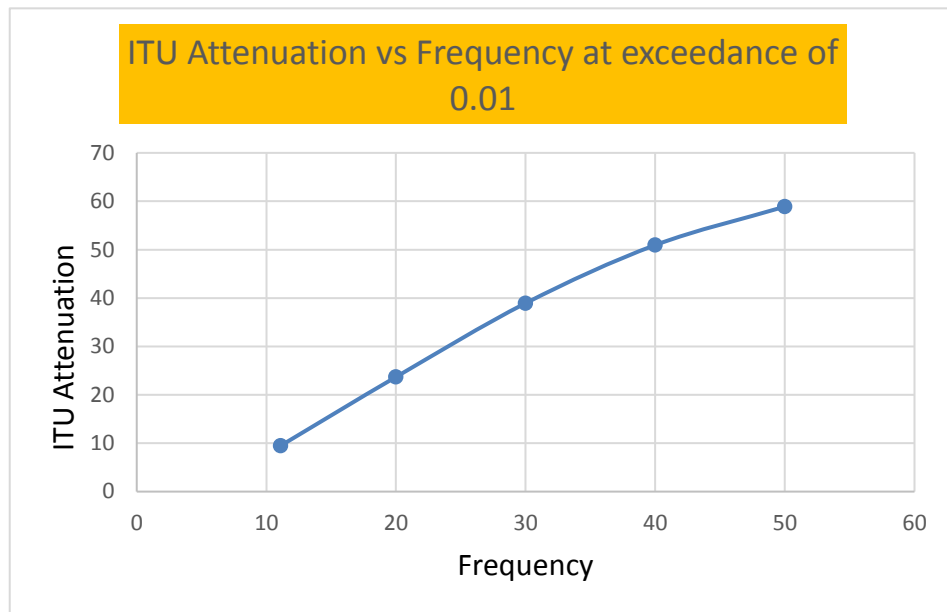


Figure 5.4: ITU attenuation vs. frequency

5.3 Proposed Rain attenuation model:

From the power regression analysis of the available rain attenuation data we propose following rain attenuation models for the rain attenuation.

5.3.1 Single component rain attenuation model:

From the power regression analysis of rain attenuation, A , as response variable and rain rate (mm/hour) R with one minute integration time as explanatory variable we propose following power law relationship between the two.

$$A(\text{Model}) = \alpha R^\beta \quad (6)$$

α, β are regression coefficients

$$\alpha = 0.1465$$

$$\beta = 0.9744$$

The regression analysis is shown graphically below. With value of coefficient of determination R^2 given by

$$R^2 = 0.9933$$

The value of R^2 shows that the model is excellent fit.

Regression analysis is shown graphically below.

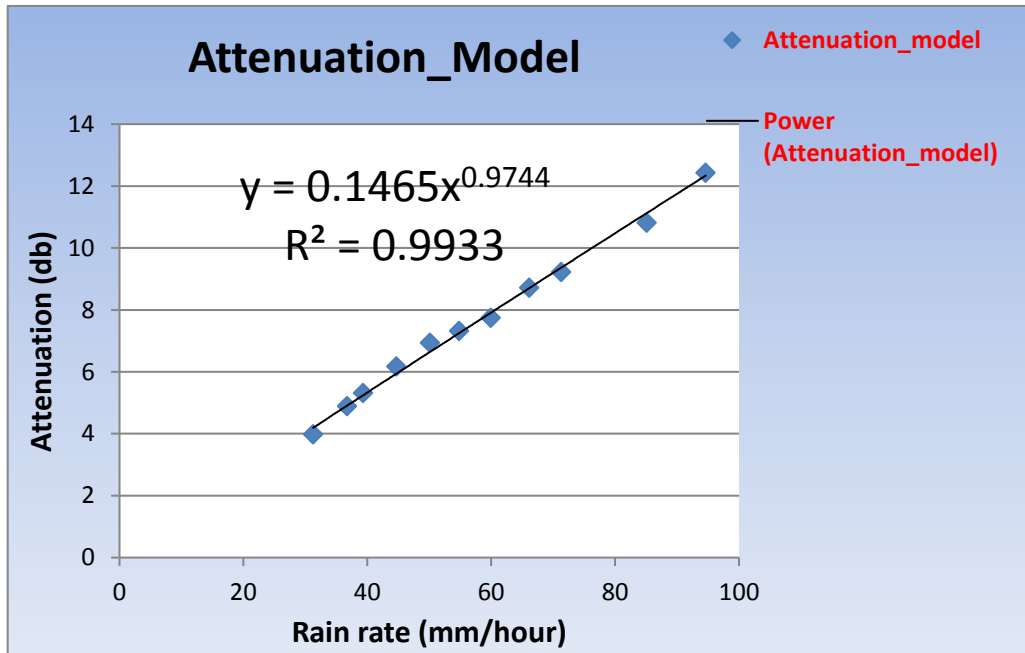


Figure 5.5: Proposed single Component Model for Rain Attenuation Ku Band

5.3.2 Two Component Rain Attenuation Model:

Since limited data is available for Ku band frequencies. To optimize the single component model we propose a two-component rain attenuation model for Ku Band.

First Component:

First component is applicable for rain rate (one minute integration time) R satisfying the following relation

$$R \leq 60 \frac{mm}{hour} \quad 7)$$

The regression equation connecting the response variable attenuation A and explanatory variable rain rate (integration time 1 minute) is given by the following power law equation

$$A(\text{Model}) = \delta R^\gamma \quad 8)$$

Where δ , and γ are regression constants

$$\delta = 0.118$$

$$\gamma = 1.0328$$

The regression analysis is shown graphically below

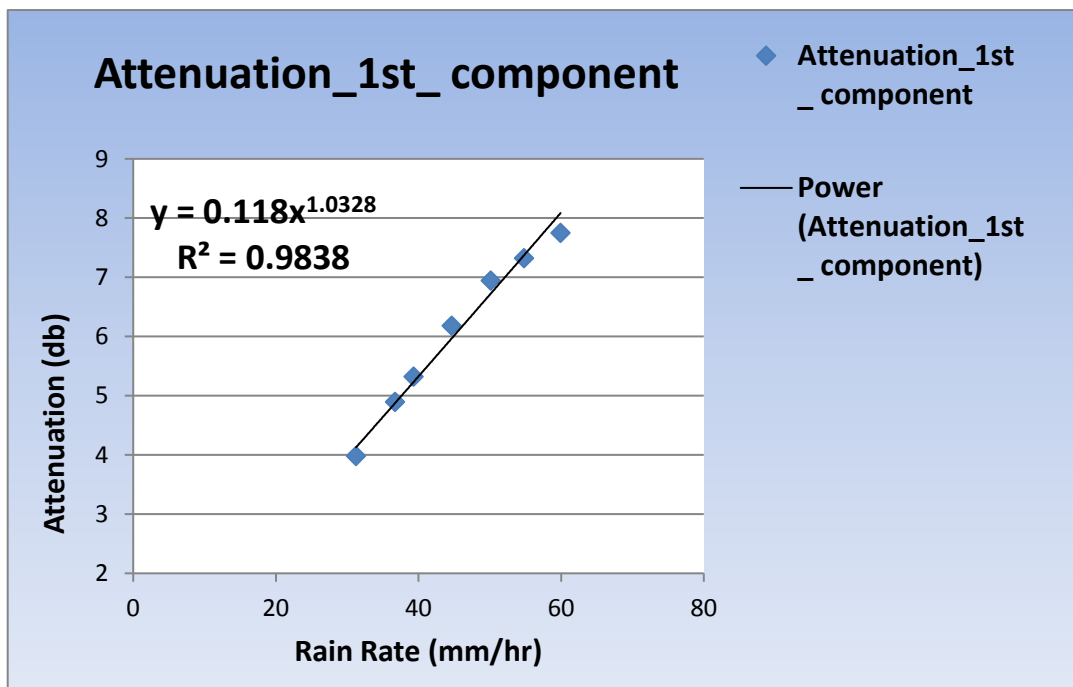


Figure 5.6: 1st component of proposed two components Attenuation Model

2nd Component:

2nd component of the model is applicable for rain rate R satisfying

$$R > 60 \text{ mm/hour}$$

Attenuation A for 2nd component is related with rain rate R by the relation

$$A (\text{Model}) = b R^d$$

9)

where b and c are regression coefficient

$$b = 0.1441$$

$$d = 0.9763$$

The regression analysis is shown graphically below.

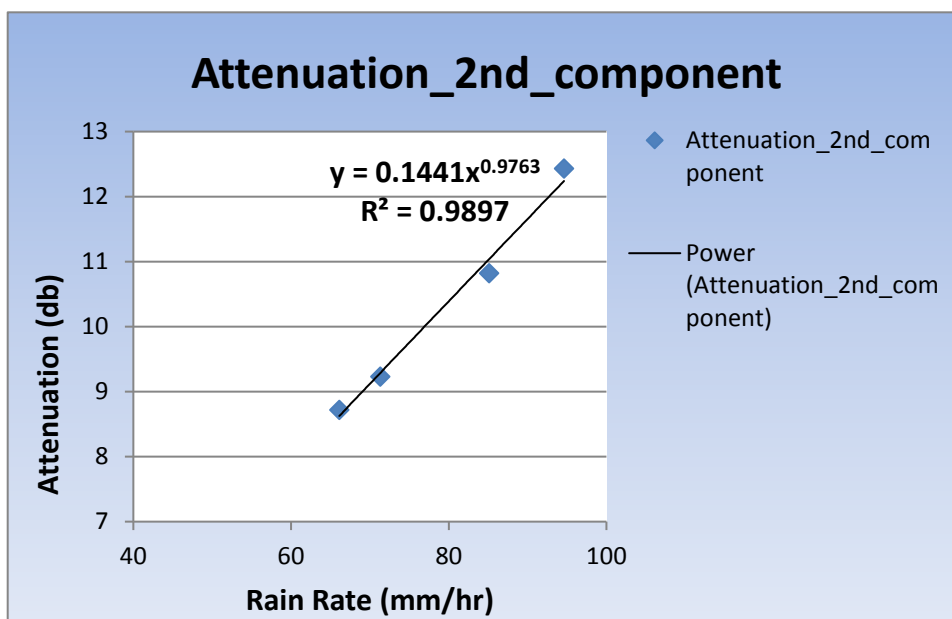


Figure 5.7: 2nd component of proposed two component attenuation model

5.3.3 Proposed Rain Attenuation Model for Different Frequencies:

From the power regression analysis of ITU predicted rain attenuation for different frequencies (Table 12), we propose a rain attenuation model for $A_{0.01}$ for different higher frequencies. $A_{0.01}$ refers to the level of rain attenuation that is exceeded for 0.01 percent of time in an average year for a specific location, and is used as a metric to evaluate the performance of satellite communication system. $A_{0.01}$ gives the value of attenuation that is exceeded only for 0.01 percent of time cumulatively over an entire year, in other words for the rest 99.99 % of time attenuation will be below this

value. Therefore if we know $A_{0.01}$ and keep this value as the rain margin in our communication system, we are sure that 99.99 percent of time, the aforesaid margin will be able to compensate the fade.

The power law relationship between frequency 'f' of signal as explanatory variable and rain attenuation $A_{0.01}$ as response variable is given by the relation.

$$R_{0.01} (\text{Model}) = a f^b \quad (10)$$

a, b are regression coefficient

$$a = 0.5434$$

$$b = 1.271$$

Power regression analysis is shown graphically below.

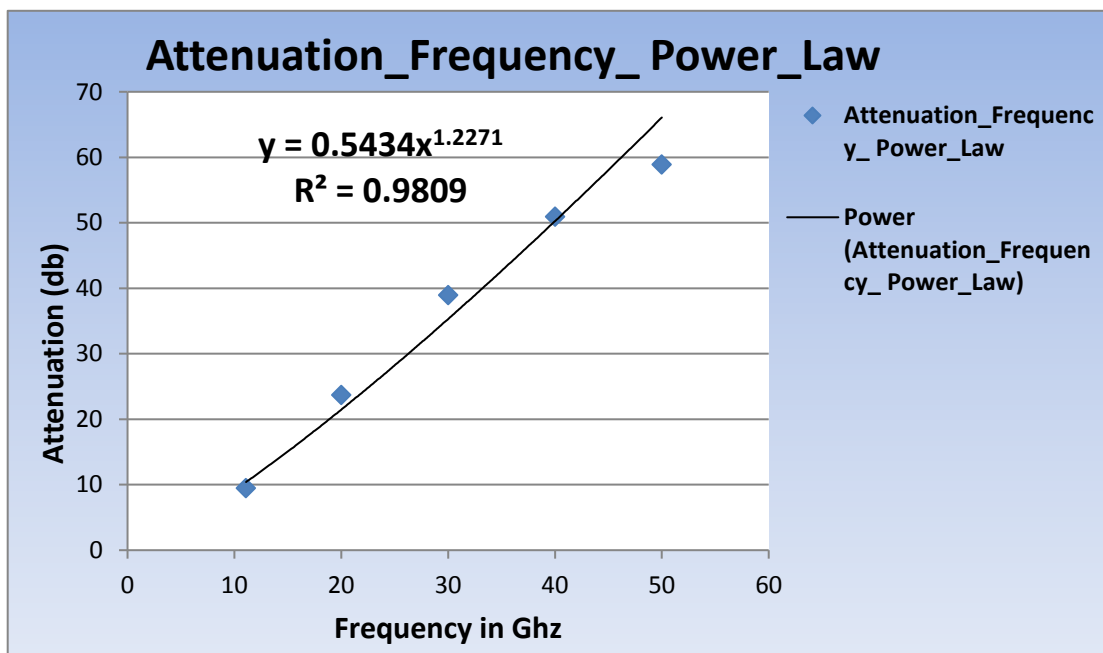


Figure 5.8: Proposed Attenuation frequency Model.

R^2 value of 0.9809 suggests the power law relationship is good fit.

5.4 Future scope of the study:

Motivation for starting the present research work was primarily based on following two observations.

1: Most of the existing rain attenuation models available in literature are based on experimental data recorded in temperate climates. They may not accurately reflect the weather pattern in north- eastern part of India.

2; No research project based on RF data measurement for rain attenuation ever carried out in North-Eastern part of India.

- The research gap identified by the current study can be a starting point for future researcher to explore various aspects of rain attenuation models in various climatic conditions.
- Another area of future research is to extend the study to cover a broader range of frequencies and locations. Since the current study collected data for single frequency at a single location, future researcher can expand the scope of study to include multiple frequencies and locations. This will provide a more comprehensive understanding of impact of rain attenuation on satellite signals.
- Fine tuning of power law rain attenuation model proposed by the current study is another potential area of the future research. Beside fine tanning the regression coefficients in power law proposed future researcher can modify the model by including other metrological parameters, such as temperature and humidity to improve its accuracy of prediction.

- During this research work we established a positive correlation between received signal $\frac{E_b}{N_0}$ and temperature (Ravindra Naithani, Thaisa Jawhly, Ramesh Chandra Tiwari). The correlation coefficients are given in table below.

Table 5.2: Correlation coefficient between $\frac{E_b}{N_0}$ and Temperature

Min. Temperature	0.75
Max. Temperature	0.79
Mean Temperature	0.81

We also developed a linear regression model for prediction signal strength $\frac{E_b}{N_0}$

in terms of atmospheric Temperature (T) and rain rate R. The mathematical equation of model is given below.

$$\frac{E_b}{N_0}(\text{Model}) = 243 + 0.32(T) - 0.17(R) \quad (11)$$

There is a scope for future researcher to fine tune the model with the measurement taken at different location.

- The reliance on rainfall data from the metrological department presents another opportunity for future research. Future researcher can conduct field study to collect rainfall data themselves and compare it with the data obtained from the metrological department. This will help to understand the reliability and accuracy of metrological data in predicting rain attenuation. An in-situ rain and RF measurement would be an ideal setup for studying rain attenuation of satellite signal.

- The proposed power law rain rate conversion model for converting rain rate from 60 minute integration time to one minute integration time can be verified and fine tuned by recording rain fall data with a disdrometer of integration time one minute.
- Another exciting area of future study could be to analyse the rain drop size distribution in the region. Such studies can improve rain attenuation modeling a great deal.

In conclusion the current study on rain attenuation at Aizawl, Mizoram can provide a reliable reference source for starting rain attenuation study in north eastern part of India.

5.5 References:

Ravindra Naithani, Thaisa Jawhly, Ramesh Chandra Tiwari,. Satellite- signal Dependence On Rain And Atmospheric Temperature., *Science and Technology Journal Vol 9 Issue 2 July 2021*ISSN: 2321-3388.

CV of the Scholar

RAVINDRA NAITHANI

Tower A-1 Flat No-701 Eldeco Elegance

Vibhuti Khand, Gomti Nagar

Lucknow226010

Contact No: - 9839029939.

ravindranaithani@prasarbharati.gov.in

ravinaithani2007@rediffmail.com

WORK EXPERIENCE

- Belong to ALL INDIA SERVICE, Indian Broadcasting Engineering Service.(IBES).
- Currently working as Deputy Director Doordarshan Kendra Lucknow.
- Experience of working with Earth station for 20 years

EDUCATION QUALIFICATION

- Student of PHD in Physics from Mizoram University.
- Student of BS Degree in Programing and Data Science, from IIT Madras.

Personal Details

Father's name	-Late Shri B.N Naithani
Date of birth	- 07April 1964
Gender	- Male
Marital status	- Married
Language	- Hindi, English.
Nationality	- Indian

List of Publication and activities

Publications

1. Ravindra Naithani, Thaisa Jawhly and Ramesh Chandra Tiwari. July 2021. Satellite-Signal Dependence On Rain and Atmospheric Temperature. Science and Technology Journal Vol 9 Issue 2 July 2021 ISSN:2321-3388. [S\(https://doi.org/10.22232/stj.2021.09.02.08\)](https://doi.org/10.22232/stj.2021.09.02.08)
2. Ravindra Naithani, Thaisa Jawhly and Ramesh Chandra Tiwari. December-3, 2021. Discrete-time series analysis of rainfall data. In 2021 International Conference on Computational Performance Evaluation (ComPE) (pp. 576-579). IEEE. (Scopus indexed);
<https://doi.org/10.1109/ComPE53109.2021.9752347>

Conference presentation

1. Comparisons and evaluation of models for conversion of rainfall distribution from several minute integration time to one minute integration time. Mizoram Science Congress (MSC-2018), **4th -5th October 2018**, Pachhunga University, Aizawl, India.
Authors:, Ravindra Naithani, Thaisa Jawhly, Ramesh Chandra Tiwari.
Presenter: Ravindra Naithani
2. Discrete- time series analysis of rainfall data. International Conference on Computational Performance Evaluation (**ComPE-2021**), **IEEE Conference ID: 531091st - 3th December 2021**, North-Eastern Hill University (NEHU), Shillong Meghalaya, India.
Authors: Ravindra Naithani, Thaisa Jawhly, Ramesh Chandra Tiwari.
Presenter: Ravindra Naithani
3. Satellite Signal Dependence on Rain and Atmospheric Temperature. International Seminar on Recent Advances in Science and Technology, **16th -**

18th November 2020, 2nd Annual Convention of North East (India) Academy of Science and Technology(NEAST)

Authors: Ravindra Naithani, Thaisa Jawhly, Ramesh Chandra Tiwari.

Presenter: Ravindra Naithani

Activities

1. Student of BS in Programming and Data Science from IIT Madras.
2. Completed Foundation level in BS degree.
3. Completed two courses titled Statistics1 and Statistics2 for three month semester duration from IIT Madras.
4. Completed two courses of three month semester duration titled Python , Programming and Data Structure from IIT Madras.
5. Attended and completed 7 days Bootcamp on Machine Learning & Python organised by devtown, Developer Student Club.

Particulars of the candidate

NAME OF THE CANDIDATE : RAVINDRA NAITHANI
DEGREE : DOCTOR OF PHILOSOPHY
DEPARTMENT : PHYSICS

TITLE OF THE THESIS : A STUDY OF WEATHER IMPACTED Ku
BAND SATELLITE CHANNEL :
PROPAGATION IMPAIRMENT AND
IMPROVEMENT IN QUALITY OF SERVICE
IN MOIST TROPICAL CLIMATE.

DATE OF ADMISSION : 13TH AUGUST 2015
APPROVAL OF
RESEARCHPROPOSAL :

1. DRC : 28TH MARCH 2016
2. BOS : 7TH APRIL 2016
3. SCHOOL BOARD : 21ST APRIL 2016

MZU REGN NO. : 1506797 of 05-04-2016
Ph.D REGN NO. & DATE : MZU/Ph.D/915 of 21.04.2016
EXTENSION IF ANY : 21.04.2021- 20.04.2023

Head
Department of Physics

ABSTRACT
A STUDY OF WEATHER IMPACTED KU BAND SATELLITE
CHANNEL: PROPAGATION IMPAIRMENT AND
IMPROVEMENT IN QUALITY OF SERVICE IN MOIST
TROPICAL CLIMATE

AN ABSTRACT SUBMITTED IN PARTIAL
FULFILMENT OF THE REQUIREMENTS
FOR THE DEGREE OF DOCTOR OF
PHILOSOPHY

RAVINDRA NAITHANI

MZU REGN NO: 1506797 OF 05.04.2016

Ph.D REGN NO. MZU/Ph.D/915 OF 21.04.2016



DEPARTMENT OF PHYSICS
SCHOOL OF PHYSICAL SCIENCES

APRIL 2023

ABSTRACT

**A STUDY OF WEATHER IMPACTED KU BAND SATELLITE
CHANNEL: PROPAGATION IMPAIRMENT AND
IMPROVEMENT IN QUALITY OF SERVICE IN MOIST
TROPICAL CLIMATE**

BY

RAVINDRA NAITHANI

Department of Physics

Name of the Supervisor

Prof. RAMESH CHANDRA TIWARI

Submitted

In partial fulfilment of the requirement of the Degree of Doctor of

Philosophy in Physics of

Mizoram University, Aizawl

ABSTRACT

Satellite communication is one of the most critical technology for data transfer in modern time. It has drastically changed the way human in modern time, receive information, navigate and conduct their day to day activities. Satellite communication systems have already proved their worth in providing seamless connectivity to remote and inaccessible areas where traditional modes of communication system are not feasible. For north- Eastern part of India satellite communication has significant importance due to its sparse population, rugged terrain and tropical weather condition.

Traditional frequencies band of satellite communication like, C Band or S band are congested because of new emerging applications and system designer are now shifting to higher frequencies band like Ku Band, Ka Band and V band where relatively higher bandwidth is available. However, higher frequencies band are subject to severe atmospheric impairments, Rain attenuation is one of most important cause of impairment for higher frequencies communication system.

Long experience of Author in the field of satellite communication has led to identification of following research gaps in the implementation/use of rain attenuation prediction models in Indian climatic conditions.

1. Most of the rain attenuation prediction models available in literature are based on experimental data recorded in temperate climatic region and as such these models do not capture the rainfall distribution of the Indian region particularly that of North-eastern part of India.
2. Absolute lack of experimental study of rain attenuation of microwave signal in North- Eastern part of India.

This thesis presents a study on weather impacted Ku band satellite channel in moist tropical climate of Aizawl, the capital city of Mizoram, a state in North- Eastern part of India. The entire thesis is running into five chapters.

- Chapter 1: This chapter gives a brief framework of all important concepts covered in the thesis.
- Chapter 2: This chapter gives a detailed, systematic and relevant review of literature related to the research problem undertaken.
- Chapter 3: This chapter describes a detailed methodology used by the author, experimental set up and rain models used such as ITU-R model, SAM, DAS and Crane Model.
- Chapter 4 describes a detailed analysis and interpretation of the experimental data, based on the various tools including various models.

- Chapter 5 contains summary and conclusion drawn from the present work and future scope of study.

As outlined in the title of thesis the soul of current work revolves around following three parts.

- Rain data analysis
- Rain attenuation data analysis
- Mitigation technique currently used in satellite communication.

Rain data analysis:

In this section the author has analyzed the historical rain data for the region. From the 30 year (1986-2025) historical rainfall data gathered from state metrological department, Government of Mizoram, both long term and short term descriptive statistics of rainfall at Aizawl were derived.

Cumulative statistics of annual rainfall depth (rain exceedance curve) was derived, by performing logistic regression analysis of cumulative statistics, author has discovered following equation connecting the annual rainfall depth Y and return period T .

$$Y = 303.011 \log_e(T) + 2456.6 \quad mm \quad (1)$$

Rain depth (mm) exceedance curve with integration time 24 hours were derived. The logistic regression analysis of the derived data we obtained the following equation relating rain depth with 24 hours integration time R_{24} and return period T .

$$R_{24} = 4.2309 \log_e(T) + 15.16 \quad (2)$$

Using equation 2 and Kothyari and Garde IDF equation (3) we derived rainfall intensity (mm/hour) with integration time of 60 minutes for various exceedance probabilities.

$$L_t^T = C \left(\frac{T^{0.20}}{t^{0.71}} \right) (R_{24}^2)^{0.33} \quad (3)$$

Rain rate with 60 minute integration time was converted to 1 minute integration time using the algorithm contained in ITU-R.P. 837.7 recommendation.

Using logistic regression analysis, Author has discovered the equation relating rain rate (mm/hour) with integration time 1 minute R_1 and exceedance probability p .

$$R_1(\text{mm/hr}) = -9.933 \log_e(p) + 27.368 \quad (4)$$

- Finally the author has proposed a power law rain rate conversion model for converting rain rate R_{60} from 60 minute integration time to 1 minute integration time R_1 .

$$R_1 (\text{Model}) = A (R_{60})^B \quad (5)$$

where A, B are regression coefficient

$$A = 2.6142 \quad (6)$$

$$B = 0.8418 \quad (7)$$

Rain Attenuation analysis:

Measured signal rain attenuation data was compared with four rain attenuation prediction models, The SAM Model, DAS Model, Crane Model and ITU model. The comparison was made using a metric comprising of , mean absolute error(MAE),mean square error (MSE), root mean square error (RMSE). Regression based coefficient of determination was also used for comparison. Author found the ITU model to be the most suited model for the region.

Finally based on logistic and power law regression analysis the author has proposed two rain attenuation model and one frequency based rain attenuation for various frequencies that could be used for the region.

Fade Mitigation Technique:

To improve the quality of satellite channel under atmospheric impairment. The author has discussed various fade mitigation Technique currently in use in satellite communication industry.